MARTIN MARIETTA ENERGY SYSTEMS LIBRARIES
3 4456 0361223 1

CENTRAL RESEARCH LIBRARY
DOCUMENT COLLECTION

ORNL-2434
Physics and Mathematics
TID-4500 (13th ed. Rev.)

5

# ELECTRONUCLEAR RESEARCH DIVISION

# ANNUAL PROGRESS REPORT

# FOR PERIOD ENDING OCTOBER 1, 1957

CENTRAL RESEARCH LIBRARY
DOCUMENT COLLECTION
LIBRARY LOAN COPY
DO NOT TRANSFER TO ANOTHER PERSON
If you wish someone else to see this document, send in name with document and the library will arrange a loan.

OAK RIDGE NATIONAL LABORATORY
operated by
UNION CARBIDE CORPORATION
for the
U.S. ATOMIC ENERGY COMMISSION

Printed in USA. Price $2.00 cents. Available from the

Office of Technical Services
U. S. Department of Commerce
Washington 25, D. C.

LEGAL NOTICE

This report was prepared as an account of Government sponsored work. Neither the United States, nor the Commission, nor any person acting on behalf of the Commission:

A. Makes any warranty or representation, express or implied, with respect to the accuracy, completeness, or usefulness of the information contained in this report, or that the use of any information, apparatus, method, or process disclosed in this report may not infringe privately owned rights; or

B. Assumes any liabilities with respect to the use of, or for damages resulting from the use of any information, apparatus, method, or process disclosed in this report.

As used in the above, "person acting on behalf of the Commission" includes any employee or contractor of the Commission to the extent that such employee or contractor prepares, handles or distributes, or provides access to, any information pursuant to his employment or contract with the Commission.

ORNL-2434
Physics and Mathematics
TID-4500 (13th ed. Rev.)

Contract No. W-7405-eng-26

# ELECTRONUCLEAR RESEARCH DIVISION

# ANNUAL PROGRESS REPORT

## For Period Ending October 1, 1957

Robert S. Livingston, Director

DATE ISSUED

APR 15 1958

OAK RIDGE NATIONAL LABORATORY
Oak Ridge, Tennessee
operated by
UNION CARBIDE CORPORATION
for the
U. S. ATOMIC ENERGY COMMISSION

MARTIN MARIETTA ENERGY SYSTEMS LIBRARIES
3 4456 0361223 1

## CONTENTS


Abstract ..... 1

Heavy-Particle Physics ..... 1
- Transfer Reactions ..... 1
- Compound-Nucleus Reactions ..... 3
- Miscellaneous Experiments ..... 4

The 86-Inch Cyclotron ..... 5
- Nuclear Physics Research ..... 5
- Applied Physics ..... 11
- Beam Deflection ..... 14

Electronuclear Machines ..... 18
- Experimental Studies ..... 18
- High-Energy Accelerator Design ..... 29

The 48-Inch Heavy-Particle Cyclotron ..... 41
- Progress on the Cyclotron as Originally Proposed ..... 41
- Revision of the 48-Inch Cyclotron Design ..... 43

Special Separations ..... 46
- Plutonium Separations ..... 46
- Chemical Recycle and Product Chemistry ..... 46
- Low-Intensity Isotope Separator ..... 48
- New Plutonium Feed Materials ..... 51
- Isotope Shipments ..... 51

Package Power Reactor ..... 54
- Army Package Power Reactor ..... 54
- Gas-Cooled Loop Design and Construction ..... 56
- Assistance to Other Reactor Programs ..... 56

Previous Progress Reports ..... 59

Papers Presented During the Period March 21, 1956–October 1, 1957 ..... 59

Articles Published During the Period March 21, 1956–October 1, 1957 ..... 61

Articles Submitted for Publication March 21, 1956–October 1, 1957 ..... 62

# ELECTRONUCLEAR RESEARCH DIVISION ANNUAL PROGRESS REPORT


## ABSTRACT

In heavy-particle physics the 28-Mev $N^{+++}$ ions accelerated with the ORNL 63-Inch Cyclotron are used in studies of transfer reactions in which a nucleon is transferred from one nucleus to the other, and in studies of reactions in which the two nuclei fuse and there is an emission of light particles.

The deflector system installed in the ORNL 86-Inch Cyclotron has proved to be very reliable. The machine is being used for a wide range of studies of proton-induced reactions in the medium-energy field, as well as for the production of radioisotopes for research and medical uses.

The successful operation of a 200-kev electron cyclotron has shown the feasibility of accelerating particles well into the relativistic region with a fixed-frequency cyclotron in which azimuthal variations in the magnetic field keep the ions focused toward the median plane. Further tests and design studies are being made in order to apply this principle to an f-f cyclotron for accelerating large currents of protons to 900 Mev.

The preparation of highly enriched isotopes of uranium, thorium, and plutonium was continued. A small 24-in. isotope separator was developed for the separation of small quantities of radioactive feed materials.

The Army Package Power Reactor, APPR-1, originally designed at the Laboratory, has shown excellent operational characteristics in performance tests. Development tests and consultation service for this and similar reactor programs were continued.


---

## HEAVY-PARTICLE PHYSICS

The heavy-particle physics program makes use of the 28-Mev $N^{+++}$ ions accelerated by means of the ORNL 63-Inch Cyclotron. The program is concerned with nuclear reactions produced by the nitrogen ions on targets ranging from beryllium to potassium. These reactions may be conveniently divided into two main types: transfer reactions in which a neutron or proton transfers from one nucleus to the other, and compound-nucleus type of reactions in which the major part of the nuclear matter fuses and there is an emission of light particles such as protons, deuterons, or alpha particles.

### TRANSFER REACTIONS

A characteristic behavior of transfer reactions has long been apparent, namely, that the cross section for such a reaction depends strongly on the energy balance, $Q$. Excitation functions for ten reactions in which a neutron transfers from $N^{14}$ to the target nucleus have now been measured. These reactions all lead to 10.1-min $N^{13}$, which is separated chemically from the target; the cross sections are then obtained by absolute beta counting.

A systematic behavior for these excitation functions is shown in Fig. 1. The abscissa, $E^*$, is the energy available in the center-of-mass system, less the Coulomb barrier, plus the $Q$ for the reaction; $E^*$ may thus be regarded as the energy available in the two-nucleus system immediately after transfer. It can be seen from the figure that most of the reactions follow a common trend. The dashed line in the graph is the excitation function for an evaporation type of reaction, $O^{16}(N^{14},2p)Al^{28}$, presented for comparison.

It is clear that the above interpretation of $E^*$ is a classical one, since it takes into account neither the quantum mechanical nature of the

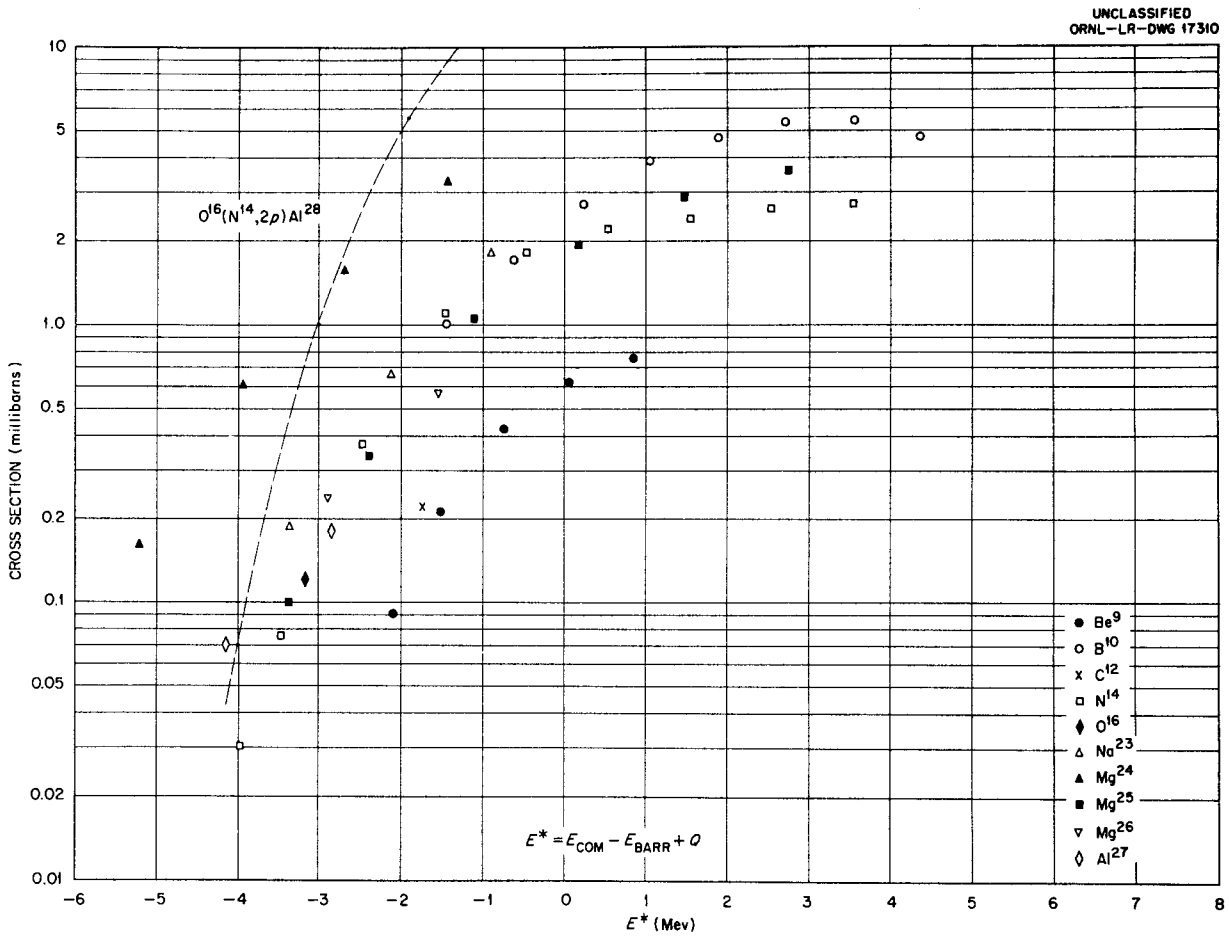


**Fig. 1. Total Cross Sections for Ten Transfer Reactions Leading to $N^{13}$, Plotted as a Function of $E^*$.**

orbits nor the details of the transfer process. The graph can therefore show only general reaction trends. The importance of the $Q$ value in transfer reactions may be understood in this way, however.

The angular distribution of $N^{13}$ was measured for the reaction $Mg^{25}(N^{14},N^{13})Mg^{26}$. The measurement of the angular distribution for a transfer reaction is complicated by the fact that the reaction products are necessarily different from the reacting nuclei by only one nucleon. Therefore, any detecting system must distinguish between the elastically scattered $N^{14}$ and the $N^{13}$, which is a reaction product. This is difficult to achieve with counters or nuclear-plate detectors. The low cross sections of the transfer reactions help matters not at all. In this experiment the half life of the $N^{13}$ served to identify the desired reaction product.

The experimental arrangement was as follows: concentric cylinders of thin phosphor bronze were mounted at various distances from a base plate, which was located 8 in. from the thin $Mg^{25}$ target. Thin aluminum strips to catch the reaction products were placed smoothly along the inner surfaces of the bronze cylinders. In this way the yields were enhanced by utilization of the entire azimuthal angle at any one polar angle. The resulting angular distribution is shown in Fig. 2. The solid line is for $Mg^{26}$ left in the ground state, and the dashed line is for $Mg^{26}$ left excited to 7.0 Mev. The dotted lines at the smallest angle are upper limits only. In this experiment there is no clear indication of which states of $Mg^{26}$ contribute to the cross section. By using cover foils over the aluminum catchers it was possible, however, to include at each angle all states up to 7 Mev.

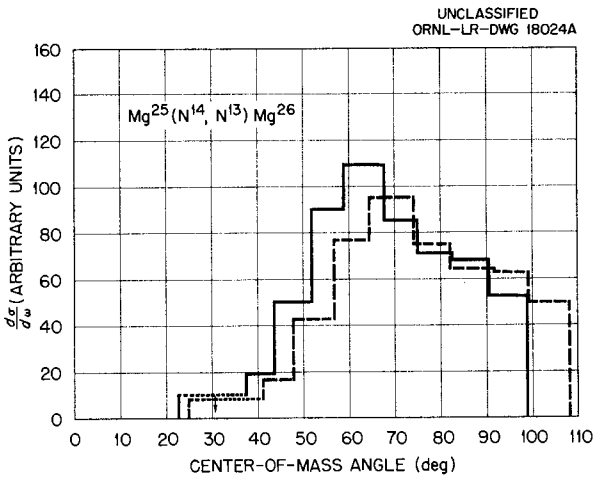


**Fig. 2. Angular Distribution of $N^{13}$ from the Reaction $Mg^{25}(N^{14}, N^{13})Mg^{26}$. The solid line represents the calculation for the ground-state transition, the dashed line represents transitions to a 7-Mev state in $Mg^{26}$, and the dotted portions are upper limits.**

Qualitative information concerning the transfer process may be obtained from a simple calculation based on classical Rutherford-scattering orbits. The orbits in a transfer reaction are similar to those in an elastic scattering of $N^{14}$ from $Mg^{25}$. Then if the transfer takes place at the distance of closest approach, and if this distance is calculated from the angle at which the $N^{13}$ is observed, it may be concluded that at the peak of the angular distribution, transitions to the ground state happen when the two nuclei are not in contact (with contact defined by $r_0 = 1.6 \times 10^{-13}$ cm).

## COMPOUND-NUCLEUS REACTIONS

Light-particle spectrometry of reactions produced by nitrogen ions in light elements was discussed in the previous progress report.[1] The following three reactions were studied in order to verify the compound-nucleus model of nuclear reactions:

$$Li^6(N^{14}, p)F^{19}$$
$$Li^7(N^{14}, d)F^{19}$$
$$Be^9(N^{14}, \alpha)F^{19}$$

According to the statistical theory the probability of the emission of a light particle depends on the phase space available, the barrier, and the level density of the residual nucleus. In the above reactions the residual nucleus is invariably the same, $F^{19}$; therefore the energy spectra of $p$, $d$, and $\alpha$ particles should be identical after the phase space and barrier corrections have been made. This is illustrated in Fig. 3, where these corrections have been applied, and it can be seen that the compound-nucleus theory works reasonably well in the case of the bombardment of light elements with nitrogen ions. Protons, deuterons, and alpha particles all show essentially the same energy dependence.

Angular distributions of protons and alpha particles were measured from the nitrogen bombardment of aluminum. Figure 4 shows the number of protons, corrected for phase space and barrier, plotted against the square root of the excitation of the residual nucleus. It may be seen that the

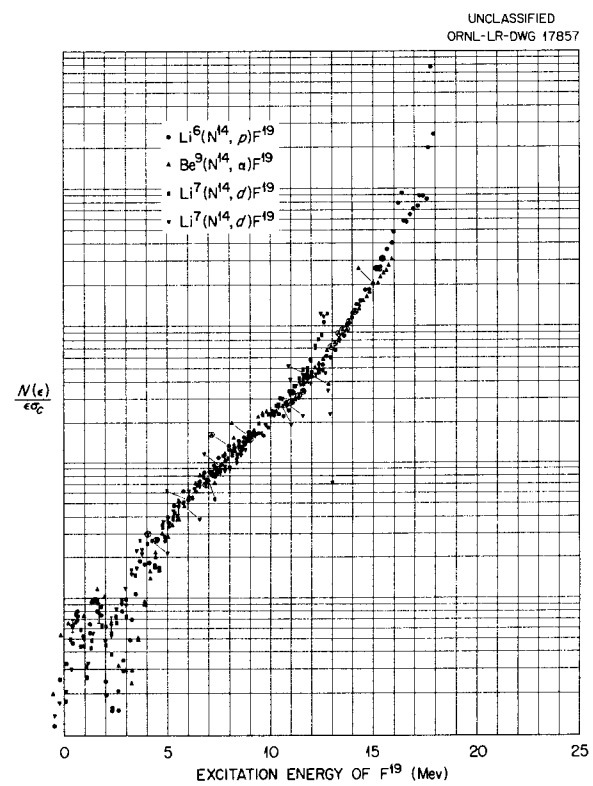


**Fig. 3. Proton, Deuteron, and Alpha-Particle Spectra from $Li^6$, $Li^7$, and $Be^9$ Bombarded with Nitrogen Ions.**

[1] *Electronuclear Research Semiann. Prog. Rep. March 20, 1956*, ORNL-2139, p 3.

energy dependence of the protons is the same at all four angles. The value of $a$ in the level-density formula

$$\omega = Ce^{2\sqrt{aE}}$$

is 5.0 ± 0.2. The angular distribution of protons is isotropic from 0 to 90 deg in the laboratory system. Alpha particles also exhibit the same energy dependence at all angles; here, however, $a = 4.0 \pm 0.5$. The angular distribution of alpha particles exhibits a forward peak, with about twice as many alphas being emitted in the forward direction as at 90 deg.

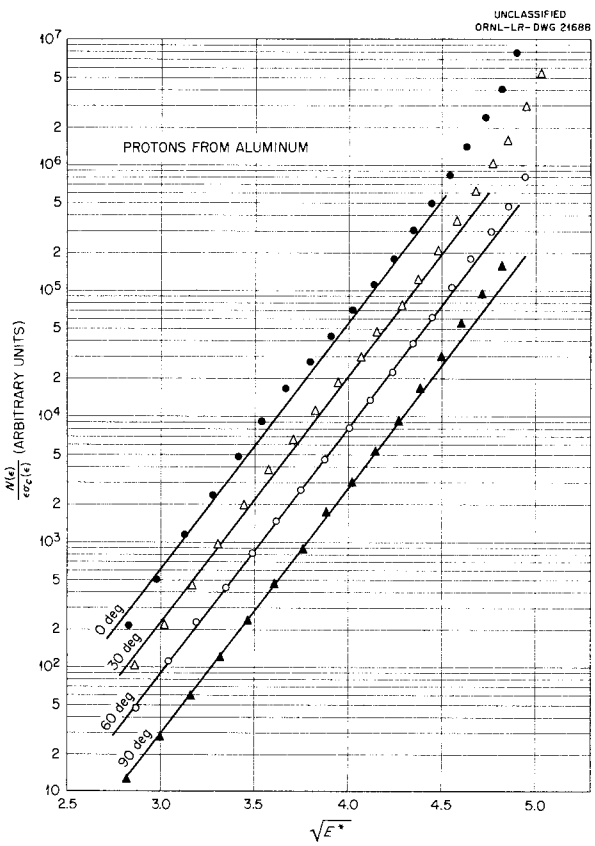


**Fig. 4. Energy Spectra of Protons from the Nitrogen Bombardment of Aluminum Measured at Four Angles.**

## MISCELLANEOUS EXPERIMENTS

A search was made for the Coulomb excitation fission of $U^{238}$ by 28-Mev nitrogen ions. The yield as measured from the production of $Ba^{139}$ indicates an upper limit for this cross section to be about $2 \times 10^{-28}$ $cm^2$.

The response of a CsI(Tl) scintillation crystal to energetic nitrogen ions was measured and is shown in Fig. 5. The CsI(Tl) response to alpha particles and gamma rays is also shown on the same graph for comparison.

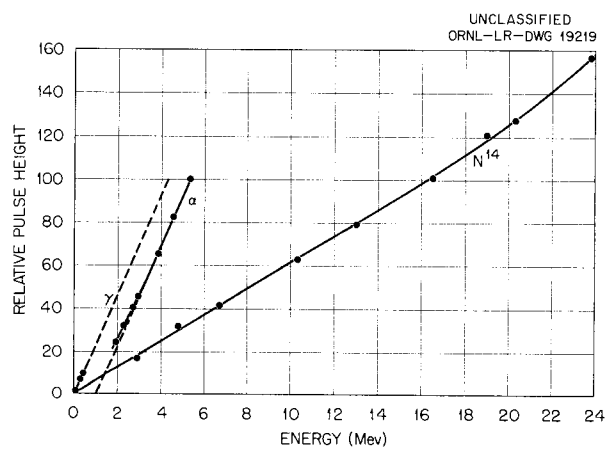


**Fig. 5. Pulse Height vs Energy of CsI(Tl) for Nitrogen Ions.**

# THE 86-INCH CYCLOTRON

Installation of the beam deflector system in the ORNL 86-Inch Cyclotron was completed; the reliability and performance of the system were improved, and the machine is now operated on a routine basis. An improved deflector septum permits operation for as long as a year without interruption because of failure of this component. A deflected beam of 80 $\mu$a of ~25-Mev protons is available at an intermediate target position. In the reaction room, 40 ft from the cyclotron, the deflected beam available exceeds requirements. For isotope production work the magnetic channel of the deflector system is readily retracted to permit exposure of large internal targets to a circulating beam of over 2 ma.

## NUCLEAR PHYSICS RESEARCH

With the reliable operation of the deflector system, the program of nuclear physics research with ~25-Mev protons is again well established. During the period of installation and development of the deflector system, a series of fission-fragment studies was conducted with a wedge-magnet spectrograph installed in the ORNL Graphite Reactor.

### Studies of Proton-Induced Reactions

**Anomalous Inelastic Scattering of 23-Mev Protons.** – Measurements of energy distributions from inelastic scattering of 23-Mev protons by heavy elements indicate the presence of very strong, apparently monoenergetic, groups; an example is shown in Fig. 6. The energies, cross sections, and angular distributions of these proton groups vary slowly and regularly with atomic number. For $Z > 40$, there is little difference between even and odd elements, or across closed shells (see Figs. 7 and 8); this complicates any explanation of these levels based on single-particle excitation.

**Inelastic Proton Scattering and $(p,d)$ Reactions.** – A previous study of anomalous inelastic scattering was extended to include heavy elements, higher excitation energies of the final nucleus, and deuterons from $(p,d)$ reactions. The energy distributions of protons inelastically scattered from each of the principal isotopes of lead and from bismuth are shown in Fig. 9; there are seven relatively well-defined groups with the same energy, cross section, and angular distribution. All elements studied with atomic number above 40 have prominent groups with $E_p - E_p' \cong 2.5$ Mev. The deuteron energy distributions from $(p,d)$ reactions in bismuth and lead isotopes are very similar (five prominent groups with the same energy and similar cross sections) in spite of differing $Q$ values (Fig. 10). There are also strong similarities in the deuteron spectra from gold and platinum, and from palladium and silver.

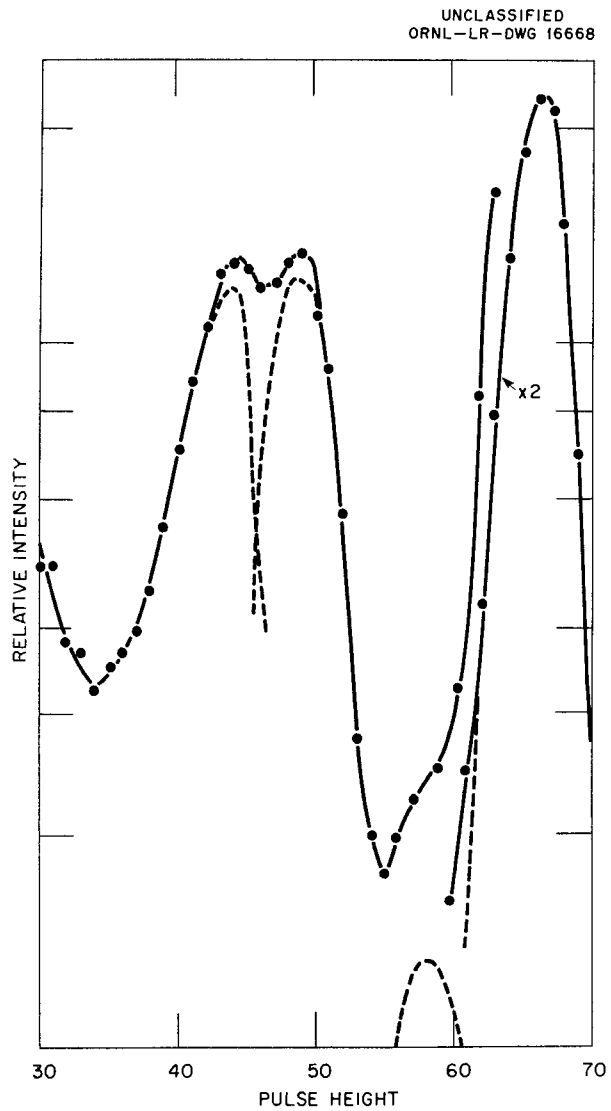


**Fig. 6. Pulse-Height Spectrum from Zirconium Target with 400 mg/cm$^2$ Aluminum Absorber Interposed.**

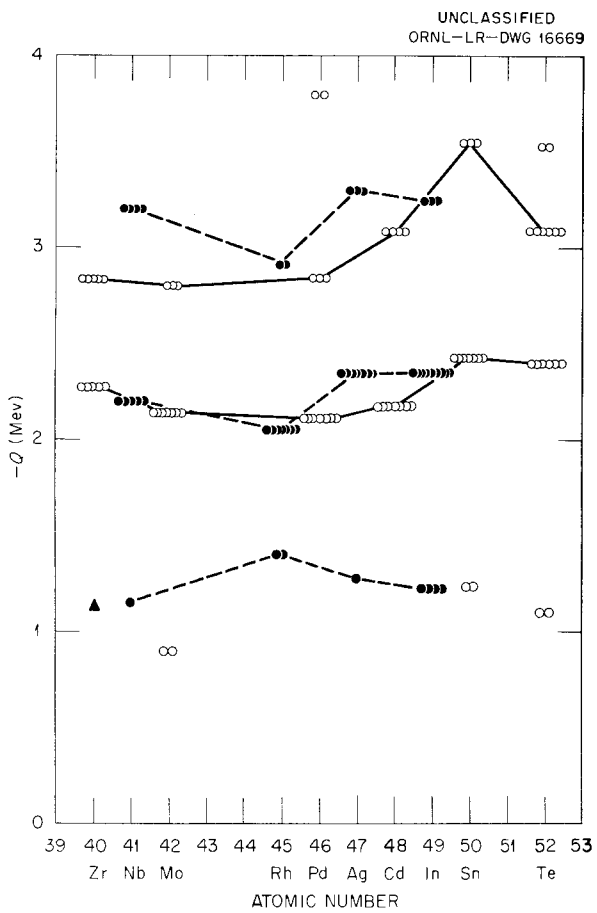


**Fig. 7. Energy Levels in Elements for $Z = 40$ to 52 Required To Explain Inelastic Proton Scattering Spectrum. Open circles, even-$Z$ elements; closed circles, odd-$Z$ elements. The number of circles gives the differential cross section at 90 deg in units of $10^{-28}$ cm$^2$/steradion; the triangle indicates $\sigma \cong 0.5 \times 10^{-28}$ cm$^2$/steradion.**

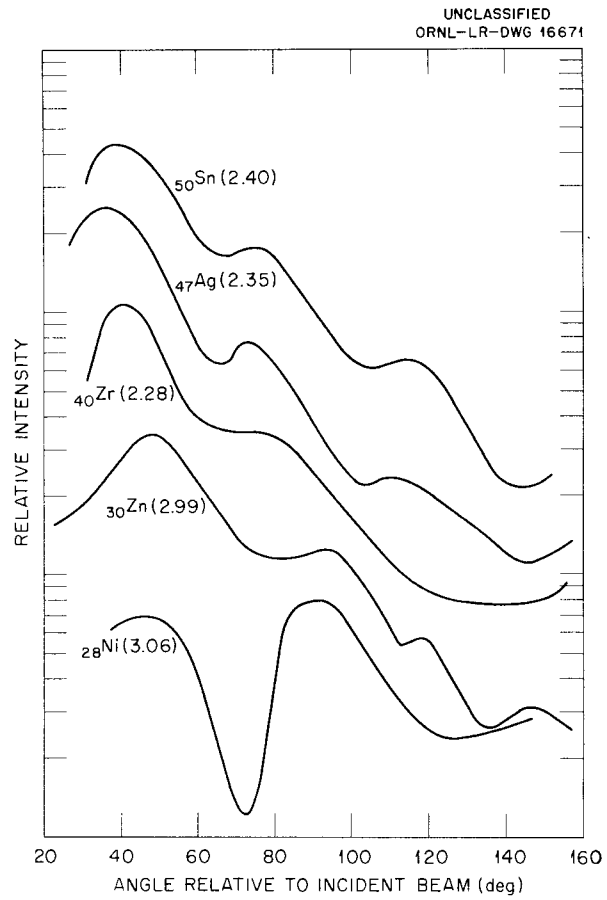


**Fig. 8. Angular Distributions of $-Q \cong 2.3$-Mev Groups in Elements for $Z = 40$–52 and $-Q \cong 3.1$-Mev Groups in Elements for $Z = 26$–30.**

**Coincidence Studies of the $Ni^{58}(p,2p)$ Reaction.** – The $Ni^{58}(p,2p)$ reaction, by far the predominant reaction in that nucleus, was studied by detecting the two outgoing protons in coincidence. Measurements were made of the energy spectra of all protons from the reaction (Fig. 11), of the spectrum of the sum of the energies of the two outgoing protons (Fig. 12), and of the angular correlations of the outgoing protons with each other and with the incident proton. The results indicate quite conclusively that the preponderance of $(p,2p)$ over $(p,pn)$ reactions in $Ni^{58}$ is not due to the relative level densities of the final nuclei, the ineffectiveness of Coulomb barriers, or a high emission energy of the "first" proton, which leaves the emission of a neutron energetically forbidden. There is strong evidence that the $(p,2p)$ reaction mechanism is predominantly a direct one in which the two protons are knocked out simultaneously.

**Recent Studies of Anomalous Inelastic Proton Scattering.** – The energy distribution of inelastically scattered protons was remeasured with 150-kev resolution (previous work was done with 500-kev resolution). Differences in the fine structure of the anomalous inelastic peaks were observed for each element. New regularities were found at lower excitation energies, and a significant structure was observed at higher excitation energies.

The dependence of the effect on bombarding energy between 23 and 12 Mev was measured. The cross section for the effect decreases slowly

as bombarding energy is decreased (about 30% over the entire range). For both $Zn^{64}$ and $Zn^{68}$, the $Q$ value of the anomalous peak shifts slowly with bombarding energy; there is some evidence for this in other elements.

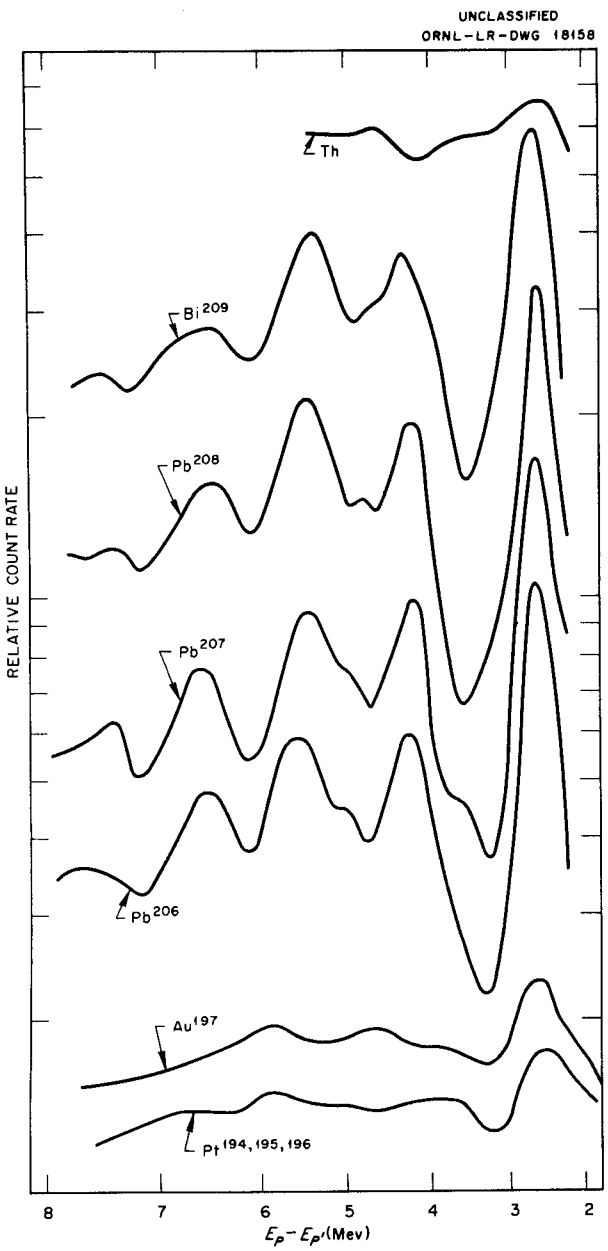


Fig. 9. Energy Distribution of Inelastically Scattered Protons. Ordinates for each curve are displaced arbitrarily. Data were corrected for contributions from carbon and oxygen contamination. The detection angle is 90 deg.

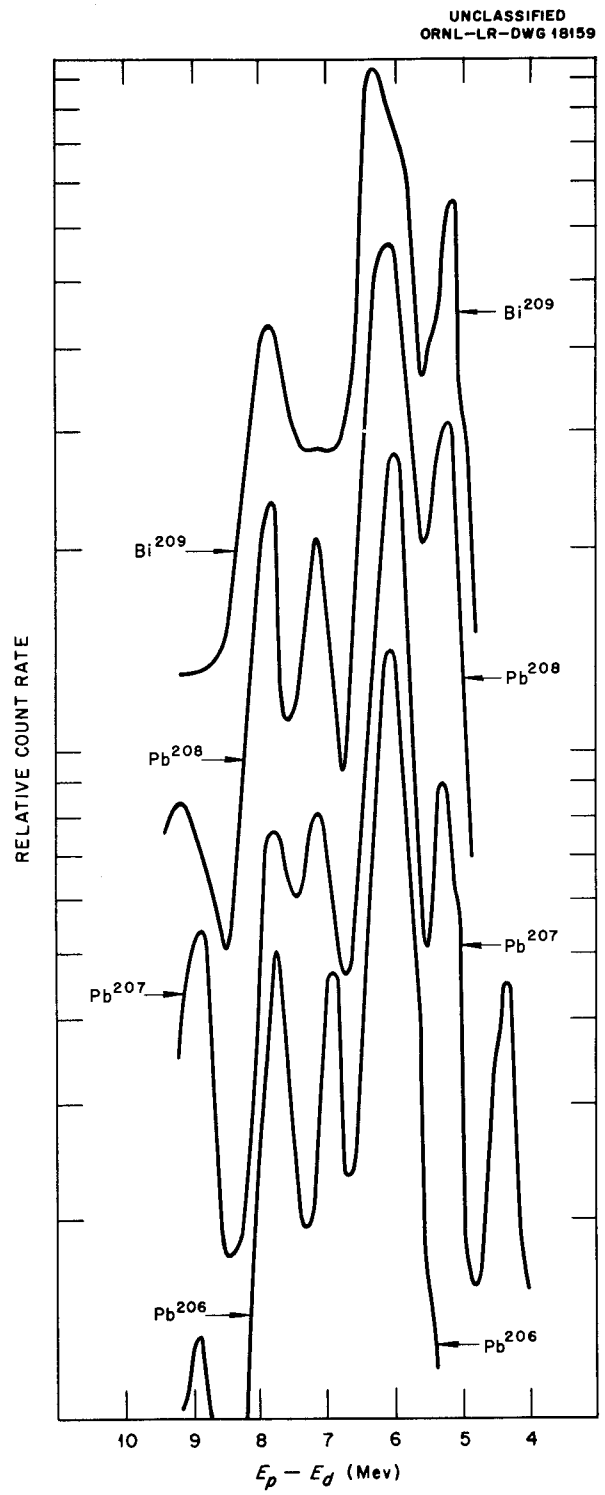


Fig. 10. Energy Distribution of Deuterons from $(p,d)$ Reactions in Bismuth and Lead Isotopes. The detection angle is 60 deg.

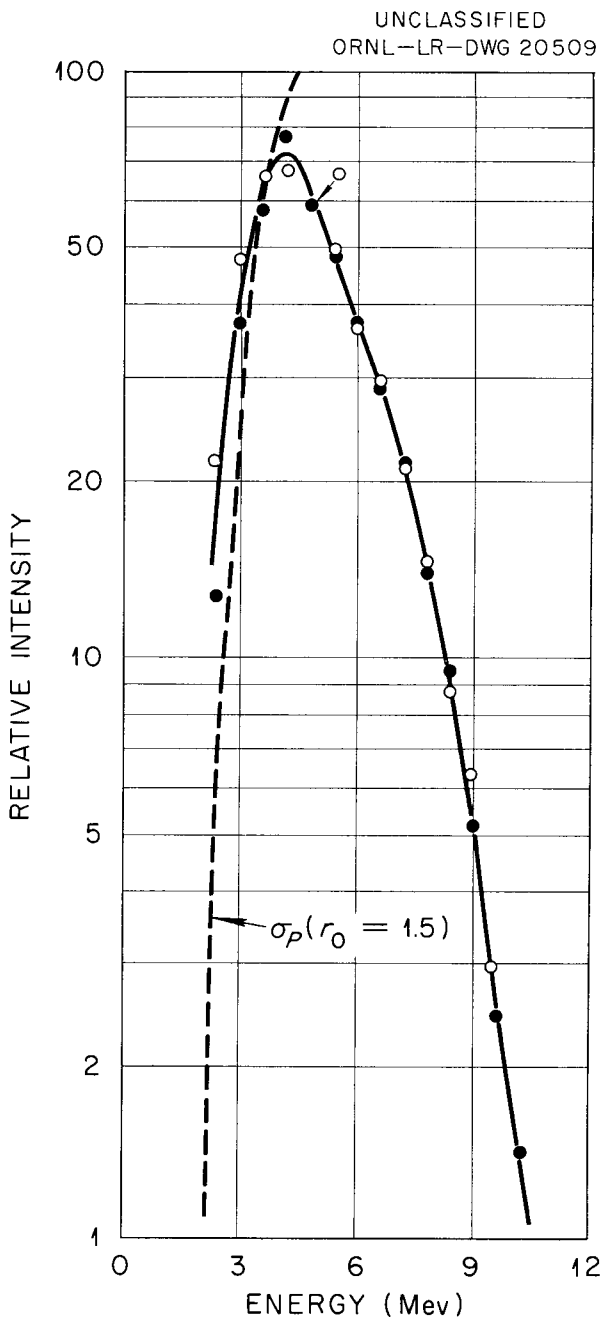


**Fig. 11. Energy Distribution of Protons Emitted in 23-Mev Proton-Induced $Ni^{58}(p,2p)$ Reactions.** Detection angles were 90 deg left and 90 deg right, but data obtained at other angles were indistinguishable except for shifts due to center-of-mass motion. The dashed curve represents, essentially, the coulomb barrier penetration factor for a nuclear radius of $1.5\ A^{1/3} \times 10^{-13}$ cm.

The gamma rays in coincidence with anomalous inelastic scattering were studied. Their energy distribution is relatively smooth, with no great preponderance or deficiency of transitions to the ground state. A few peaks were observed.

**Activities in Rare-Earth Nuclei.** – The series operation of the calutron isotope separators, the 86-in. cyclotron, and ion exchange columns produced excellent rare-earth radioactive sources for use in a 180-deg, permanent magnet, photorecording spectrograph. Decay rates of the internal-conversion lines were measured, and these data, along with activation data and use of enriched isotopes, made it possible to make mass assignments for 10 new activities and to elaborate upon 18 others. The following new isomeric transitions were

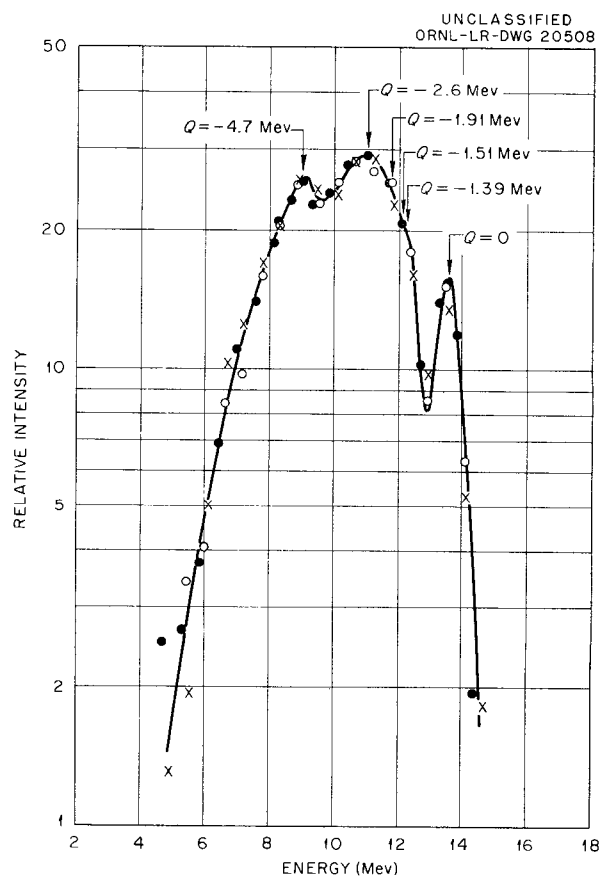


**Fig. 12. Distribution of the Sum of the Energy of the Two Protons Emitted in $Ni^{58}(p,2p)$ Reactions.** Detection angles were 90 deg left and 90 deg right, but data obtained at other angles were essentially indistinguishable except for shifts due to center-of-mass motion.

observed: $Tb^{156m}$ (5.5 hr), 88.2 kev ($E3$); $Ho^{160m}$ (5.0 hr), 60.4 kev ($E3$); $Er^{167m}$ (2.5 sec), 208 kev ($E3$); and $Yb^{171m}$ ($T_{1/2?}$), 75.8 kev ($E3$).

New and more precise data were obtained on the energies of the first and second excited states of a dozen even-even nuclei. It appears that, for the region of neutron number 94 to 108, the value of the moment of inertia has a dependence on proton number and is slightly smaller for a higher $Z$ element (for the same neutron number) (see Fig. 13).

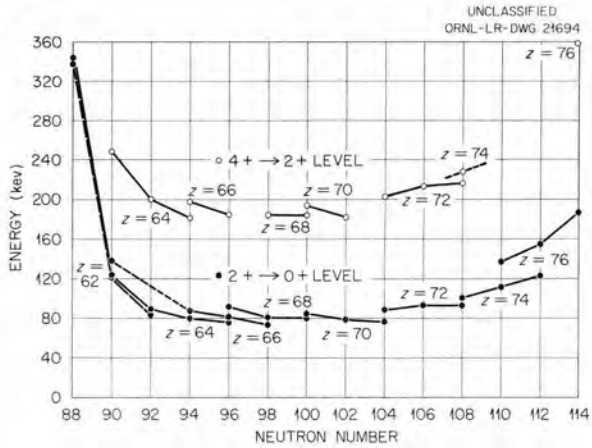


**Fig. 13. Energies of First and Second Excited States in Even-Even Nuclei, for $88 < N < 114$ with $Z$ as a Parameter.**

### Fission-Fragment Spectrograph Studies

A wedge-magnet mass spectrograph, Fig. 14, was built for the analysis of fission fragments originating in the ORNL Graphite Reactor. The $3\frac{1}{2}$-in.-dia 16-ft-long aluminum tube (1) is placed

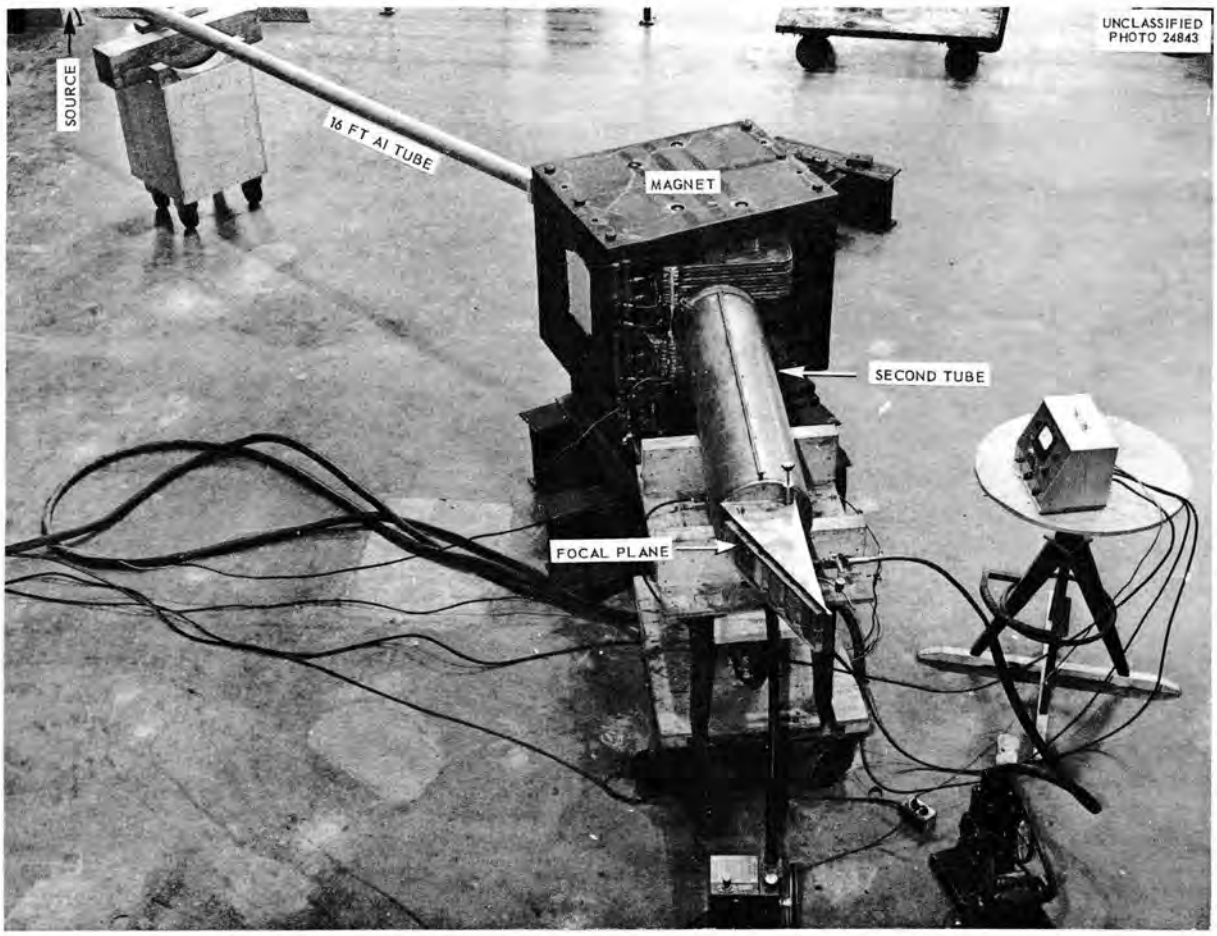


**Fig. 14. Fission-Fragment Spectrograph.**

with the far end inside the reactor core. The source (2), a 40 $\mu g/cm^2$ plating of $U^{235}$, $2\frac{1}{4}$ by $\frac{3}{8}$ in., is mounted inside the end of the tube, in a flux of $5 \times 10^{11}$ neutrons·cm$^{-2}$·sec$^{-1}$. Thus, fission fragments are produced at a rate of about $2.5 \times 10^8$ per second. Those neutrons emitted in the proper direction (about 1 in $10^5$) travel down the tube and are analyzed in the magnet (3), which focuses them through the tube (4) to a line (for a given $H\rho$) on the focal plane (5) 6 ft beyond. There, they are stopped in a 0.001-in. aluminum foil. After a bombardment of some hours the foil is removed, cut in strips corresponding to given $H\rho$'s, and radiochemically analyzed; the resulting activity is measured with end-window counters.

**Energy Distribution of Mass-97 Fission Fragments.** – The energy distribution of mass-97 fragments from thermal-neutron-induced fission of $U^{235}$ was measured. The fragments were caught in an aluminum foil which, after the irradiation, was cut into strips that were radiochemically analyzed individually for $Zr^{97}$. The $H\rho$ distribution is complicated by the large energy width, which leads to overlapping of momentum distributions from successive charges. An analysis of the shapes of the $H\rho$ distributions obtained with different relative charge populations indicated that the width of the energy distributions was 11.4 ± 0.8%, corrected for broadening due to prompt-neutron emission. This result is in agreement with measurements of the distributions of the number of neutrons per fission but is in sharp disagreement with the predictions from the theory of the fission process. The most probable energy is 174.7 ± 2 Mev for the mass-97 fission mode, and about 164.5 ± 3 Mev for the mass-91 mode.

**Fission-Fragment Mass Separator.** – An energetic fission fragment passing through a gas changes its charge frequently by electron capture-and-loss collisions with gas molecules. Its average charge, $\bar{e}$, is found to be very nearly proportional to velocity, so that magnetic deflection depends only on the mass; thus, passing fission fragments through a gas-filled magnetic spectrograph gives mass separation. At low pressure the resolution is limited by the statistics of the electron capture-and-loss process; increasing the pressure to reduce this effect is eventually limited by energy loss and the resulting multiple scattering. However, before this occurs, there is a pressure range where the resolution is limited by the nuclear charge distribution of fragments of a single mass. All these effects were studied experimentally. The best resolution obtained for mass-97 fragments was 3.5% full width at half maximum (with helium at 20 mm Hg), of which 2.1 ± 0.3% was due to the width of the nuclear charge distribution. Combining this resolution with the results of a study of the dependence of $\bar{e}$ on nuclear charge gave the width of the nuclear charge distribution for mass-97 fragments as 2.3 ± 0.5 units. This value is in agreement with determinations from yields of shielded isotopes but is in disagreement with the predictions of most theories. The best obtainable resolution from the mass separator is 4.5 mass units for light fragments (Fig. 15).

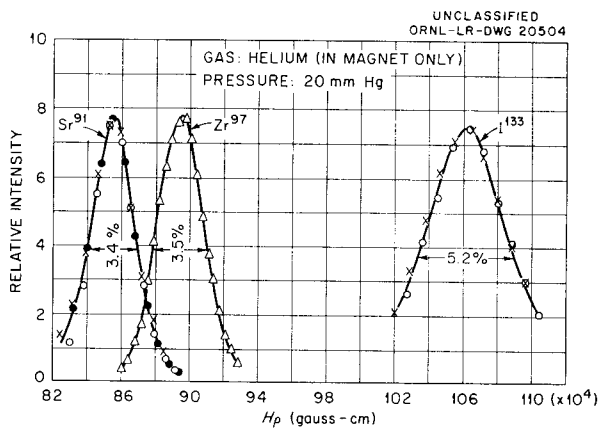


**Fig. 15. The $H\rho$ Distribution of Mass-91, -97, and -133 Fission Fragments.**

**Equilibrium Charges of Fission Fragments in Gases.** – The magnetic analysis method was used to measure the equilibrium charges of median light and heavy fission fragments in hydrogen, helium, air, and argon, and of mass-97 fragments in helium for wide ranges of fragment velocity and gas pressure. The data for the fragments in hydrogen, air, and argon showed pressure effects on the equilibrium charge which yielded estimates of the mean radiative lifetime of excited ionized fragments that agree within 25%, in contrast with previous estimates differing by a factor of 10. An experimental test of the Bohr assumption, that the equilibrium charge of a heavy ion is equal to the number of electrons whose orbital velocities are lower than the translational velocity of the ion, showed the assumption to be only a rough

approximation. Measurements of equilibrium charge as a function of atomic number of the stopping gas agreed with previous measurements.

**Scintillation Response of CsI(Tl) Crystals to Fission Fragments.** – A thin CsI(Tl) crystal was used as the phosphor of a scintillation detector of fission fragments. Light and heavy fragments from reactor-neutron fission of $U^{235}$ were magnetically separated, and the scintillation pulse heights in CsI(Tl) crystals were determined as a function of range in various gases and metals. The relationship between pulse height and fragment energy was found to be linear. Specific fluorescence of fission fragments in the crystal increases monotonically with specific energy loss (Fig. 16). Energy vs range curves (Fig. 17) were obtained for median light and heavy fragments in $H_2$, He, air, A, Al, Ni, and Au.

**Magnetic Analysis of the Long-Range Particles from Fission of $U^{235}$.** – The long-range particles from reactor-neutron fission of $U^{235}$ were studied with a high-resolution magnetic spectrograph. The particles were detected with a CsI(Tl) crystal scintillator; differential pulse-height analysis was used. Data for scintillation pulse height vs $H\rho$ show that the particles have the same value of $e^2/m$ as do alpha particles. The range-energy relationship for the particles in aluminum showed that the particles have the same value of $me^2$ as do alpha particles. Therefore these long-range particles have the same values of $e$ and $m$ as do alpha particles; this confirms that they are alpha particles, as was indicated by previous studies. The energy distribution of the particles, Fig. 18, is in good agreement with previous determinations by other methods.[1,2] An extensive search revealed no fine structure in the energy distribution. The shape of the energy distribution indicates that the particles are formed at the instant of fission.

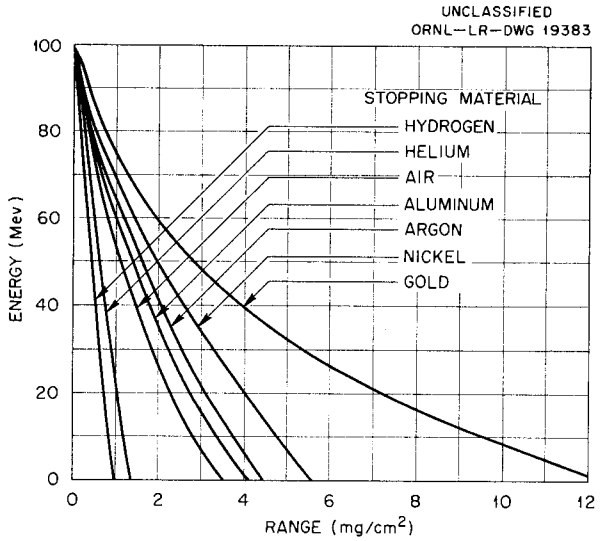


**Fig. 17. Energy of Median Light Fission Fragments as a Function of Range in Various Materials.**

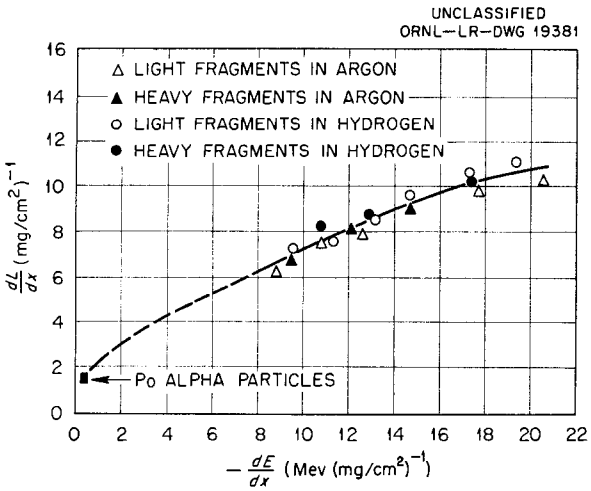


**Fig. 16. Specific Fluorescence as a Function of Specific Energy Loss of Fission Fragments in CsI(Tl) Crystals.**

## APPLIED PHYSICS

Since the startup of the 86-in. cyclotron, after installation of the beam deflection system, the efforts of the Applied Physics Group have been directed toward better understanding and control of the cyclotron when it is used for isotope production. Commercial interest in the use of the cyclotron for production of radioisotopes has continued to be steady. The isotopes are produced in service irradiations for outside concerns who handle the processing and distribution. These service irradiations are billed under the full-cost recovery policy of the AEC. The production of radioisotopes in the cyclotron is summarized in Table 1.

[1] K. W. Allen and J. T. Dewan, *Phys. Rev.* 80, 181 (1950).

[2] E. W. Titterton, *Nature* 168, 590 (1951).

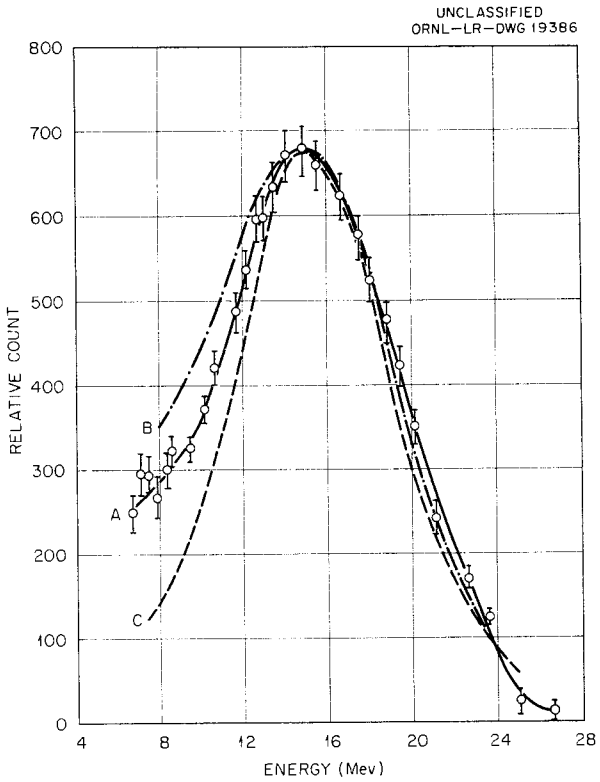


**Fig. 18. Energy Distribution of Long-Range Alpha Particles from Reactor-Neutron Fission of $U^{235}$. Distributions *B* and *C* were determined by Allen and Dewan (see ref 1) and by Titterton (see ref 2), respectively.**

The use of $As^{74}$ has increased during this time; 240 mc was produced in the first six runs and 480 mc in the last six. Two runs for $As^{74}$ production were made with target material enriched to >90% in $Ge^{74}$. The expected increase in yield was not obtained. This point is under further study.

As noted in Table 1, two runs were made for the production of $Mn^{54}$, one with natural chromium and one with ~840 mg of chromium enriched to 80% in $Cr^{54}$. The enriched target stood up very well under bombardment; its use resulted in a twenty-fold increase in the production rate for $Mn^{54}$ and a marked decrease in the undesired $Mn^{52}$ activity.

In addition to these production runs for commercial organizations, the 86-in. cyclotron was used to make an additional 18 radioisotopes for research use in ORNL and other laboratories. Those isotopes produced for other laboratories were $F^{18}$, $Ag^{105}$, $I^{125}$, $Ba^{133}$, $Ce^{139}$, $W^{181}$, $Os^{185}$, $Au^{194,196}$, and $Bi^{205,206}$. The run for the $W^{181}$ production lasted 18 hr and averaged 1500 $\mu$a on a tantalum sheet brazed to a 6 × 7 in. copper target. It was performed for UCRL at Livermore. The yield reported was one-tenth of that estimated. A bombardment of a small target in the external beam was made in order to check the yield determination. Bismuth-205,206 was produced by bombarding radiogenic lead supplied by the customer; bombardment conditions were chosen to enhance the ratio $Bi^{205}/Bi^{206}$.

Two large programs were carried out at the request of Laboratory personnel. In one case 35 runs were made in order to produce $F^{18}$ for use in studies of fluorine exchange kinetics. Small (50 mg) samples of various alkali fluorides were placed in 2-in. lengths of ⅛-in.-OD × 0.008-in.-wall aluminum tubing; the ends were then flattened and the tube bombarded for 15 to 20 min in an A-1 head. The other program consisted of 12 runs for the production of $Kr^{79}$; this was also largely development work. The target finally chosen was KBr fused in a vented nickel capsule. The other isotopes produced for research use within the Laboratory were $Ti^{44}$, $Y^{88}$, $Nb^{90}$, $Mo^{93}$, $Tc^{95m}$, $Te^{121}$, $Ce^{139}$, $Dy^{159}$, and $Bi^{207}$.

The targets used for isotope production are of three types: the 6 × 7 flat plate,[3] the capsule,[3] and the A-1 head.[4] In most cases the 6 × 7 in. target is used. The standard 6 × 7 in. aluminum-target base shows plastic deformation and surface crazing at currents in excess of 950 $\mu$a, while the standard 6 × 7 in. copper-target base has handled 2400 $\mu$a without any signs of deterioration. Because of this, the copper base with the target material intimately bonded to it is usually used. Electroplated deposits with thicknesses of 0.008 to 0.020 in. are used whenever possible. This method was used successfully for Mn, Fe, Ni, Cd, Cr, Zn, Ag, and Sn. Other methods used to bond the target material to the copper are casting (Li, Na, Tl, and Pb), furnace brazing (Ta, W, and V), and vacuum evaporation (Mg and Ca).

---

[3] *Electronuclear Research Semiann. Prog. Rep. Sept. 20, 1954*, ORNL-1795, p 5 (classified).

[4] R. S. Livingston and A. L. Boch, *The Oak Ridge 86-Inch Cyclotron*, ORNL-1196 (June 12, 1952).

Table 1. Summary of the Production of Radioisotopes in the ORNL 86-Inch Cyclotron

| Isotope | Reaction | Amount Produced (mc) | Runs | Production Rates (mc) | | Target | Maximum Average Current ($\mu$a) | Maximum Time per Run (hr) |
|---|---|---|---|---|---|---|---|---|
| | | | | Per hr | Per ma-hr | | | |
| $Al^{26}$ | $Al^{27}(p,pn)$ | $3.2 \times 10^{5*}$ | 1 | $1.6 \times 10^{4*}$ | $1.6 \times 10^{4*}$ | 6 × 7 in. Al | 980 | 20 |
| $Al^{26}$ | $Mg^{26}(p,n)$ | $3.0 \times 10^{4*,**}$ | 1 | $3.0 \times 10^{3*,**}$ | $3.3 \times 10^{3*,**}$ | 6 × 10 in. Mg | 920 | 10 |
| $As^{74}$ | $Ge^{74}(p,n)$ | 786 | 13 | 14 | 76.9 | Capsule | 190 | 6 |
| $Be^{7}$ | $Li^{7}(p,n)$ | 340 | 5 | 28 | 140 | Li on 6 × 7 in. Cu | 200 | 4 |
| $Bi^{207}$ | $Pb^{208}(p,2n)$ | 0.3 | 1 | 0.2 | 0.5 | Pb on 6 × 7 in. Al | 400 | 1.3 |
| $Cd^{109}$ | $Ag^{109}(p,n)$ | 8.5 | 1 | 1.9 | 1.1 | Ag on 6 × 7 in. Cu | 1750 | 4.3 |
| $Co^{57}$ | $Ni^{58}(p,pn)$ + $(p,2n)$ + $(p,2p)$ | 175** | 1 | 88** | 50** | Ni on 6 × 7 in. Cu | 1750 | 2 |
| $Fe^{55}$ | $Mn^{55}(p,n)$ | 37 | 2 | 5.0 | 5.3 | Mn on 6 × 7 in. Al | 950 | 4 |
| $Mn^{54}$ | $Cr^{54}(p,n)$ | 2.9 | 1 | 0.5 | 0.28 | Natural Cr on 6 × 7 in. Cu | 2025 | 5 |
| $Mn^{54}$ | $Cr^{54}(p,n)$ | 112 | 1 | 11 | 6.2 | Enriched $Cr^{54}$ on 6 × 7 in. Cu | 1800 | 10 |
| $Sr^{85}$ | $Rb^{85}(p,n)$ | 105 | 5 | 3.1 | 17.3 | Capsule | 190 | 8 |
| $Y^{88}$ | $Sr^{88}(p,n)$ | 8 | 2 | 3.6 | 20 | Capsule | 190 | 1 |
| $Zn^{65}$ | $Cu^{65}(p,n)$ | 90 | 2 | 20 | 8.4 | 6 × 7 in. Cu | 2400 | 3 |

*Disintegrations per minute.
**Preliminary values.

The materials run in the capsule target were rare-earth oxides, alkali and alkaline-earth halides, and metal powders. In the case of oxides, care must be taken that the material is fully converted; the presence of unconverted oxalates, nitrates, or carbonates generally results in explosive rupture of the capsule during bombardment. Because of the high (>1000°C) temperatures prevalent at the center of the capsules, the alkali metals were bombarded as alkali halides, and nickel was chosen as the capsule material. These halide targets gave more trouble than all others put together. The halides are generally deliquescent and in some cases have water included in the crystal structure. A sequence of six failures (ruptures), with even more care taken in drying the material on each succeeding run, suggested the use of a capsule target in which vapor from the target material is vented to the cyclotron vacuum. This was first tried on RbCl for $Sr^{85}$ production and extended (again by necessity) to KBr for $Kr^{79}$ production. In the latter case the product is a noble gas which must be trapped within the crystalline lattice of the target material. The first such run was successful, but there was some difficulty in repeating it.

Another modification of the capsule target is the development of a vented capsule for use with small quantities, ~50 mg, of target material. A small slot is milled in a solid aluminum plug, the material is placed in this slot as an alcohol-base paste, and the plug and aluminum capsule are dusted with graphite before the plug is inserted in the capsule. Since the capsule is not welded, the plug can be removed after bombardment for easy access to the target material. The use of this target design greatly lowers the radiation exposure of the investigator.

The A-1 head was used for bombarding small metal foils, for the $F^{18}$ runs, and for three runs on 10- to 20-mg samples of $Zr^{90}O_2$.

The development work of the group has been directed toward feasible targets for the production of $Na^{22}$ and $Ca^{47}$. Sodium-22 is produced by the $Mg^{25}(p,\alpha)$ and $Mg^{26}(p,\alpha n)$ reactions. The production rate on a normal magnesium target is 0.4 mc/ma-hr or 0.3 mc/hr. Magnesium-25 is present to only 10% in natural magnesium, so that the use of a target enriched in $Mg^{25}$ would increase the production rate. Experiments on vacuum-deposited, natural magnesium targets, weighing about 300 mg or 3 mg/cm$^2$, gave a yield of 0.13 mc/hr. Extrapolated to similar thin targets of enriched $Mg^{25}$, this is a yield of 1.3 mc/hr, or a fourfold increase in production rate over a full-thick natural magnesium target. The magnesium can be recovered for reuse, so that the isotope cost per run is only a fraction of the total value of the enriched material used.

Calcium-47, the other isotope undergoing development work, is of great interest to biologists because of its short half life (4½ days) and the presence of a 1.3-Mev gamma ray. Attempts were made to fabricate a flat-plate calcium target. One such successful target gave a yield of 46 ± 15 μc/hr from 200 ± 40 mg of natural calcium (0.18% $Ca^{48}$). This extrapolates to 5 mc/hr for target material enriched to 20% in $Ca^{48}$.

Work on both the $Na^{22}$ and the $Ca^{47}$ was performed in cooperation with the Isotopes Division.

## BEAM DEFLECTION

Operation of the 86-in. cyclotron with the beam deflector system, Fig. 19, is now on a routine basis. The reliability of the components of the system and the quality of the deflected beam have been greatly improved since the initial installation.

The water-cooled septum was redesigned, and ¼-in. aluminum tubes flattened to 0.090 in. are used instead of the 1/16-in. tubes originally used. The new design makes it easier to maintain alignment of the tubes, the electrical gradient at the tubes is smaller because of their shape, and the heavier wall (0.028 in. as opposed to 0.010 in.) is much less likely to be punctured by sparking. The first model of the improved septum operated for one year before it developed a leak. During this period, water flowed through the septum tubes at 90 fps for over 5000 hr, and the cyclotron was operated with a deflected beam for a total of 2000 hr. The septum is mounted on one of the dees (Fig. 20).

Additional iron was placed in the magnetic channel to reduce the radial gradient of magnetic field inside the channel, and thus reduce the divergence of beam in the radial direction.

A deflected beam of 80 μa out of a 470-μa circulating beam has been focused on a spot 0.6 in.$^2$ in area by a set of 2-in.-aperture quadrupole focusing magnets. The focused beam in this case was about 70% of the available deflected beam.

UNCLASSIFIED
ORNL-LR-DWG. 17979

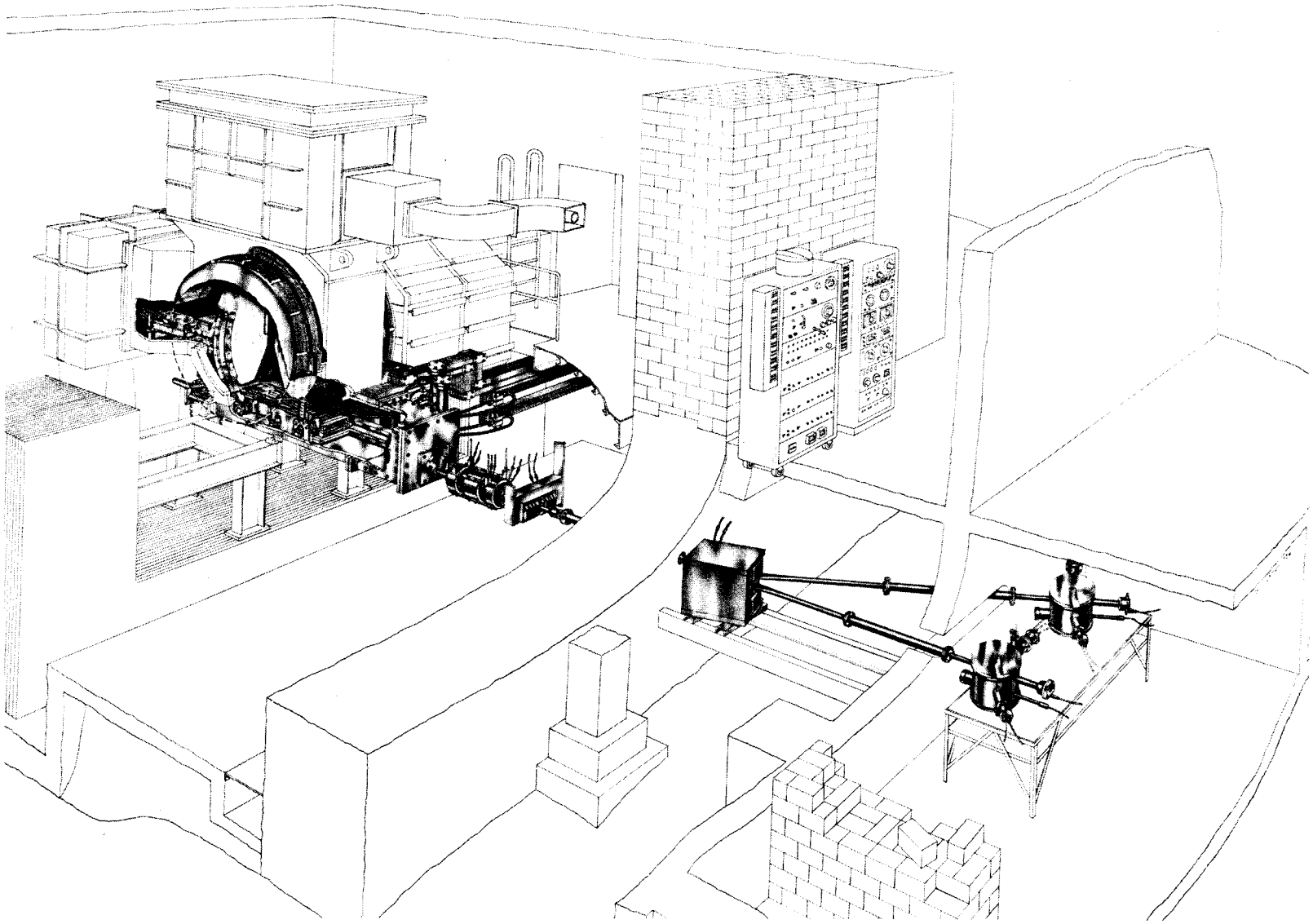

Fig. 19. Deflector System Installed in the 86-in. Cyclotron.

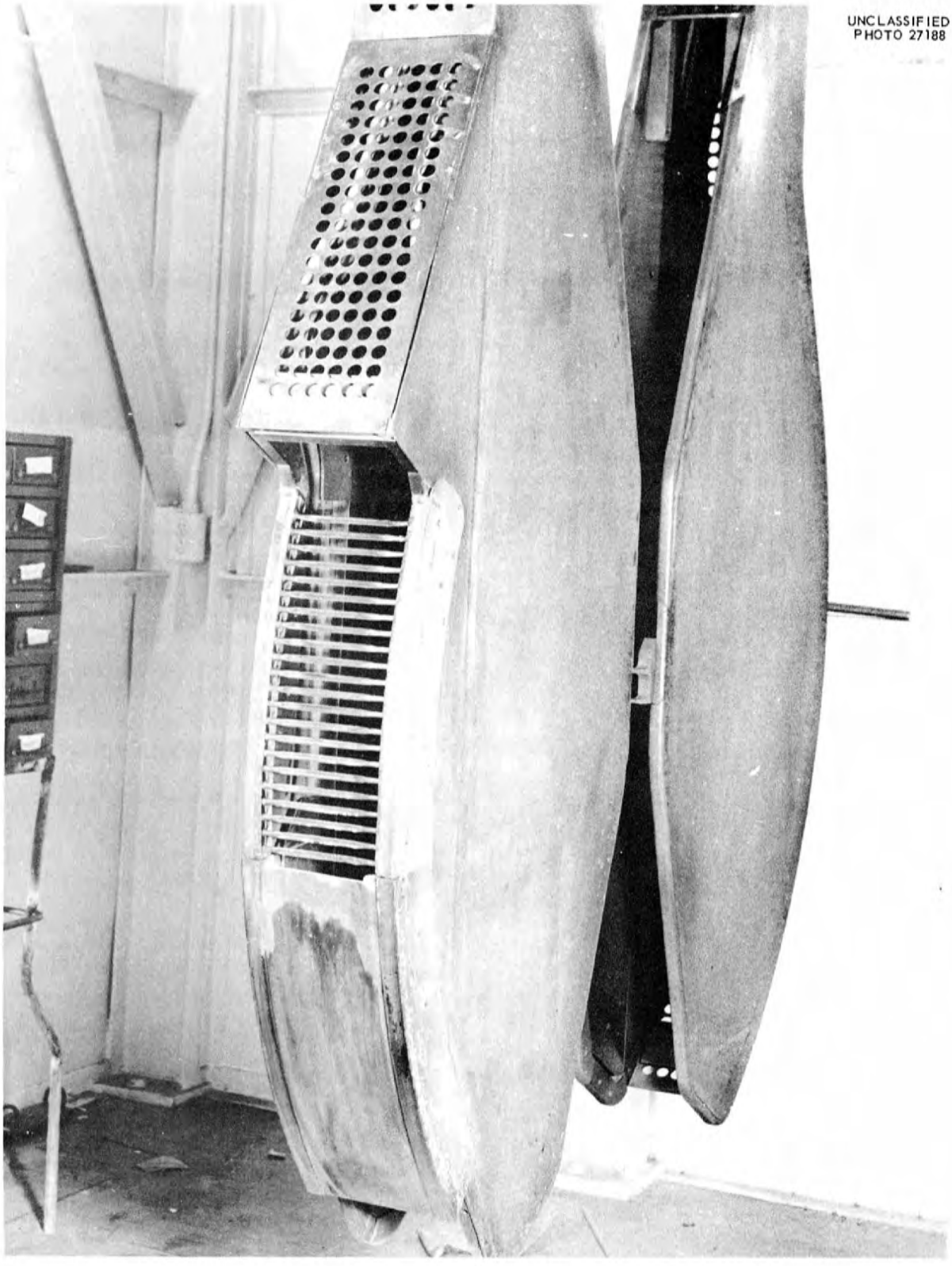


Fig. 20. Water-Cooled Tube Septum Mounted in Dee.

A set of 3-in.-aperture magnets has been constructed so that all the deflected beam can be focused on a target.

For basic physics experiments the deflected beam is piped to the reaction room, 40 ft from the cyclotron. Because of the nature of the experiments and because of the limited shielding of the reaction room, the deflected beam is defined and reduced to less than 1 $\mu$a. In Fig. 21 the deflected beam is shown issuing through a 0.001-mil aluminum foil into the reaction room. The 23-Mev protons travel 13.5 ft before their luminous path in air is interrupted by a wall at the left; the full range in air would be 16 ft.

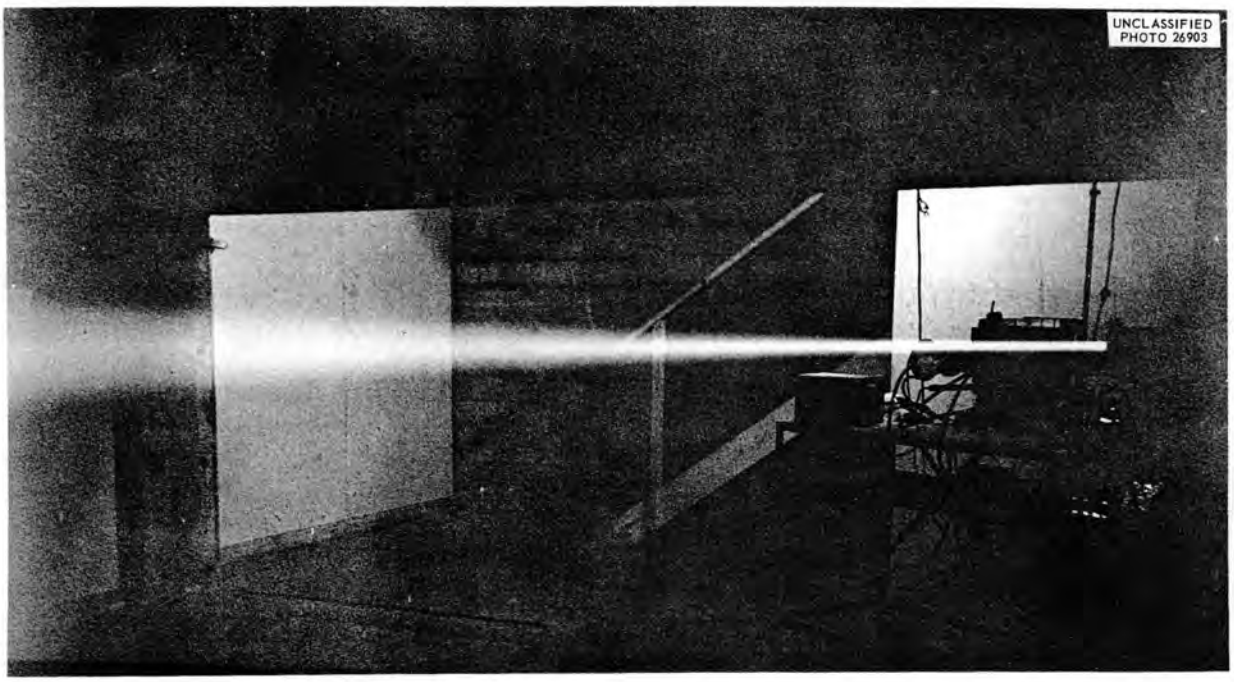


Fig. 21. Deflected Beam of ORNL 86-in. Cyclotron.

## ELECTRONUCLEAR MACHINES

The feasibility of a fixed-frequency cyclotron for accelerating large proton currents to ~900 Mev is being investigated. An azimuthally varying field (AVF) would be used to provide focusing forces in a magnetic field which increases radially to compensate for the relativistic increase in the mass of the protons. Further studies are being made of the practicability of using such an AVF cyclotron for injecting protons into an ~10-Gev proton synchrotron. Theoretical studies have been made, and operating electron models are being used to verify theoretical conclusions and design techniques. The theoretical work is being done in collaboration with the Physics Division.

### EXPERIMENTAL STUDIES

To confirm experimentally the theoretical studies of orbit dynamics in cyclotrons of the AVF type, an electron model was constructed, and a second model is being designed. The design and fabrication of the first model, Cyclotron Analogue I, was completed, and the machine is now being used in an investigation of factors affecting orbits and resonances and in an evaluation of theoretical studies and techniques of calculation. The conditions in the central region of the cyclotron which may initially affect properties of the beam are also being investigated in the 44-in. proton cyclotron.

#### Cyclotron Analogue I: Design and Fabrication

The principal design features of Cyclotron Analogue I (Fig. 22) are as follows:

| | |
|---|---|
| Central field | 40 gauss |
| Orbit frequency | 112 Mc/sec |
| Number of sectors | 4 |
| Beam radius, max | 12 in. |
| Magnetic field at maximum radius, av | 50 gauss |
| Energy, max | 200 kev |
| Energy, 3/2 resonance | 140 kev |

The hills and valleys of the four cycles of azimuthal variation are radial (no spiral). The field in the valleys approaches zero, and along the hills it approaches 100 gauss.

The magnetic field of the Analogue contains no ferromagnetic materials. A pair of large circular coils produces the main field. Layers of concentric coils are used in trimming the field. The fourfold azimuthal pattern is produced by eight pairs of wedge-shaped sector coils. All these coils are contained within the vacuum chamber. Two pairs of large square coils and one pair of circular coils are placed around the vacuum chamber; these Helmholtz-type coils are used to neutralize stray magnetic fields.

Since the Analogue magnet contained no magnetic materials, it was possible to calculate, by use of the Oracle, a coil design which would give the desired orbit properties. The problem to be solved was of a relatively high degree of complexity; 200 hr of computer time was spent in the development and testing of calculational techniques; 300 hr of computer time was required for the actual solution of the problem.

With the exact coil design calculated, considerable effort was expended to obtain maximum precision in coil fabrication so that a clear-cut test of the theory and the techniques of calculation could be obtained relatively unbeclouded by structural errors. A composite view of the coil structure of the Analogue is shown in Fig. 23. The layers of azimuthal windings (Fig. 24) used to produce the hills and valleys of the field were wound on an aluminum structure and cast in plastic. The coils are believed to be among the most precise ever fabricated. Detailed checks of the accuracy of the completed coils indicate an average error of no more than 0.005 in. in the placement of individual wires.

The radio-frequency accelerating system is of the single-dee type and is driven at a frequency of 112 Mc/sec by a crystal oscillator with power amplifier. The vacuum system is two-chambered; the various resin-impregnated coils are housed in a separate chamber which is kept at about $10^{-2}$ mm Hg. This chamber is separated by a thin metal membrane from the beam space, which is kept at a pressure of $10^{-6}$ mm Hg by a mercury diffusion pumping system. The double vacuum system reduces the possibility of contaminating the chamber containing the resonant system with vapors evolving

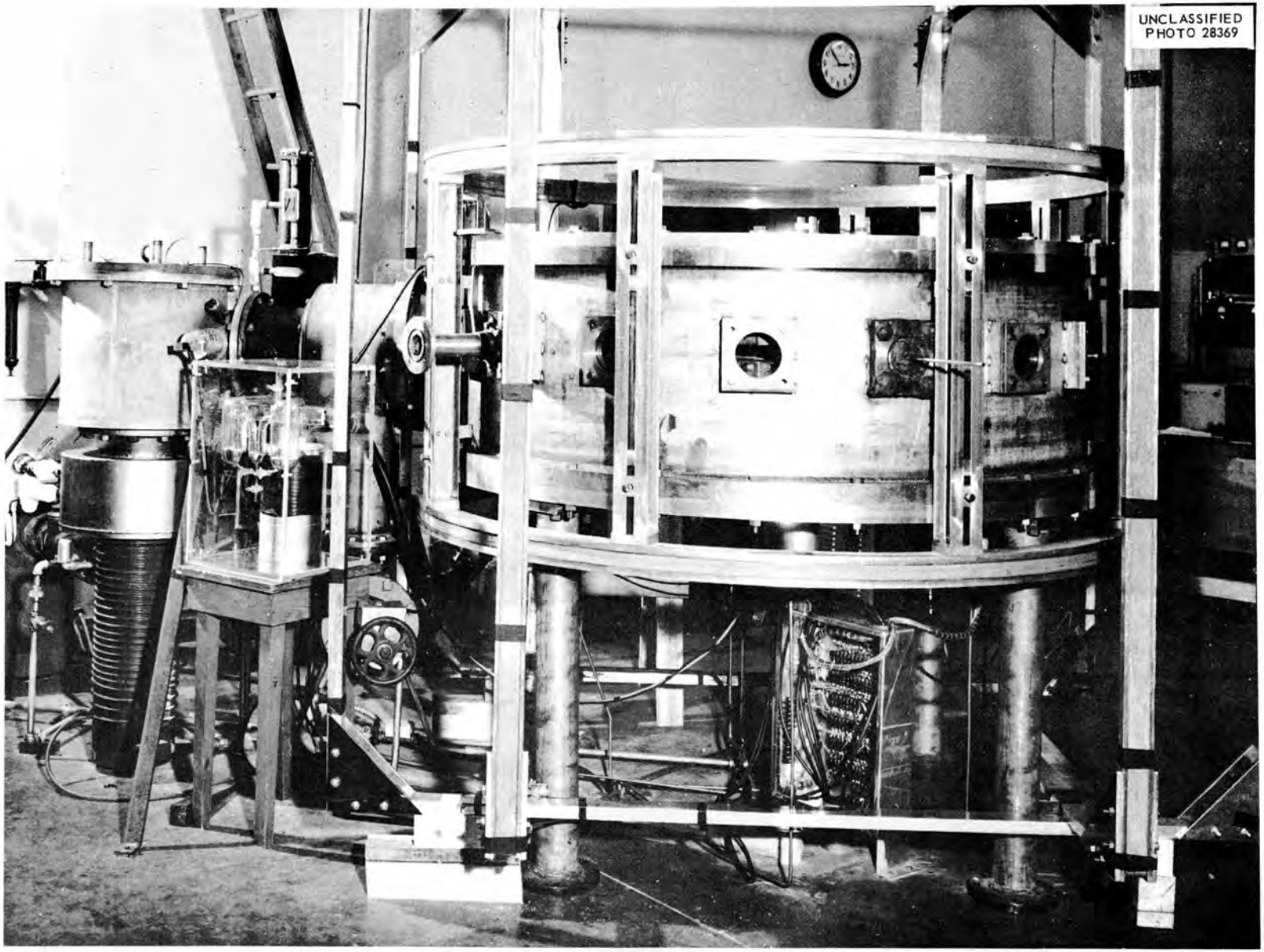


Fig. 22. Cyclotron Analogue I.

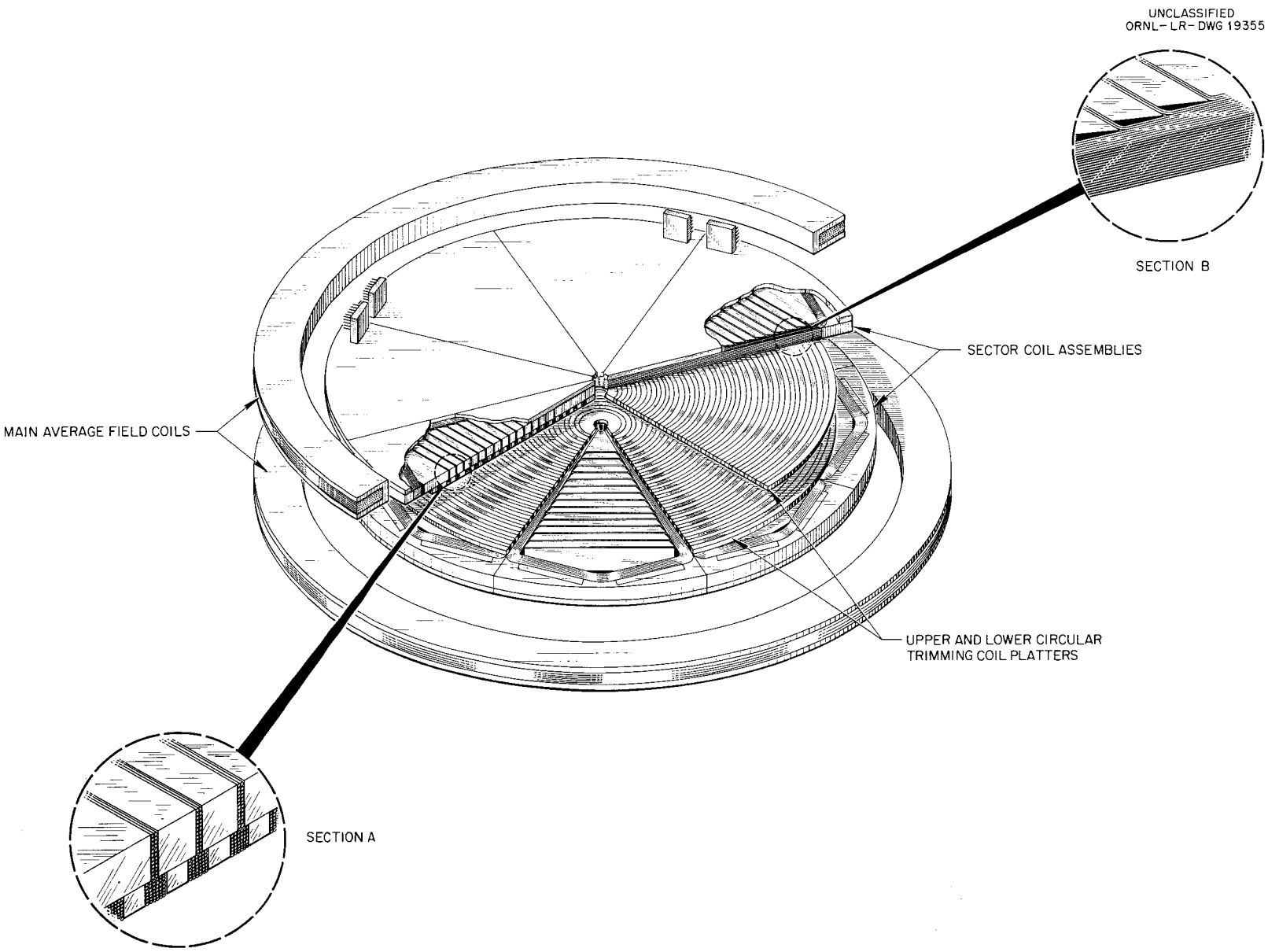


**Fig. 23. Coil Structure of Cyclotron Analogue I.**

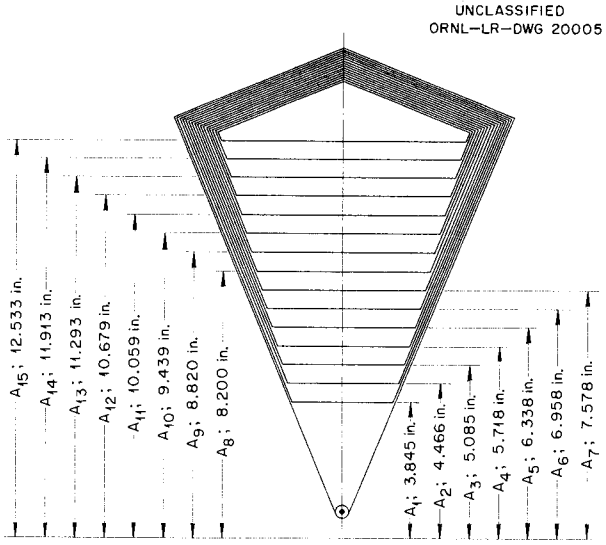


**Fig. 24. Sector Coil Configuration.**

from the resins used in bonding the coils. Power for the various coils is obtained from a group of electronically current-regulated d-c supplies. Currents are measured by inserting a high-precision standard resistor in series with each power supply and comparing the potential drop across the resistor with that of a standard cell by means of a precision potentiometer.

### Cyclotron Analogue I: Beam Measurements

A vertically focused beam was obtained in Analogue I on March 27, 1957. The subsequent measurement program has been concerned with experimental verification of calculable beam properties and observation of the passage of the beam through resonances.

Visual observation of the beam on fluorescent probes shows that the beam is vertically focused and goes through noticeable changes at radii corresponding to the resonances $\nu_r - \nu_z = 1$, $\nu_r = 4/3$, $\nu_r + \nu_z = 2$, and $\nu_r = 2$. Photographs of a fluorescent probe are shown in Fig. 25. In the top band, the probe was withdrawn while the camera shutter was open so that the envelope of the beam pattern can be observed. From right to left are the hot-wire electron source, a defining aperture, and the trace made on the fluorescent probe. The vertical striations are due to irregularities in the motion of the probe.

In the second band the probe is at a radius smaller than that for $\nu_r = 4/3$. There is only a small radial penetration of the beam on the probe.

In the third band the probe is beyond $\nu_r = 4/3$. There are two components of the beam: that which has blown up at the 4/3 resonance and has a very large penetration on the probe, and that which has passed through the resonance undisturbed and still has a small penetration on the probe.

The fourth band shows the probe at the approximate position of $\nu_r = 2$. The picture is qualitatively similar to that of the third band, except that the spill beam from the 4/3 resonance is narrower vertically.

The fifth band shows the probe beyond $\nu_r = 2$; the second component of the beam now shows radial blowup.

The three resonances inside $\nu_r = 2$ at which beam disturbances have been noted are $\nu_r - \nu_z = 1$, $\nu_r = 4/3$, and $\nu_r + \nu_z = 2$. The identification is based principally on radial position. In the case of $\nu_r - \nu_z = 1$, it was determined that increasing $\nu_z$ by increasing the sector-coil currents moves the position of the beam disturbance radially outward to a position of larger $\nu_r$, and that decreasing $\nu_z$ moves the disturbance to a smaller radius. This is the correct qualitative behavior of the resonance $\nu_r - \nu_z = 1$. At $\nu_r + \nu_z = 2$, the corresponding radial motion was too small to be observed with certainty for changes in $\nu_z$ small enough to get a beam at the large radius.

The effect of $\nu_r - \nu_z = 1$ is discernible in the top band of Fig. 25 as a vertical spreading of the beam, although it is slightly masked by the vertical striations in the picture; $\nu_r + \nu_z = 2$ is clearly discernible in the left half of the band.

All these resonances are nonlinear in nature and are observable only because of the large radial amplitudes which are present in the beam and which are due to conditions near the source. Large amplitudes are expected with the present source geometry because of asymmetries in the electric field around the source. The effect of altering this field is most easily observed in the pulsed-beam oscillograms of Fig. 26. The abscissa is time (2 $\mu$sec/div), and the ordinate is the intensity of the electron pulse arriving at a detector placed just inside the radius corresponding to $\nu_r = 2$. The source puts out a pulse of beam about 1 $\mu$sec in duration, starting at the left side of the coordinate grid. The first pulse, in time, is due to a beam which is accelerated through proper orbits up to $\nu_r = 4/3$ and then blows up radially.

UNCLASSIFIED
PHOTO 29952

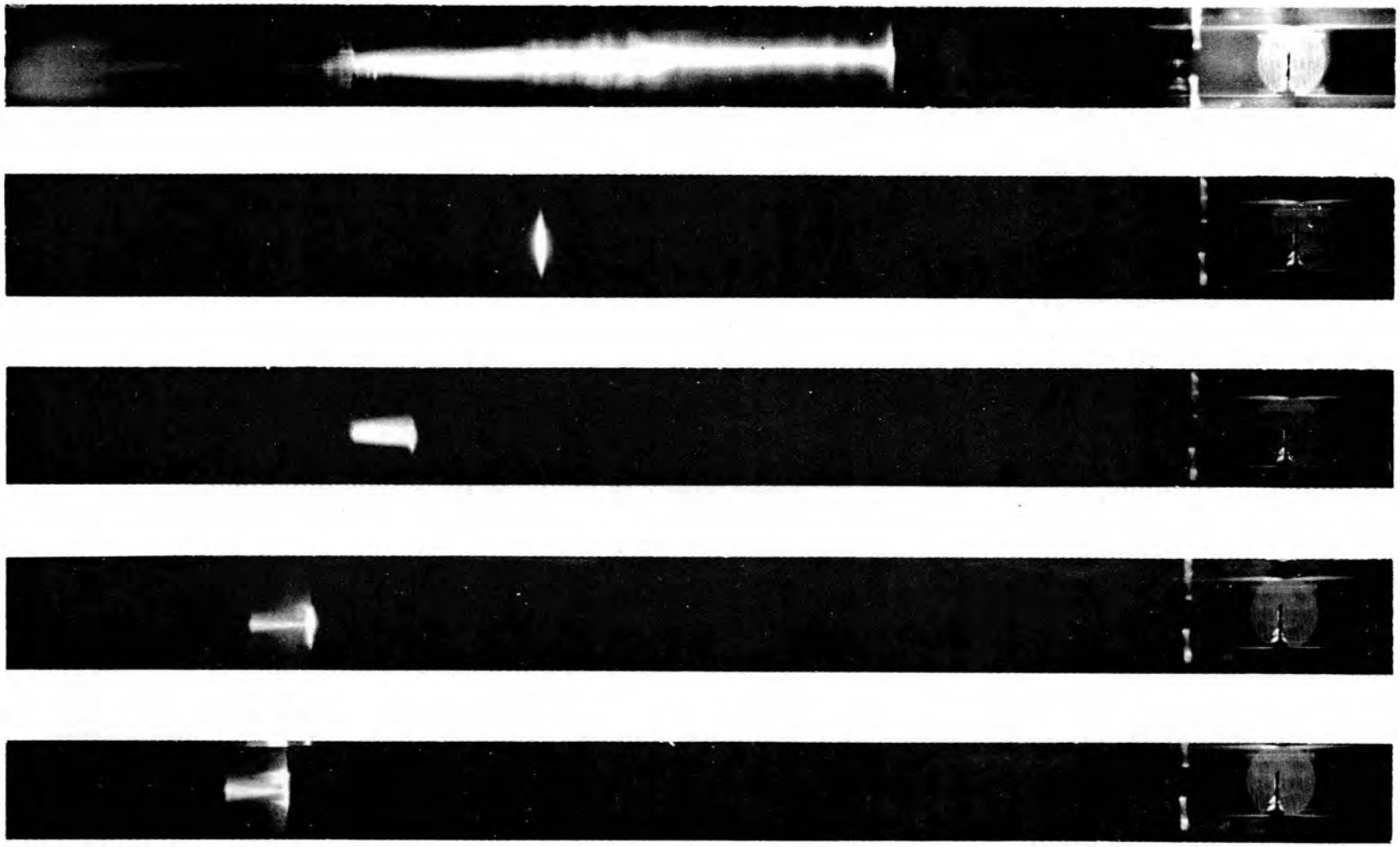

Fig. 25. Fluorescent Probe in Cyclotron Analogue I.

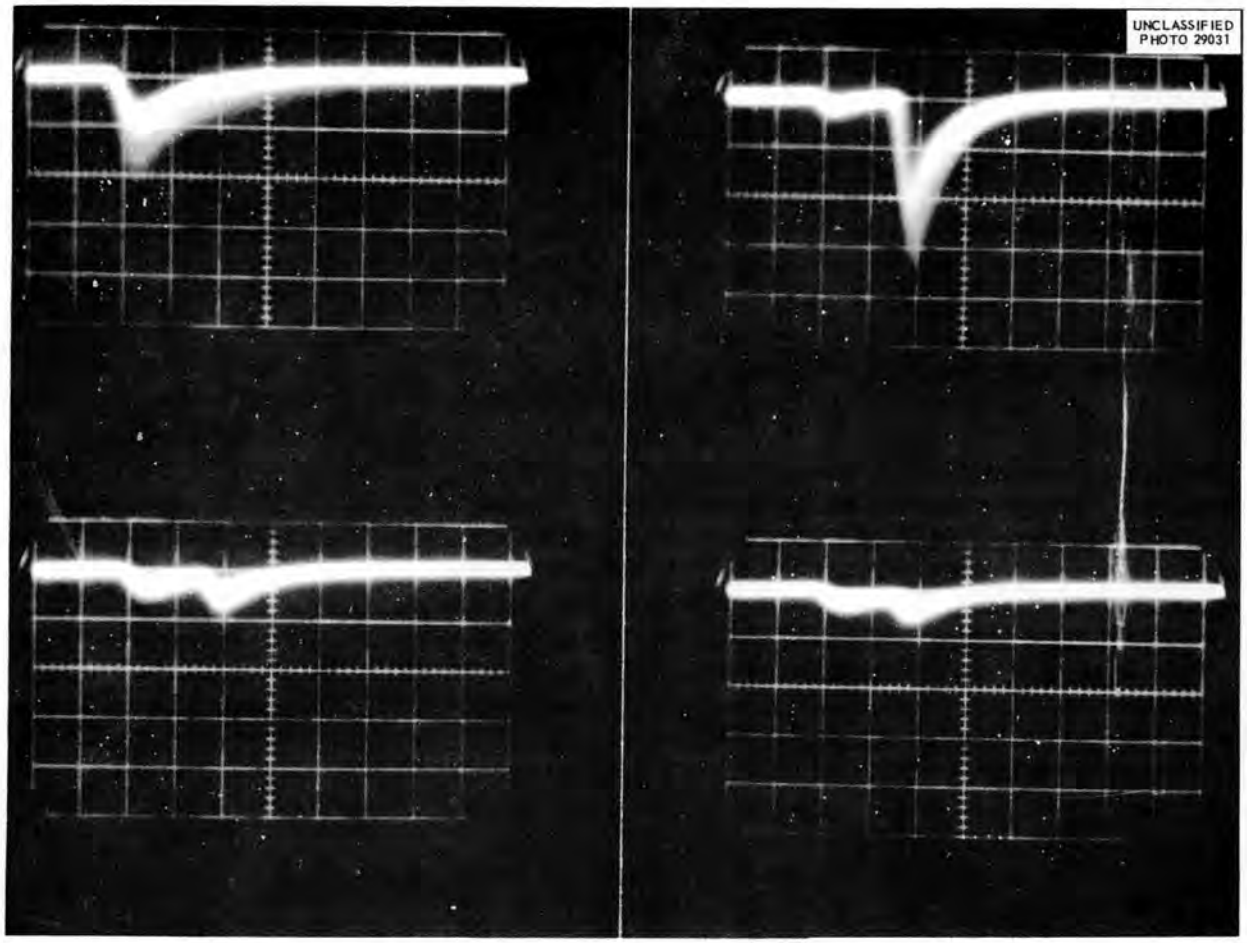


Fig. 26. Oscillograms of the Pulsed Beam in Analogue I. The time scale is 2 $\mu$sec/div.

The second pulse is due to a beam which does not blow up at $\nu_r = 4/3$ but which continues to be accelerated out to the detector probe.

The two oscillograms at the left show the effect of tuning the average field on the blowup of the beam. A reasonable interpretation is that in the case at the upper left, the field is mistuned so that the beam arrives at the 4/3 resonance in an unfavorable phase with respect to the accelerating voltage, goes through the resonance slowly, and then blows up radially. In the case at the lower left, the beam arrives in a more favorable phase and traverses the resonance rapidly enough so that part of the beam goes through. In the case at the upper right, the d-c bias on the source was adjusted to maximize the beam which goes through the resonance. The d-c bias affects the radial amplitudes in the beam leaving the source, and therefore affects the amount of the beam which blows up at the 4/3 resonance. At the lower right the bias was changed, with all other conditions kept constant.

The orbits in the Analogue are accurately isochronous, as can be inferred from measurements of threshold voltage and time of acceleration. A threshold dee voltage corresponding to an energy gain of 140 ev per turn was observed with the hot-wire electron source, and a maximum acceleration time of about 12 $\mu$sec was observed with a pulsed source. Both these measurements indicate that the beam can make about 1300 turns without being decelerated. Since the beam would be decelerated if it got $\frac{1}{4}$ turn out of phase with the dee voltage, the measurements indicate that the isochronism is good, on the average, to about 1 part in 5000.

The effective magnet current required to produce the average field for resonance differed from the calculated value by only 1 part in 4000.

Measurements of $\nu_r$ and $\nu_z$ were made with r-f knockout techniques. The results are shown in Figs. 27 and 28. Both measurements show some differences from the calculated values. The discrepancies in the $\nu_z$ measurement could be due to small flutter errors, since $\nu_z$ is very sensitive to the flutter value. The reason for the consistent discrepancy between the measured and the calculated values of $\nu_r$ is being sought.

### Cyclotron Analogue II: Design

Cyclotron Analogue II is a fixed-frequency electron cyclotron with an eight-sector azimuthally

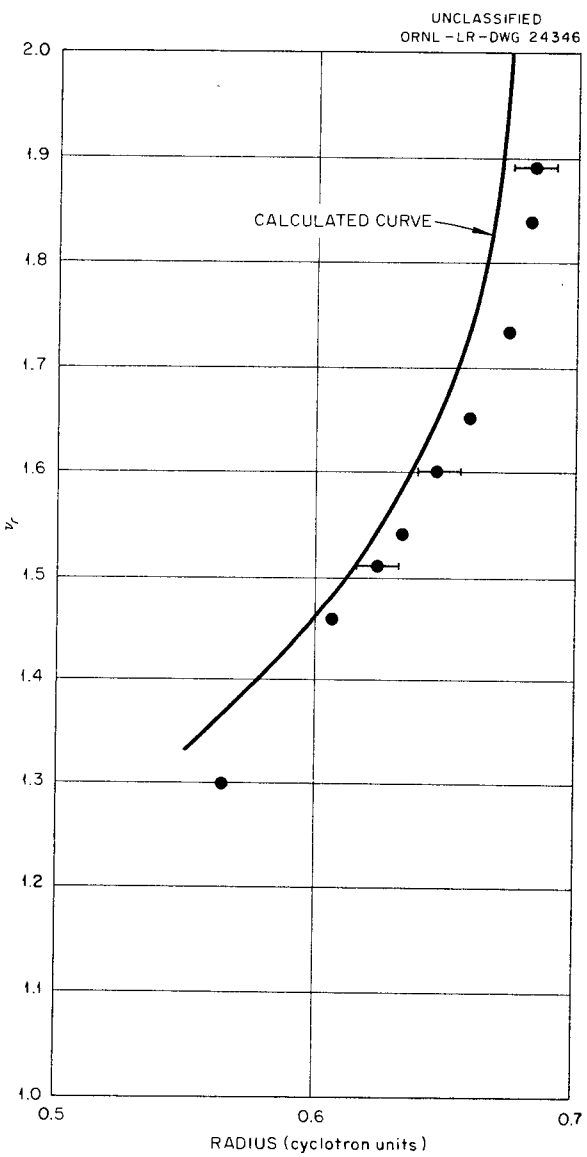


Fig. 27. $\nu_r$ as a Function of Radius.

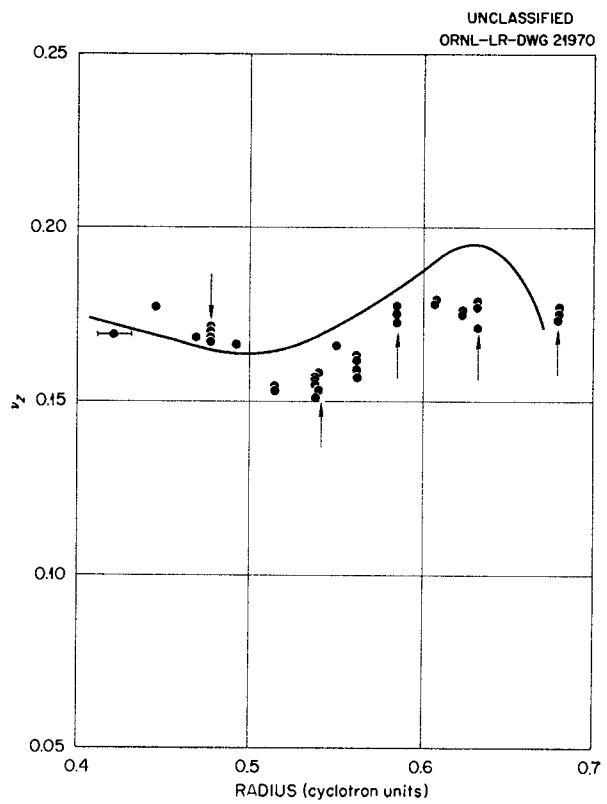


Fig. 28. $\nu_z$ as a Function of Radius.

varying magnetic field designed to focus the beam and to hold the period of the orbits constant to energies beyond the $\nu_r = 2/1$ resonance. The sectors will be spiraled to reduce the flutter requirement and to increase the particle energy at which the resonances occur. The magnetic field is given by the following equation:

$$B = \langle B \rangle \; [1 + f(r) \cos 8 (\theta - \xi)] \; ,$$

where

$B$ = total magnetic field in the median plane,
$\langle B \rangle$ = average field in median plane,
$f(r)$ = flutter,
$r$ = radius (cyclotron units),
$\theta$ = azimuth (radius),
$\xi$ = spiral angle (radians).

Here, $\xi = r^2$. That is, if $r = 1$ cyclotron unit, the sector will have spiraled through one radian.

The machine is to be a prototype of the AVF cyclotron with which it is proposed to inject ~900-Mev protons into an ~10-Gev synchrotron

ring. Therefore, the Analogue will be used primarily to study beam deflection; a method using the $\nu_r = 2/1$ and 8/4 resonances has been described elsewhere.[1] Since the higher the injection energy, the smaller the required synchrotron field and frequency variations, the magnetic field of the Analogue is being designed so that passage through the $\nu_r = 2/1$ resonance may also be studied.

The cyclotron unit for this machine has been selected as 16.000 in. This value then fixes the central field, $B_0$, as 41.926 gauss and the ion rotational frequency as 117.399 Mc/sec. The vertical focusing frequency, $\nu_z$, is to be held near 0.2 at all radii. The resonance diagram for this machine is shown in Fig. 29.

**Coil System.** – Like Analogue I, this machine is being designed with an air core for the magnetic field so that the exact field can be calculated for the coils. These calculations, which are quite lengthy, require the use of a digital computer. In order to obtain the average field to an accuracy of about 5 parts in $10^4$, the sector coils must be positioned radially to about ±0.003 in. Winding the coils with magnet wire or tape, and holding this tolerance on all dimensions, was found to be impractical because of the negative radius of curvature on one side of the spiral coils. Instead, the coils are being designed with but four turns in series and will carry a large current, 582 amp. One of the turns goes into the center of the machine (Fig. 30) and is shaped to produce the required flutter out to a radius of about $r = 0.75$. From $r = 0.75$ to 0.92, it was necessary to introduce three additional turns in order to fit the required flutter curve (Fig. 31). This design is based on the use of ¼-in.-square copper tubing as the conductor. A set of trimming coils is located between each pair of the main sector coils. At large radii these coils can change the flutter by 5%; the change is over 10% at smaller radii. The construction details of these coils have not been determined.

Four of the sector coils go nearer the center of the machine than do the other four. This four-sector field at the center allows the flutter to be increased at small radii so that vertical focusing can be obtained at a radius corresponding to less than that for 500-v electrons. For the eight-sector symmetry the corresponding energy would be 3 kev. Fourier analysis of the magnetic field shows that the four-sector, $4\theta$, component of field drops off rapidly with radius as the $8\theta$ field builds up; at the radius of the $\nu_r = 4/3$ resonance, the $4\theta$ component is less than 1 part in 140,000 of the $8\theta$ component.

The circular coils, which produce the average field not supplied by the sector coils, will be similar to those of Analogue I. The average field produced by the sector coils and the required average field, according to the smooth approximation, are shown in Fig. 32. The difference between these two curves gives the average field which must be produced by the circular coils. The vertical spacing of the coils and the dees is shown in Fig. 33.

**Digital Computer Codes.** – All the coil design work is based on computations made with the Oracle. The codes written for this purpose are

[1] M. M. Gordon and T. A. Welton, *Phys. Semiann. Prog. Rep. Sept. 10, 1957*, ORNL-2430, p 6.

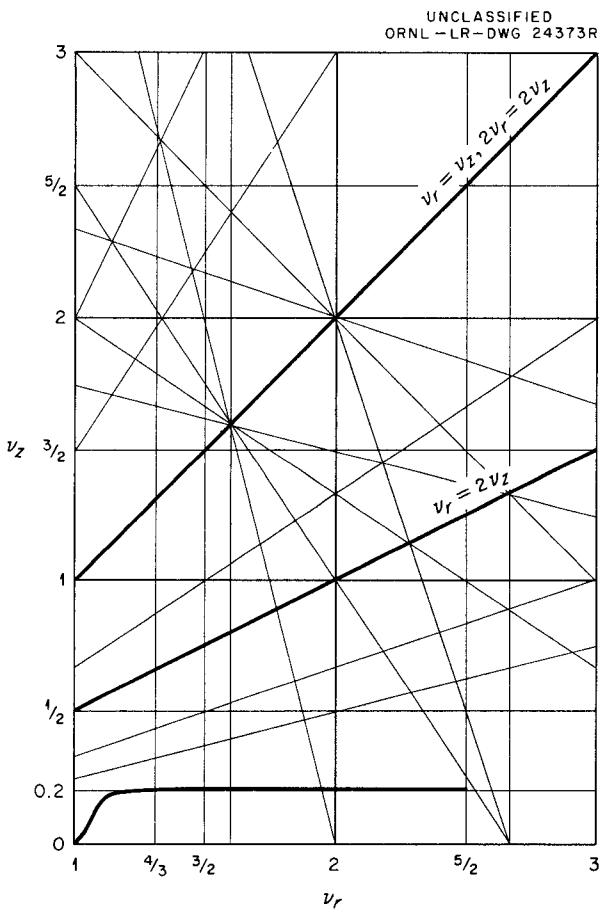


**Fig. 29. Resonance Diagram, Analogue II.**

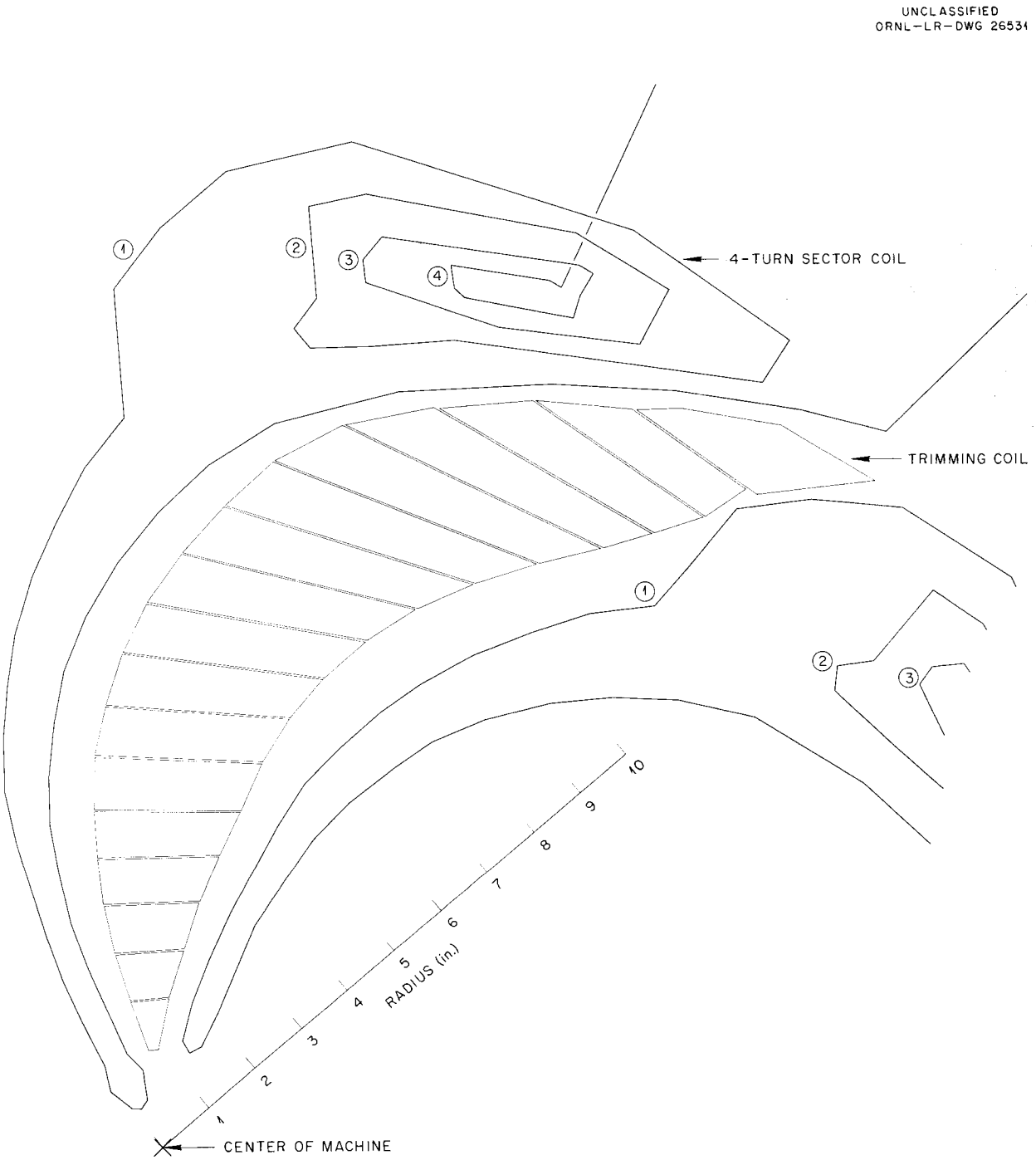


**Fig. 30. Sector Coils, Analogue II.**

listed below, with a brief description of each:

1. The Spiral Coil Code computes the magnetic field of any shape of coil that can be specified in terms of short, straight segments. This code was used in computing the field of the sector coils.

2. The Flutter Fitting Code uses the relative fields from a set of azimuthal coils to compute the relative current necessary in each of the coils to produce a given flutter. The method is that of successive approximations with a least-squares fit.

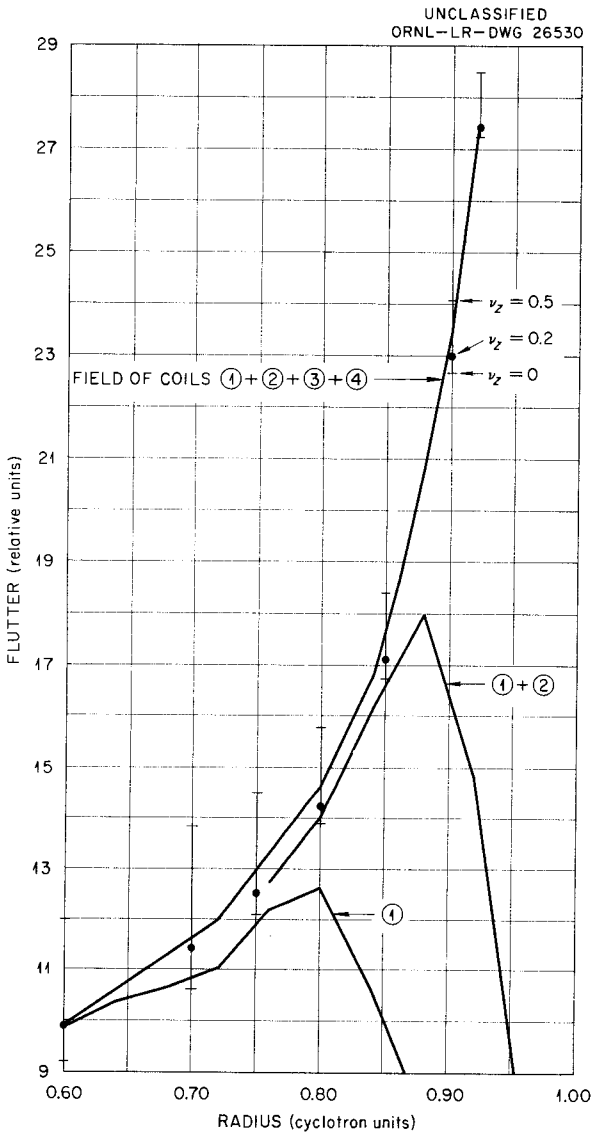


**Fig. 31. Flutter Field Obtained with Four-Turn Sector Coils, Analogue II.**

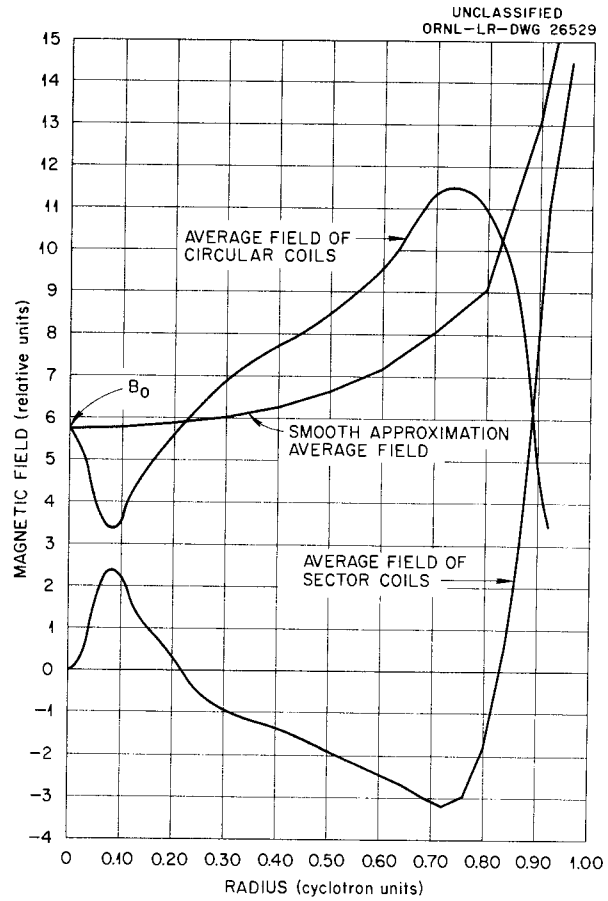


**Fig. 32. Average Fields, Analogue II.**

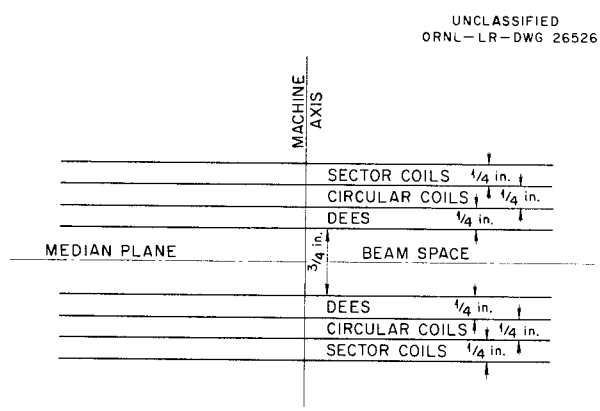


**Fig. 33. Vertical Spacing of Dees and Coils in Analogue II.**

3. The Preparation Code adds an average field to the fields given by the Flutter Fitting Code, then computes the radial derivatives and arranges this data in a special order for use in the Orbit Code. The Preparation Code also prepares the parameters for the Orbit Code and runs the Orbit Code and the Iteration Code automatically.

4. The Orbit Code computes the orbit characteristics of the particles at equal momentum steps, using a 16-step Runga-Kutta integration formula upon the data provided by the Preparation Code. The output consists of $\nu_r$ and $\nu_z$, the radial and vertical focusing frequencies; $T$, the time of each orbit; $\langle r \rangle$, the average radius of each orbit; and $p$, the momentum for each orbit.

5. The Iteration Code checks the times at each momentum step given in the output of the Orbit Code. If they are constant, it stops; if they are not, it computes a new average field and inserts this into the Preparation Code. This process is repeated until the times are constant.

6. The Circular Coil Codes compute the relative fields of the circular coils and then determine the current required in each circular coil to give the best least-squares fit to the average field, as obtained in the last step of the Iteration and Preparation Codes.

**R-F System.** – More than two accelerations per revolution must be used to prevent any cos $2\theta$ fields from arising in the r-f system. Four have been selected because of symmetry with the eight-sector magnetic field and for simplicity of the r-f electrodes. There will be two 90-deg dees and two 90-deg dummy dees (Fig. 34). The space inside the dummy electrodes offers a maximum vertical height for probes. The 90-deg dees must be driven at double the ion rotation frequency of 234.799 Mc/sec to prevent any cos $2\theta$ voltage from affecting particles which are not phased exactly with the r-f peak voltage.

To determine the shape of the electrode, that is, the shorting bar position and shape, and the shape of the edge between the shorting bar and the lip, a code written for the Oracle is being tested. The rather tedious job of finding and tracing equipotentials and current flow lines in the electrodes made this code necessary. The goal is to find the electrode configuration which is practical to build and which still has a sufficient flat-voltage–standing-wave ratio along the lip. A set of electrodes was constructed, and the frequency and voltage standing wave along the dee

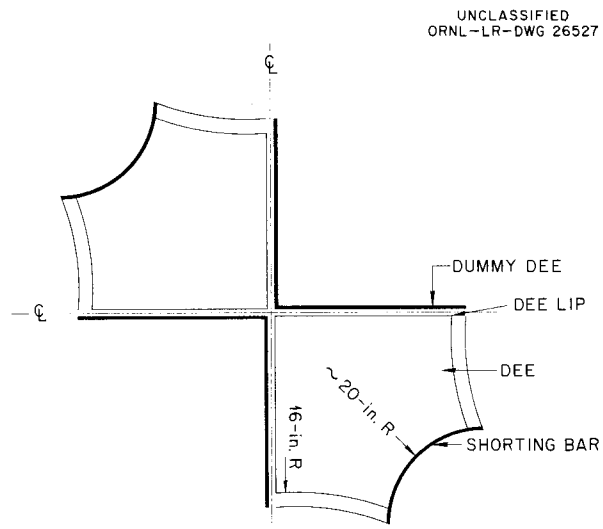


**Fig. 34. Ninety-Degree Dees, Analogue II.**

lips was measured. The results of one measurement gave the results shown in Fig. 35; the $Q$ of this resonator was 678.

One requirement for an efficient deflection system is that the accelerating voltage be held constant to about 1 part in $10^4$; the beam can then be positioned precisely for the energy at which deflection is to begin. Design work is in progress for this regulator system, along with the power amplifier for Analogue II.

**Conversion of Analogue I.** – As many of the Analogue I components as possible are being used for the Analogue II. The complete vacuum system can be used as it is. To improve operation, however, Freon baffles were ordered which will replace the two dry-ice traps in the roughing lines. The power supplies, of course, will be used. Also, most of the r-f transmitter will be re-used. Since the coil system will be quite different from that in Analogue I, the inner vacuum system and the coil support plates must be replaced. The power supply for furnishing the high current to the sector coils will be designed; it must be current-regulated and ripple-free to about 1 part in $10^4$.

### Beam Studies with the ORNL 44-Inch Cyclotron

In the region close to the center of cyclotrons, the magnetic focusing forces of either the conventional or of the AVF type are effectively zero over a region with a diameter of about twice the

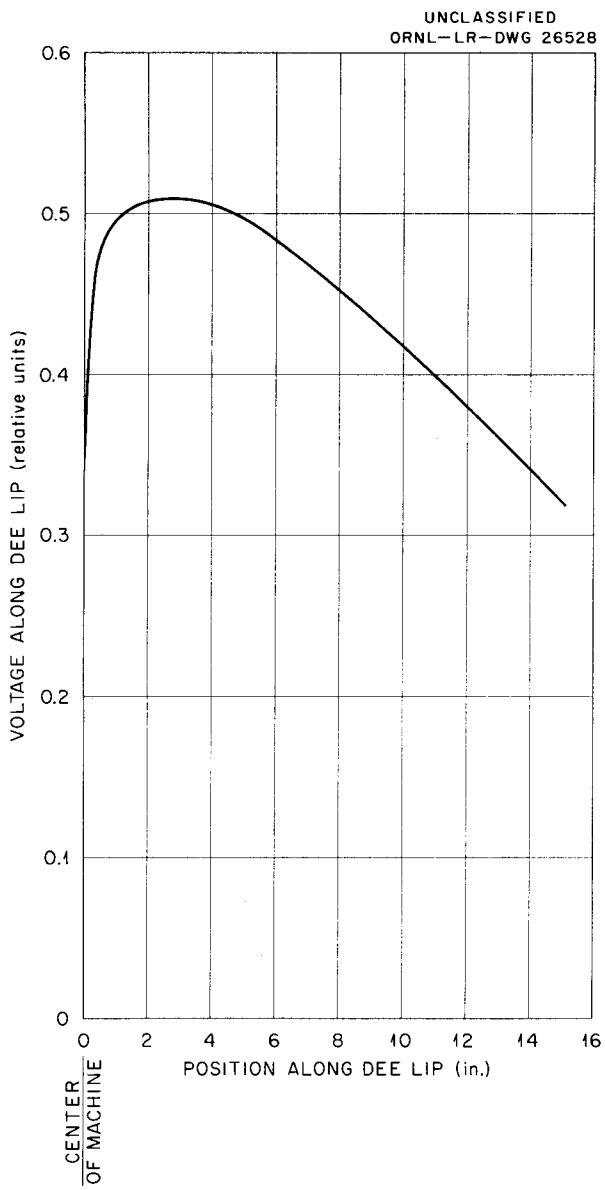


**Fig. 35. Voltage Standing Wave Along Dee Lip, Analogue II.**

vertical gap of the magnet. Properties of the beam ultimately obtained at the outside of the cyclotron are largely determined in this central region. Experimental studies are being performed to explore mechanisms for utilizing electrical forces at the center of the cyclotron in order to maintain control over particle motion. The 44-in. cyclotron is being used in these investigations.

Two main types of mechanisms are being explored. The first employs various schemes for causing the particles to cross the accelerating gap after the peak of the r-f voltage so that, due to the transit time across the gap, the electric field is stronger in the first or focusing half of the gap than in the defocusing half, with a net gain in focusing. The second type of mechanism involves the use of grid-type structures on the entering edge of the dees in order to shape the electric field in a fashion which eliminates the defocusing half of the gap. For conventional dee voltages (50 to 100 kv), individual turns of the beam in the central region of a cyclotron are very markedly separated. This makes it possible to place the grids between turns, thereby avoiding loss of beam due to collision with the grid structure.

Experiments with the grid-type structures have indicated rather strong focusing effects which, therefore, allow large beams to be obtained in considerably smaller magnet gaps. Experiments exploring the transit-time type of focusing have uncovered a number of difficulties which, at present, make that line of approach appear less promising.

## HIGH-ENERGY ACCELERATOR DESIGN

Major progress has been made in the conception and planning of an ultrahigh-energy accelerator especially suited to the needs of physicists working at Oak Ridge and at universities of the South. A committee consisting of members of ORNL and eight southern universities spent a substantial amount of time reviewing possible accelerators or combinations of accelerators. A document[2] summarizing the conclusions of this study and describing results of the Laboratory's associated experimental and theoretical investigations was transmitted to the AEC. The proposed Southern Regional Accelerator (SRA) consists of a 900-Mev AVF fixed-frequency cyclotron which injects into a rapidly pulsed (~60 cps) proton synchrotron of 8 or 12 Gev energy. Conceptual designs for proposed installations are shown in Figs. 36 and 37.

In August and in September of 1957, further information regarding the accelerator was presented to an accelerator subcommittee of the AEC's General Advisory Committee. Revised and

[2] F. T. Howard *et al.*, (eds.), *Proposal for a Southern Regional Accelerator*, ORNL CF-57-4-30 (April 1957).

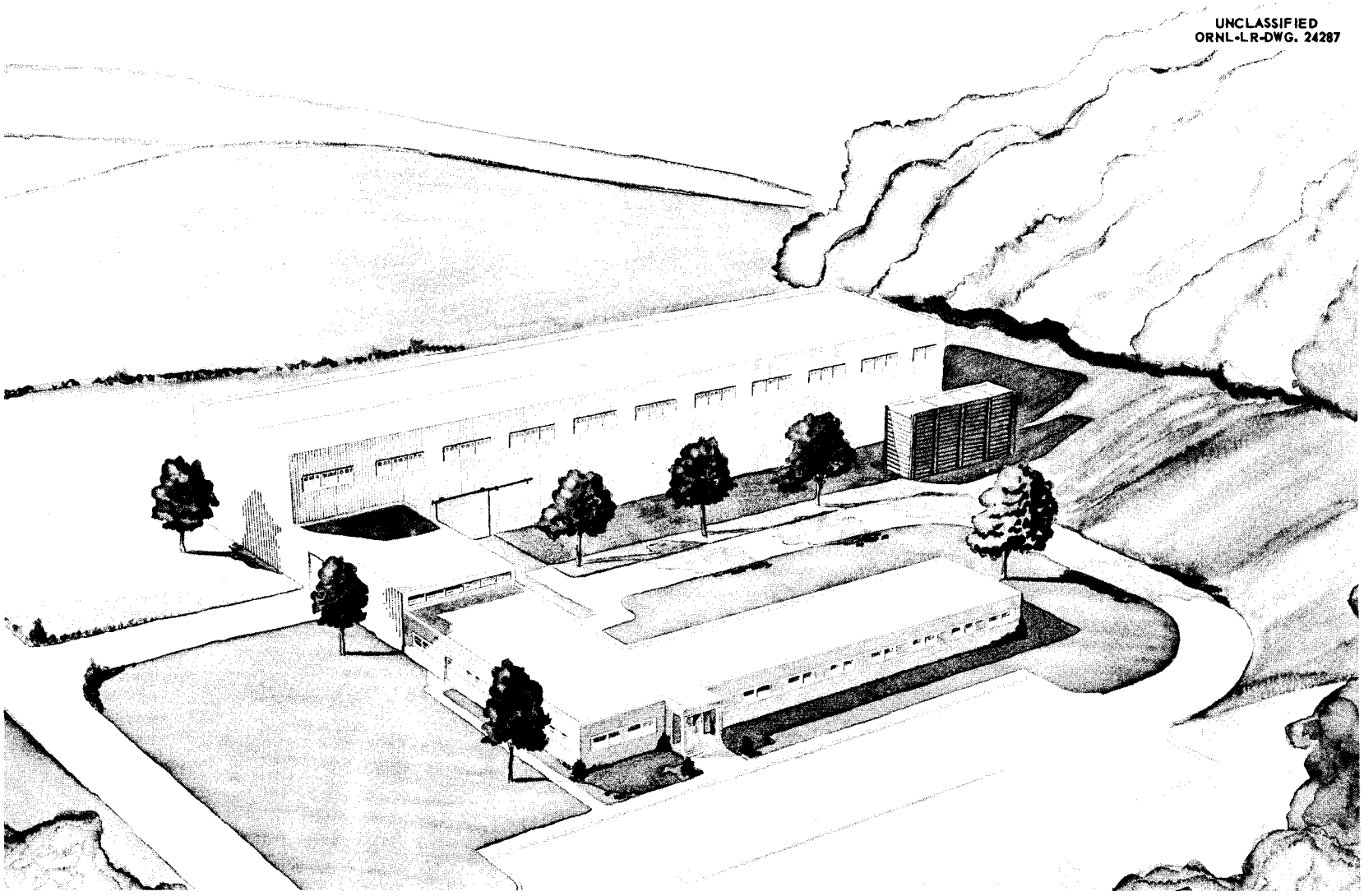


Fig. 36. Building for Proposed 900-Mev Cyclotron and Laboratory.

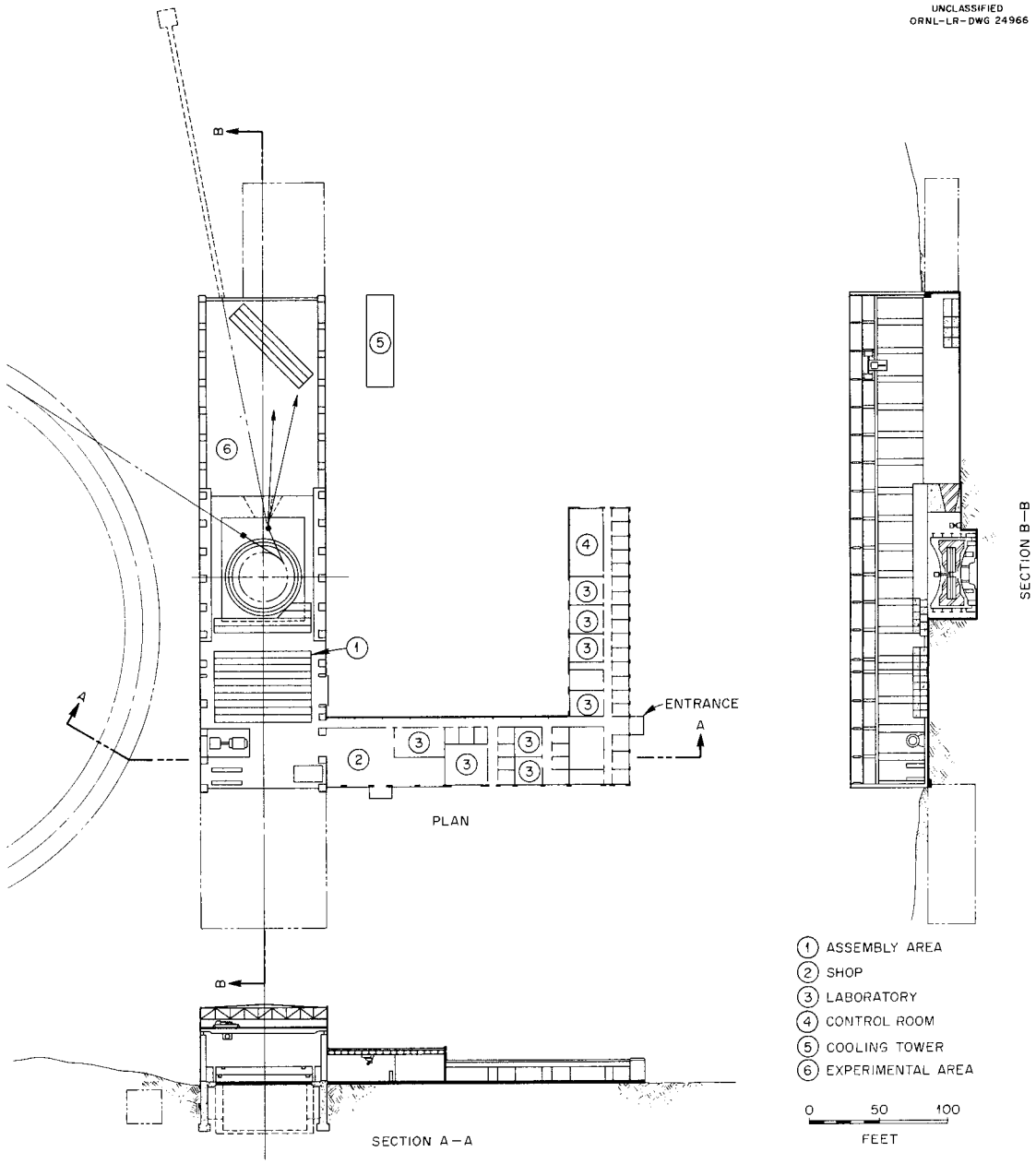


**Fig. 37. Plan and Section of Proposed Installation for the Southern Regional Accelerator.**

improved cost estimates were prepared and transmitted to the AEC early in October. Pertinent excerpts from these documents are included in the following description.

Major attention has been given to the 900-Mev cyclotron; proposed specifications for this machine are given in Table 2. Preliminary specifications for the synchrotron ring are outlined in Table 3. Cost estimates for the cyclotron are itemized in Table 4, and the estimated over-all costs for the cyclotron installation and its operation are summarized in Table 5. The experimental development work with the Cyclotron Analogue has been described above. The results of design studies of the major features of the cyclotron are described in the following sections.

**Table 2. Specifications for Proposed 900-Mev Cyclotron**

| General Features | |
|---|---|
| Design energy (protons) | 900 Mev |
| Beam radius, max | 17.1 ft |
| Orbital frequency | 8.25 Mc/sec |
| Azimuthal sectors | 8 |
| Volume of vacuum system | 26,300 $ft^3$ |
| Ion source, type | Hot cathode |
| Beam extraction type | Integral resonance (Le Couteur) |
| Duty cycle | Continuous or pulsed (see beam properties) |

| Magnetic Field | |
|---|---|
| Gap, max | 8 in. |
| Gap, min | 6 in. |
| Strength, center, av | 5400 gauss |
| Strength, outside, av | 10,600 gauss |
| Strength, max | 22,000 gauss |
| Magnet power | 4000 kw |
| Magnet weight | 2600 tons |
| Magnet winding | 150 tons |
| Cooling | Water |

| R-F System | |
|---|---|
| Oscillator | Master oscillator; power amplifier |
| Pre-exciter | None |
| D-C input, max | 2000 kw |
| R-F output, max | 1000 kw |
| Accelerator voltage, per cavity, peak | 250 kv |
| Accelerator cavities | 4 |
| Accelerator voltage, per turn, peak | 1 Mev |

| Beam Properties | |
|---|---|
| For Injection | |
| Injection beam pulse length | 100 $\mu$sec |
| Injected beam pulse | $10^{12}$ protons |
| Repetition rate | 60 pulses/sec |
| Injected current, peak | 10 ma |
| Injected current, av | 60 $\mu$a |
| Injected beam power | 55 kw |
| For Independent Research | |
| Duty cycle | Continuous |
| Repetition rate | $10^7$ r-f pulses/sec |
| R-F pulse length | $10^{-8}$ sec |
| Beam intensity | $6 \times 10^7$ protons/r-f pulse |
| Average beam current | 100 $\mu$a |
| Beam power | 90 kw |

## Conceptual Design of the Magnet and Vacuum System

The following is a general description of the conceptual design and suggested method of assembling the 900-Mev AVF cyclotron. The final design can come only after model magnet tests and many other tests of the various design features.

The magnet is designed with eight sectors. The steel cores of the sectors are essentially rectangular in cross section, and are tapered and spiraled out from the center. Spiraling the sectors reduces the flutter requirement and results in a smaller machine for the desired energy. In order to achieve sufficient flutter to produce the desired focusing, the magnetic gap must be small. A gap of 6 in. at the outer edge was chosen, leaving a clear gap of 4 in. between the pole-face windings. With this gap, the required tolerance for aligning the pole faces with the median plane is ±0.003 in.

Since the gap is small, a system of accelerating with cavities perpendicular to the median plane has been adopted. Two r-f cavities are inserted vertically in the space between adjacent sectors; they cross at the center of the machine (Fig. 38). Thus the magnet sectors are not structurally connected at the center of the machine.

**Magnet Design.** – The maximum magnetic field, which occurs at the outer edge, was chosen as 22 kilogauss. This value decreases to 5.4 kilogauss at the center. The field is produced by eight pairs of coils, one pair on each sector. All turns of each coil pass around the outermost edge

of the sector core; the windings then pass inward along the vertical side of the sector and, at selected intervals, cross the pole face for the return, as shown in Figs. 38 and 39. At a current density of 2000 amp/in.$^2$, approximately 150 tons of copper would be required, and the magnet power requirements would be approximately 3 Mw. In order to provide for fine trimming of the field, small coils are wound in with the sector coils.

Each sector is supported and positioned in the magnet by an inner yoke which extends inward from the outer yoke. Where enough space is allowed for cavities between adjacent yokes, the

**Table 3. Tentative Specifications for Synchrotron Ring**

| | |
|---|---|
| **General Features** | |
| Design energy (protons) | 8 Gev |
| Orbit radius, max | 122 ft |
| Injector | 900-Mev cyclotron |
| Orbital frequency, at injection | 1.095 Mc/sec |
| Orbital frequency, at extraction | 1.270 Mc/sec |
| Acceleration time | 1/120 sec |
| Repetition rate | 60 pulses/sec |
| **Magnetic Field** | |
| Type of field | Alternating gradient |
| Number of sectors | 30 to 36 |
| Magnet current | Pulsed, 60 cps, d-c bias |
| Magnetic field, max | 10,000 gauss |
| **R-F System** | |
| Frequency modulation | 49.3 to 58.9 Mc/sec |
| Accelerator cavities | 2 to 4 |
| Energy gain, max | 2.0 Mev/turn |
| **Beam Properties** | |
| Pulse length, variable | 10 $\mu$sec to 1 msec |
| Proton current | $10^{11}$ to $10^{12}$ protons/pulse |
| Proton current, av | 1 to 10 $\mu$a |
| Beam power | 8 to 80 kw |

**Table 4. Cost Estimates for Proposed 900-Mev Cyclotron**

| | |
|---|---|
| Magnet iron | $1,600,000 |
| Magnet coils | 650,000 |
| Magnet power supplies | 500,000 |
| R-F cavities | 200,000 |
| R-F supplies | 390,000 |
| D-C supplies for r-f systems | 225,000 |
| Vacuum tank | 125,000 |
| Vacuum system | 240,000 |
| Beam deflection and focusing apparatus | 150,000 |
| Ion source, including supplies | 15,000 |
| Miscellaneous controls, instrumentation, safety radiation detection equipment | 100,000 |
| | $4,195,000 |
| Contingencies, 10% | 420,000 |
| Engineering, 15% | 700,000 |
| Total | $5,315,000 |

**Table 5. Summary of Cost Estimates for 900-Mev Cyclotron Installation and Operation**

| | | |
|---|---|---|
| 900-Mev cyclotron | $4,195,000 | |
| Shielding | 1,240,000 | |
| Building | 1,915,000 | |
| Site development, utilities, etc. | 924,000 | |
| | | $ 8,274,000 |
| Contingencies | 828,000 | |
| Engineering | 1,149,000 | |
| | $1,977,000 | |
| | | $10,251,000 |
| Development for cyclotron | 2,500,000 | |
| Operating costs, per year | 770,000 | |
| Research costs, per year | 1,000,000 | |

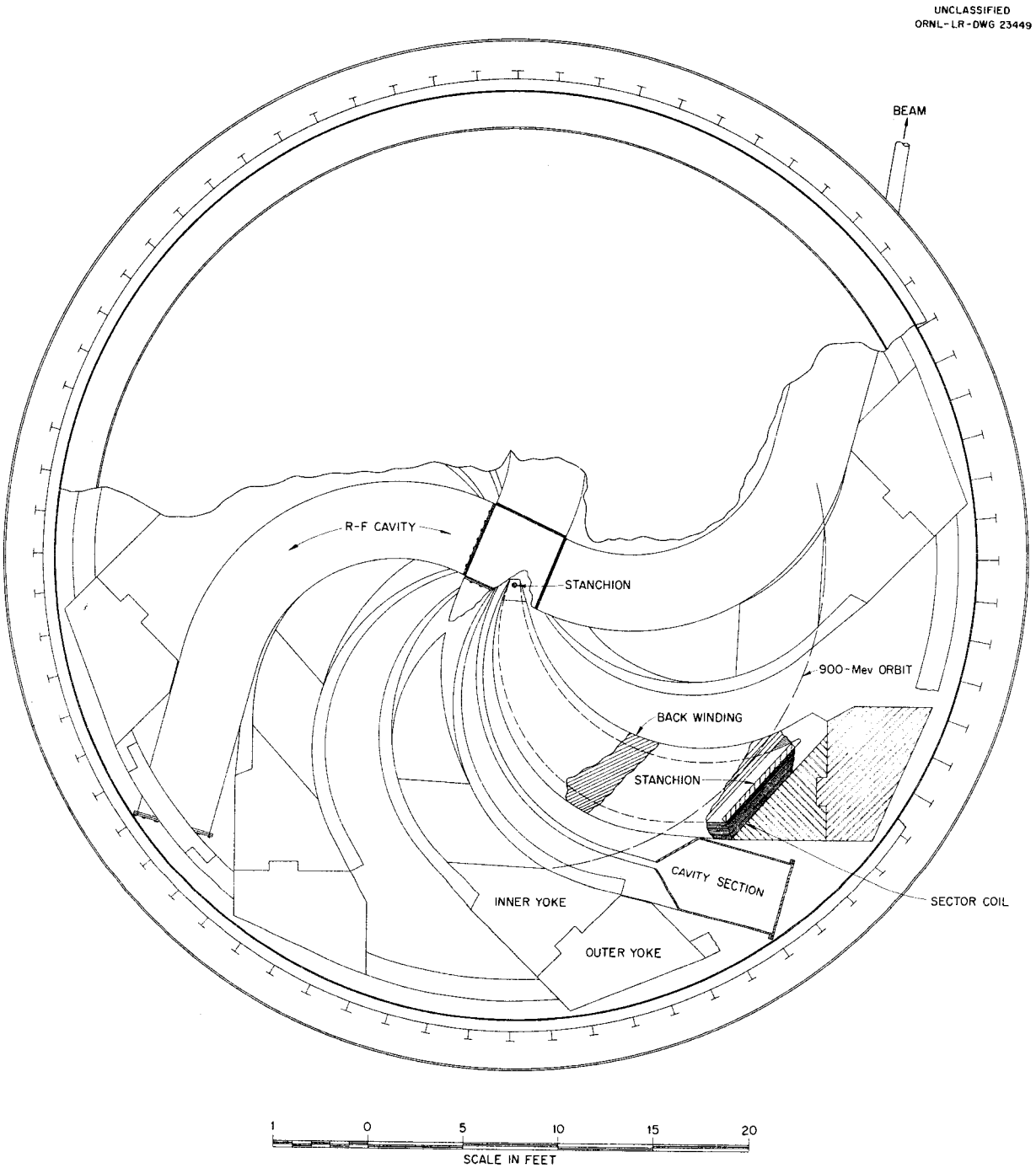


**Fig. 38. AVF Cyclotron, Plan and Section.**

UNCLASSIFIED
ORNL-LR-DWG 24348

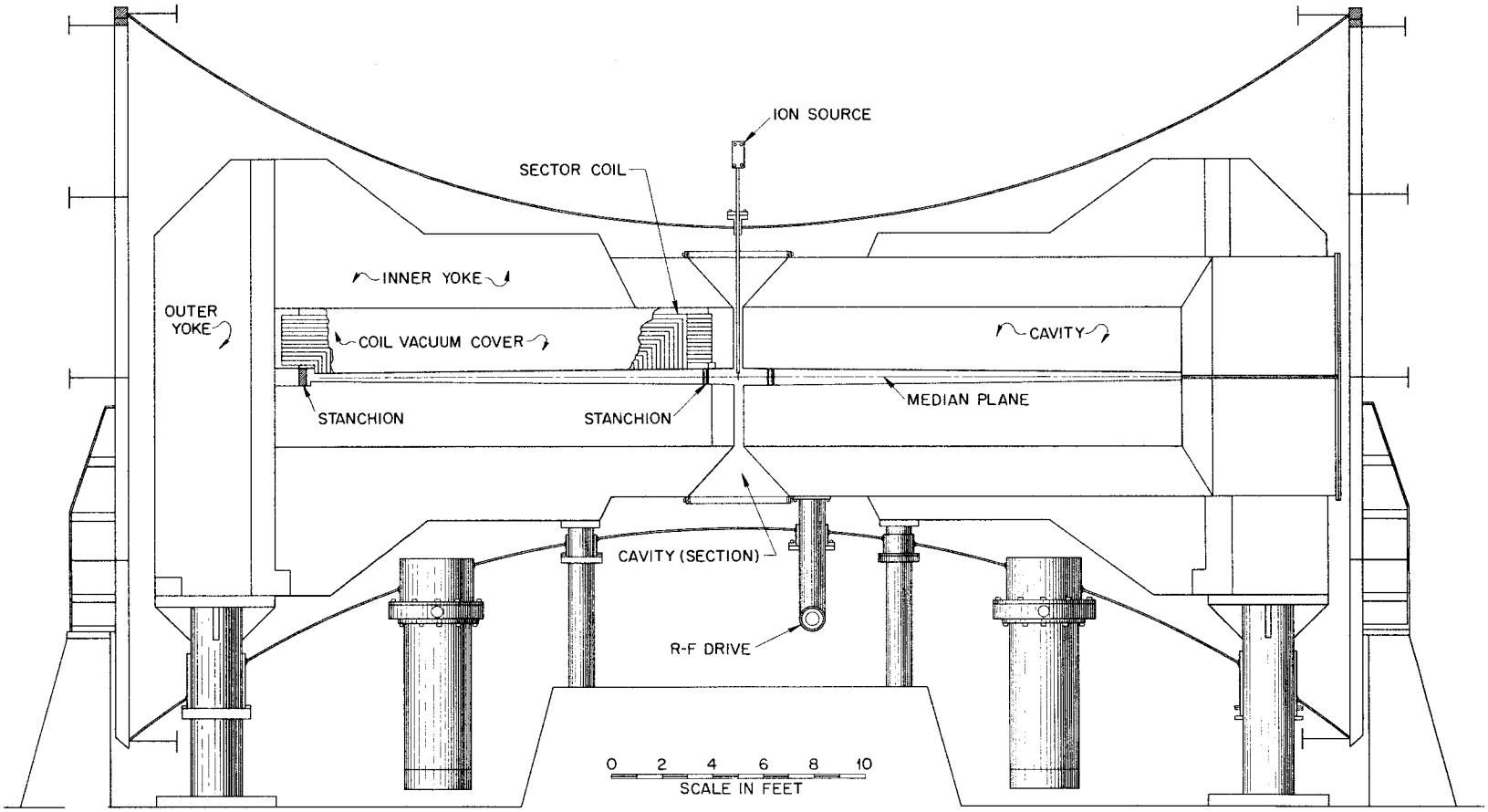


**Fig. 39. AVF Cyclotron, Vertical Section.**

height of the yoke is determined by the average flux density the yoke is to carry. The maximum yoke height is 6 ft at the 17.1-ft radius. This is tapered down to 3 ft, as shown in Fig. 39. The outer yokes serve as the main base for aligning and supporting the sectors, in addition to carrying the flux. These yokes are 17½ ft high, and each yoke has a cross section of about 40 $ft^2$. The final size will be determined by model magnet studies.

The magnet is supported at the outer edge by eight large posts connected by a ring of girders in order to form a rigid structure. In the central area the sectors are supported by four posts capped by a heavy girder in order to provide a support platform. These posts pass through the bottom vacuum chamber and are sealed in a manner that allows movement. All these posts are to be temperature-regulated so that relative expansion can be controlled.

**Magnet Assembly.** – The components of this large structure must be designed especially with the problems of assembly in mind. The coils are wound on the sector cores separately, then each sector is attached to a yoke extension or inner yoke. The coil is then enclosed in a stainless steel case which forms a vacuum tank and which is pumped on separately. This prefabricated sector is installed or removed as a unit. Since the cyclotron components are large and heavy, the assembly will be done from overhead. To permit this, the vacuum tank is provided with a removable upper head. The outer yokes are individually lowered into position, aligned, and formed into a rigid circular structure by ring girders. Next the eight lower sectors are fastened to the outer yokes and are aligned with jacks mounted from the central support platform.

Due to a large voltage gain per turn, and to the consequent large orbit separation near the center, it is possible to use stanchions in the magnet gap to prevent deflection of the poles and to maintain the critical gap tolerance. Stanchions are also used outside the maximum beam orbit on each sector. The upper yokes and sectors are individually lowered and fastened in place, with the stanchions being used as precise spacers. The cavities can then be installed and aligned with the gap.

**Vacuum System Design.** – Because of the magnet gap tolerance, ±0.006 in. over an area within a 17.1-ft radius, no distortion of the poles due to vacuum loading can be tolerated. For this reason the vacuum chamber completely encloses the magnet and is independently supported.

The tank is 50 ft in diameter by 28 ft in height and weighs approximately 90 tons. The net volume of the main vacuum chamber is 26,300 $ft^3$ or 745,000 liters. In addition, each sector coil is enclosed in a separate vacuum system; this excludes insulation, hoses, and other organic materials from the main high-vacuum chamber.

The tank walls are constructed from ½-in. plate reinforced with ring girders and longitudinal stiffeners. Appropriate reinforcing is used around the many openings in the tank wall and heads. The two heads are dished in rather than out in order to produce tensile stresses under vacuum in preference to compressive stresses. They are made of ½-in.-thick steel, thickened to ¾ in. near the edge. The top head is removable and is sealed with a gasket.

This very large vacuum chamber presents special pumping problems. A thorough study being made of all known types and sizes of vacuum pumps has revealed two types of large-capacity and reasonably priced roughing pumps. The first is a six-stage steam ejector pump with a capacity of 100,000 cfm at a pressure of $10^{-2}$ mm Hg. The second is a positive-displacement type of Roots blower which has capacities to 5000 cfm at $1 \times 10^{-3}$ mm Hg.

The investigation also includes large 20,000- to 40,000-liter/sec oil diffusion pumps with extremely low backstreaming rates. Their design eliminates the need for refrigerated baffles, thereby eliminating the large pumping-speed losses inherent with baffles. Another type of high-vacuum pump being considered is the Evapor-ion pump. This type is different from oil diffusion pumps in that the pumping action is principally by gettering, and by ionization for the inert gases. At present these pumps are available in only the relatively small capacity of 2000 liters/sec.

The final selection of pumping components will be made after the results of this study are evaluated and upon completion of a testing program.

### Design Study of R-F System

The r-f accelerating system for the 900-Mev cyclotron will consist of two cavities oriented at right angles to each other, as shown in Figs. 38 and

39. These cavities will be driven by two power amplifiers; a crystal oscillator will be used to determine the frequency.

The cavity voltage must not be zero at any radius and must be symmetrical about the center of the machine. The simplest mode that will give a suitable accelerating voltage in a rectangular cavity is the $TE_{011}$. For this mode, with rectangular coordinates parallel to the edges at one corner of the cavity, the electric field will have only one direction, say $E_y$. The magnetic field will then have $x$ and $z$ components, circulating about $E_y$. The voltage standing wave will be one-half sine wave as a function of $x$ and/or $z$.

Since the particle rotates through 180 deg from one cavity side to the other, the r-f must go through an odd multiple of 180 deg to accelerate the ions. Therefore, the cavities must operate on an odd harmonic of the ion rotational frequency. The lowest usable frequency for these cavities is three times the ion frequency, or 24.9 Mc/sec; operation at the ion frequency would introduce a cos $2\theta$ r-f field component for any particles not in phase.

For the $TE_{011}$ mode, the frequency of a cavity having dimensions $X_0$, $Y_0$, and $Z_0$ is given by

$$f_{011} = \frac{c}{2}\sqrt{\frac{1}{X_0^2} + \frac{1}{Z_0^2}} \; .$$

The value of $Y_0$ affects the $Q$ but not the frequency. Note that for a given frequency, as $X_0 \to \infty$, $Z_0 \to C/2f = \lambda/2$; this is the condition for a wave guide operating at the cutoff frequency. In this case, if $X_0$ is the cavity dimension in the median plane, $X_0$ would extend along the poles through the machine and some distance beyond in order that the accelerating voltage would still be large at the last orbit. The electrical length of the cavity is 180 deg and is made to extend 30 deg beyond the last orbit, so that with a sinusoidal voltage standing wave the accelerating voltage would be one-half as large at the last orbit as in the center of the machine. Then, $X_0$ is so large, 60 ft, that $Z_0$ nearly equals $\lambda/2$ or 19.8 ft.

A cavity having uniform $Y_0$ determined by the allowable separation (not more than 4 in.) between magnet sectors would not be very efficient. The cavity is held at this small $Y$ dimension only near the median plane; at as small a $Z$ dimension as possible, the $Y$ dimension is increased. This enlarging of the cavity has the advantage of increased $Q$, in addition to smaller height, $Z_0$, for a given frequency. The energy storage, which is proportional to volume, is increased, and the power loss, which is proportional to surface area, is decreased.

The sides of the cavity are tapered linearly to simplify the analysis. Since the cavity operates somewhat like a wave guide near cutoff, the effect of taper may be found by treating the cavity as sections of quarter-wave shorted transmission line.

Mechanically, the ideal place to couple a driving signal to the cavity would appear to be at the ends. However, the magnetic field at the ends of the cavity is so small that a loop with a practical value of input impedance is impossible there. Near the center, a 50-ohm loop requires only 1 ft$^2$ of area; hence, the cavities should be driven there.

The cavities would have a $Q$ of 23,000 and require an average driving power of 300 kw each in order to obtain an accelerating voltage of 1 Mev/turn at the center of the machine. The stored energy is about five times that of the ORNL 86-Inch Cyclotron. A tube such as the A2332 could readily drive one of these cavities.

### Shielding Estimates

The 900-Mev cyclotron will be erected below ground level in order to obtain maximum advantage from earth fill for shielding material, as shown in Fig. 37. Three sides of the cyclotron room are shielded in this manner; the fourth faces the experimental area and is shielded with iron and heavy concrete. Beam holes piercing the shield are located out of line with the deflector, where most of the beam loss in the accelerator is expected to occur. In this way, leakage through beam holes should be substantially reduced. The analyzing and focusing magnets are located within the main cyclotron enclosure. Preliminary estimates of the shield thicknesses are given in Table 6.

The proton beam will pass through the experimental area in an evacuated pipe and stop at the end of a 200-ft tunnel. The use of thin targets will minimize the radiation level in the experimental area. At present no overhead shielding is planned for this area. Local shielding for individual experiments will be provided where required.

**Table 6. Estimates of Shield Thicknesses**

| Location | Material | Thickness (ft) |
|---|---|---|
| Side walls (not facing exptl area) | Earth | 100 |
| Wall facing exptl area | | |
| 30-deg cone from deflector | Iron | 15 |
| Remainder of wall | Barytes concrete | 15 |
| Roof* | Concrete | 10 |

*Provision will be made for additional thickness of concrete over collimators, meson-producing targets, deflector, etc., as needed.

### Site Investigation

Some preliminary evaluations have been made of possible locations for the proposed energy accelerator. Prior to the preparation of the SRA proposal, a geologist from the University of Tennessee and ORNL representatives had established five possible sites in the vicinity of ORNL (X-10). Subsequent to the release of the proposal, it developed that the first sites were rather restricted in area; the accelerator concepts had grown larger and the shielding requirements more severe than in the early estimates. ORNL staff members next selected six additional sites with larger usable areas. Two of these were core-drilled for rough geological information, and a detailed layout was made on one site to provide a more definite basis for estimates. The location of this tentative site is shown in Figs. 40 and 41. It is expected that still other sites will be investigated, and, at a time when it seems appropriate, a careful and detailed study of the most likely site will be made. The principal criteria adopted for the SRA site were as follows:

*Stability.* – The tolerance for individual horizontal or vertical motions under varying conditions of load, temperature (either daily or seasonal), or any other disturbing influence should be held to 1 mm.

*Power Available.* – Power requirements may approach 20 Mw.

*Dimension of Site.* – An area of at least 600 × 1000 ft is required. For design purposes the synchrotron tunnel is assumed to be 25 ft high and 25 ft wide.

*Shielding.* – The site should have an easily movable overburden which can be used to provide the major portion of shielding. The horizontal center line will be 10 to 15 ft below normal grade. This requirement is intended to provide a minimum of 100 ft of earth shielding.

*Proximity to Other Facilities.* – The site should be as close to other X-10 buildings as practical.

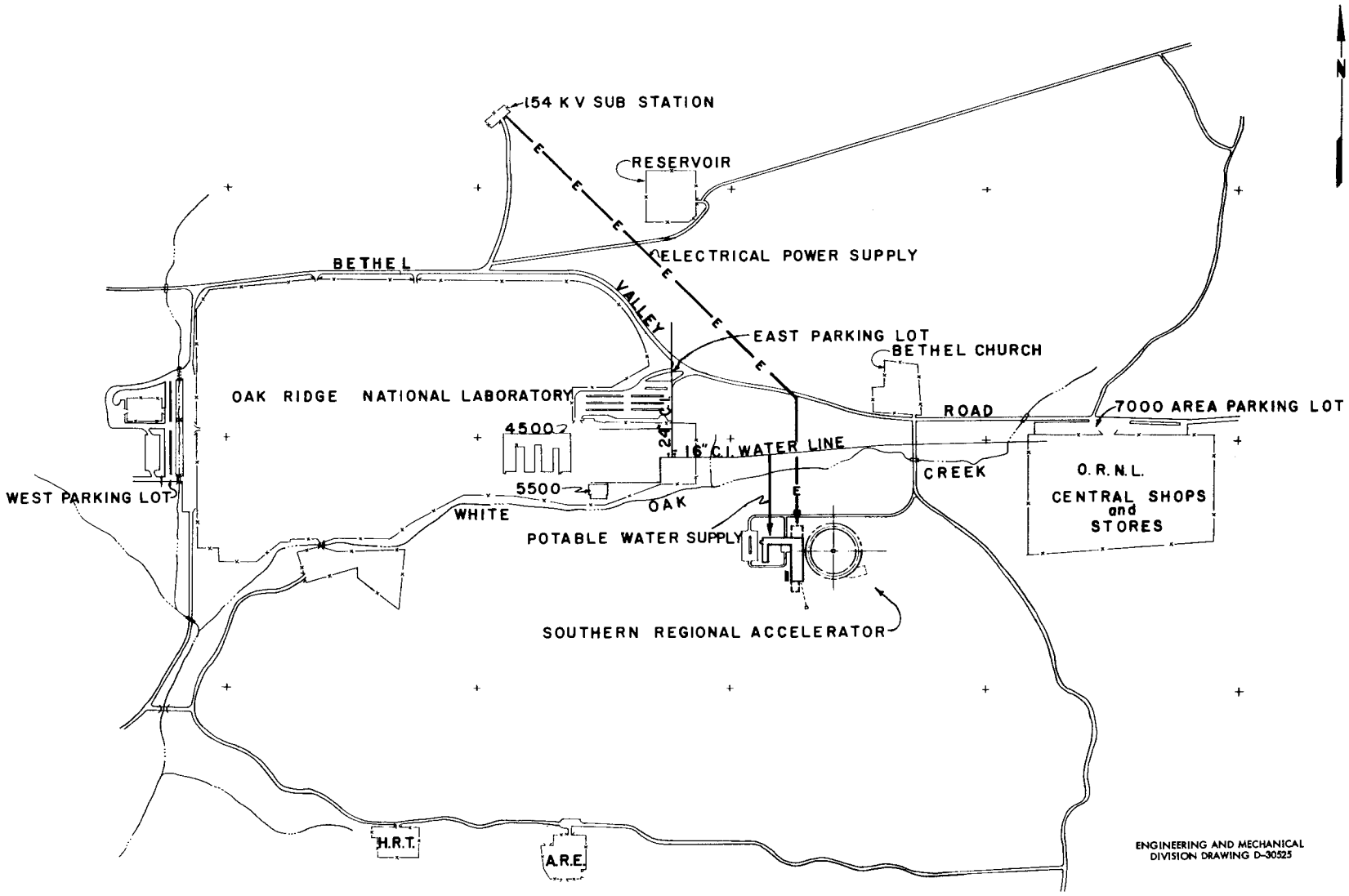


Fig. 40. Tentative Site Location for SRA.

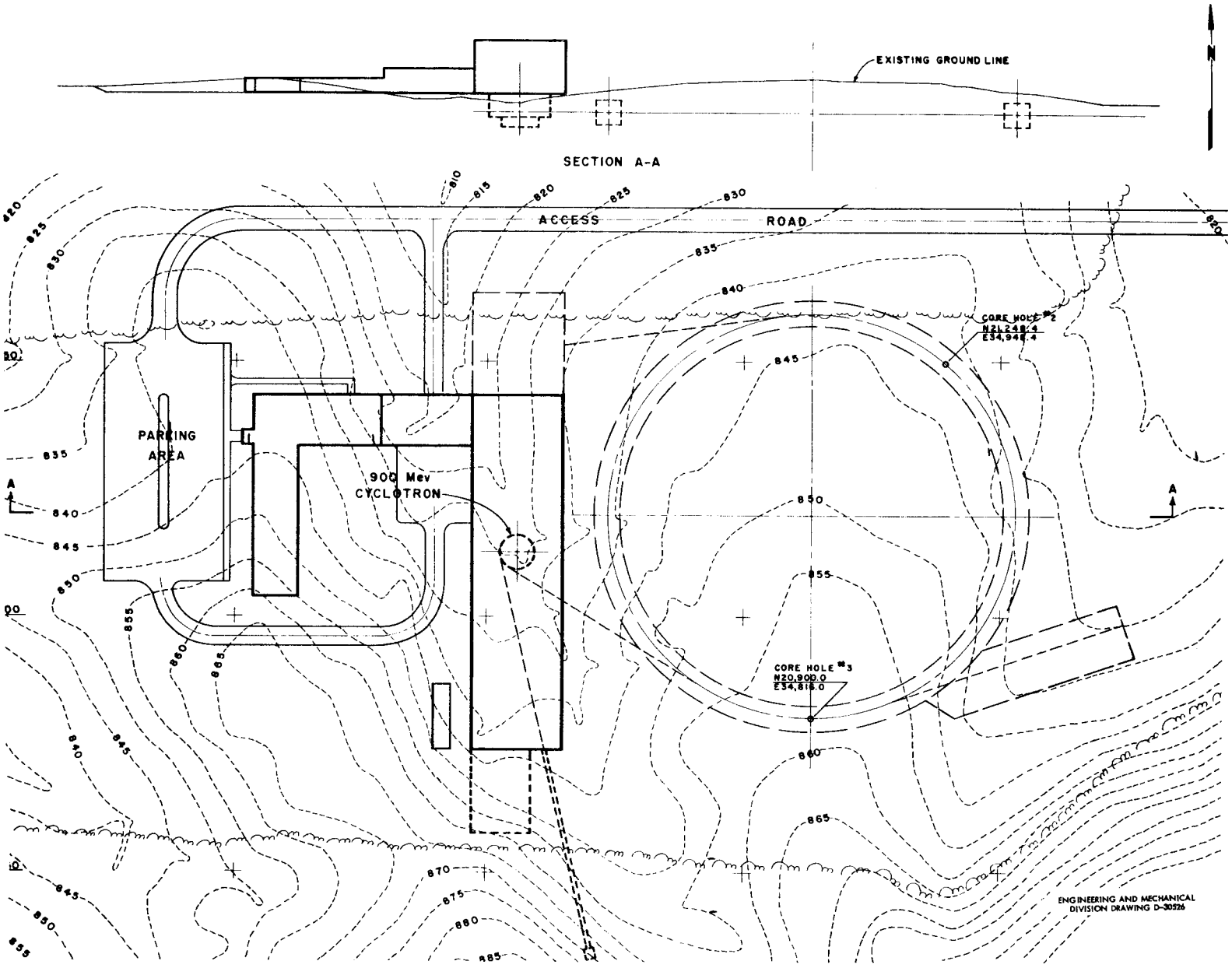


Fig. 41. Topographic Plan and Section at Tentative Site.

## THE 48-INCH HEAVY-PARTICLE CYCLOTRON

A 48-in. cyclotron for the acceleration of nitrogen and carbon ions to energies up to 88 Mev is being constructed. The complete r-f system is already constructed and is being operated in a Beta magnet, as the 44-in. cyclotron. Protons are accelerated to ~2 Mev for ion transmission studies. A new magnet is being designed which will permit acceleration of heavy particles to the higher energies. The 48-in. cyclotron is now being designed to operate as a conventional fixed-frequency cyclotron; the r-f would be adjustable, in steps, from 7.5 to 10.5 Mc/sec in order to obtain resonance for several heavy-ion species.

Other developments and the recent successful operation of Cyclotron Analogue I strongly support a proposal to revise plans for the 48-in. cyclotron in order to take advantage of the azimuthally-varying-field (AVF) principle. The revision being studied would produce heavy ions of considerably higher energy. The specifications of the original design and of the revision are given in Table 7. The AVF cyclotron would be designed to operate with a variable magnetic field and variable r-f. Such a versatile machine should provide for the acceleration of a wide range of particles, some to energies exceeding 110 Mev (see Fig. 42).

### PROGRESS ON THE CYCLOTRON AS ORIGINALLY PROPOSED

The design, fabrication, and preparation for construction of the ORNL 48-Inch Heavy-Particle Cyclotron have progressed satisfactorily. The engineering on the building is approximately 90% complete. The structure is designed for 3-ft-thick poured concrete walls and roof. Precast concrete beams will be utilized as a form for pouring the concrete roof and will remain in position as part of the shielding. Access to the building will be

Table 7. Specifications for the 48-Inch Cyclotron, Present and Revised (AVF Cyclotron)

| | Conventional Cyclotron | AVF Cyclotron |
|---|---|---|
| Nitrogen (4+) energy, Mev | 56.5 | 29–103 |
| Nitrogen (5+) energy, Mev | 88.5 | 29–117 |
| Carbon (4+) energy, Mev | 66 | 25–100 |
| Protons, Mev | | 5–75 |
| Diameter of magnet pole tips, in. | 56 | 76 |
| Maximum radius of orbit, in. | 20 | 31.5 |
| Magnetic field at exit radius, kilogauss | 20.0 | 17.5 (av) |
| Magnetic field drop-off at maximum radius, gauss | 400 (or 2%) | AVF |
| Magnetic field gap, min, in. | 13.5 | 9 |
| Radio-frequency, max, Mc/sec | 10.5 | 24 |
| Radio-frequency, min, Mc/sec | 7.5 | 12 |
| Orbit frequency, max, Mc/sec | 10.5 | 24 |
| Orbit frequency, min, Mc/sec | 7.5 | 4 |
| Dee-to-dee r-f voltage, design, kv | 200 | 200 |
| Dee-stem length, ft | 7 | 9 |
| Dee-stem diameter, in. | 7 | Oval |
| Dee diameter, in. | 44 | 67 |
| Dee-to-dee gap, in. | 2 | 2 |
| Dee aperture, in. | 6.5 | 3 |

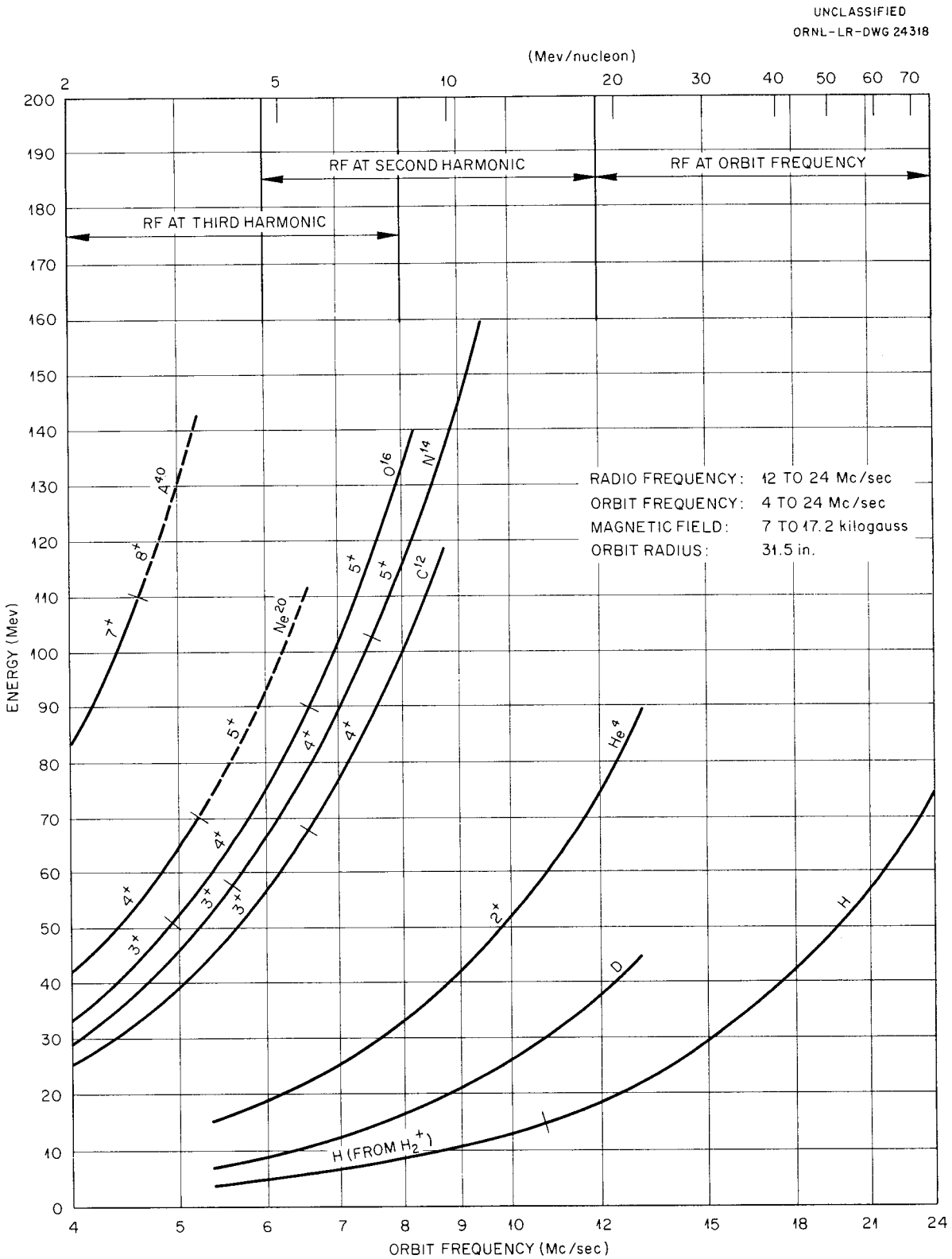


**Fig. 42. Energy Ranges of Particles Potentially Available in the Revised 48-in. Cyclotron.**

through two hung, vault-type doors weighing approximately 20 tons each. Utilities lines will enter the building through an underground tunnel.

Core drillings for the building and magnet base showed rock approximately 9 ft below grade level. A few limestone cavities were encountered; most were small, but some will need to be pressure-grouted.

The magnet design is 80% complete. The yoke and pole bases, amounting to some 200 tons of steel, are being fabricated. The steel has been cast and forged. Ladle analysis of the steel gave the following very satisfactory composition:

| | Pole Base | Yoke |
|---|---|---|
| C | 0.13 | 0.11 |
| Mn | 0.37 | 0.33 |
| P | 0.010 | 0.010 |
| S | 0.018 | 0.030 |
| Si | 0.12 | 0.15 |
| Ni | 0.05 | 0.06 |

The aluminum for winding the main magnet coils was received. The conductors are 1.137 in. square, with a circular water passage 0.7 in. in diameter. There are 16 strands, each 1070 ft long. The d-c power for exciting the magnet coils will be furnished by a 1750-kw Beta motor-generator (M-G) set. The conductors and coils of the magnet are designed for a resistance of 0.070 ohm, to match the M-G set. The engineering for installing the M-G set in line with and adjoining the two M-G sets now in Building 9201-2 is complete.

The resonant dee system was successfully checked out in a Beta magnetic field gap. Protons are accelerated to approximately 1.5 Mev. Beam properties and ion transmission problems are being studied.

## REVISION OF THE 48-INCH CYCLOTRON DESIGN

The modifications in the designs of both the magnet and the r-f system which would be required for the revision of the 48-in. cyclotron being considered are now under study.

### Revision of Magnet Design

A series of model magnet studies is being made in order to determine the feasibility, details, and limitations of a conversion of the partially fabricated yoke and coil structure of the 48-in. cyclotron magnet to an AVF magnet with a wide range of flexibility of operation. Sector coils would be attached to the pole faces so as to produce the azimuthal variations in the field. Initial studies include experimental measurements of the fields produced by a number of pole-face and conductor configurations; an approximately $\frac{1}{8}$-scale model of the magnet is used. Orbit properties were derived from the measured fields by use of approximate analytic formulas. These initial studies indicate that a usable average $H\rho$ of about 550,000 gauss-inches can be obtained in the magnet, with adequate azimuthal variations for focusing a wide variety of particles. These studies also indicate that the field strength can be successfully varied over a wide range; variations from full strength to $\frac{1}{4}$ full strength, while a satisfactory field shape is still maintained, appear quite feasible.

### Revision of R-F System

Two specifications must be considered in the design of the r-f system. The dee-to-ground voltage should be at least 100 kv to assure efficient emission from the ion source and to permit reasonable tolerances in magnetic field specifications. Also, the r-f system for the revision being considered should provide for the acceleration of various ions which have orbit frequencies from 4 to 24 Mc/sec. The use of several separate r-f systems to cover this wide-range variable frequency would not be very practicable. A better solution to this problem would be to make use of mode acceleration.

**Mode Acceleration.** – A cyclotron with 180-deg dees and the r-f equal to the ion orbit frequency is operated in what is called the fundamental mode. Ions which rotate at one-third the accelerating frequency could also be accelerated; the ion would travel 180 deg in the dee while the r-f goes through 3 × 180 deg. The allowable phase spread of the ions relative to the r-f voltage would only be one-third as great, but there would be three bunches, compared with a single bunch, in a machine operating on the first or fundamental mode. For example, $HD^+$ can be accelerated under the same conditions as those for protons, except that the cyclotron would be operating on the third mode.

Similarly, with 180-deg dees, ions could be accelerated on any mode having an odd number. The mode number is the ratio of the r-f to the ion rotation frequency.

Mode acceleration has been discussed by Jakobson and Schmidt.[1] They have developed the following equation for the voltage gain per turn, $\Delta W$, in a two-dee system:

$$\Delta W = 2qV_0 \cos\left(\frac{\omega}{\Omega}\phi\right) \sin\left(\frac{\omega}{\Omega}\frac{\theta}{2}\right) \times \times \left[1 + \cos\left(\frac{\omega}{\Omega}\pi + \psi\right)\right],$$

where

$q$ = charge of ion,
$V_0$ = dee-to-ground voltage,
$\theta$ = angle the dee subtends,
$\phi$ = phase angle of ion with respect to oscillator voltage,
$\omega$ = accelerating frequency,
$\Omega$ = ion frequency,
$\psi$ = 0, dees operating in phase,
= $\pi$, dees operating out of phase.

The following data show what could be obtained with two dees:

| $\theta$ (deg) | Dee Phase (deg) | $\omega/\Omega$ | $\Delta W/qV_0$ |
|---|---|---|---|
| 90 | 180 | 1 | 2.83 |
| 90 | 0 | 2 | 4 |
| 90 | 180 | 3 | 2.83 |
| 120 | 180 | 1 | 3.46 |
| 120 | 0 | 2 | 3.46 |
| 190 | 180 | 1 | 4 |
| 180 | 0 | 2 | 4 |
| 180 | 180 | 3 | 4 |

It should be pointed out here that the size of the orbits, and hence the radius of the dees, is such that the large capacitance of 180-deg dees makes the dee stems too short to be practical. The 180-deg dees are included in the above table for comparison only.

[1]M. J. Jakobson and F. H. Schmidt, *Phys. Rev.* **93**, 303 (1954).

Use of the 90-deg dees and an r-f of 12 to 24 Mc/sec would appear to be one solution. The second mode would cover 12 to 6 Mc/sec for deuterons and alpha particles, and the third mode would cover 8 to 4 Mc/sec for the heavy particles. If the r-f system could be tuned from 24 to 8 Mc/sec, the mode-2 operation could be eliminated.

**Methods of Tuning Resonators.** – Standard cyclotrons are tuned by varying the dee-to-ground capacitance for small frequency changes and moving the shorting bar along the dee stems for larger frequency variations. To vary the resonant frequency over the large range of 24 to 12 or 24 to 8 Mc/sec by moving the shorting bar would require dee stems of an unreasonable length. Also, continuous frequency variation would be impractical because of the difficulty of continuous movement of the shorting bar.

A better method is to vary the characteristic impedance, $Z_0$, of the dee stems along with a minimum movement of the shorting bar. The maximum stem length would be reduced by a factor depending on the amount which $Z_0$ could be varied. Also, the variation of $Z_0$ could probably be made continuous in order to allow continuous frequency and, hence, continuous energy control.

A resonant system employing a transmission line of variable $Z_0$ is shown in Fig. 43. The dee stem and dee-stem liner form, in effect, a strip transmission line in which the conductor spacing may be changed in order to vary the characteristic impedance, $Z_0$, of the line. Such a system is being considered as a solution to the tuning problem of the revised 48-in. cyclotron.

For the desired frequency range it was calculated that the characteristic impedance of the dee stems would have to be variable from 12 to 35 ohms and that two positions of the shorting bar would be required; the farthest position would be approximately 155 in. from the center of the cyclotron. At 24 Mc/sec and with 100 kv dee-to-ground, the r-f power required was computed to be 150 kw.

The system which has been considered for the revised cyclotron consists of a master oscillator, a driver, and a power amplifier driving each dee stem through a suitable coupling network. This system should be adaptable to the automatic control and alignment which would be essential if the operating frequency is to be changed often.

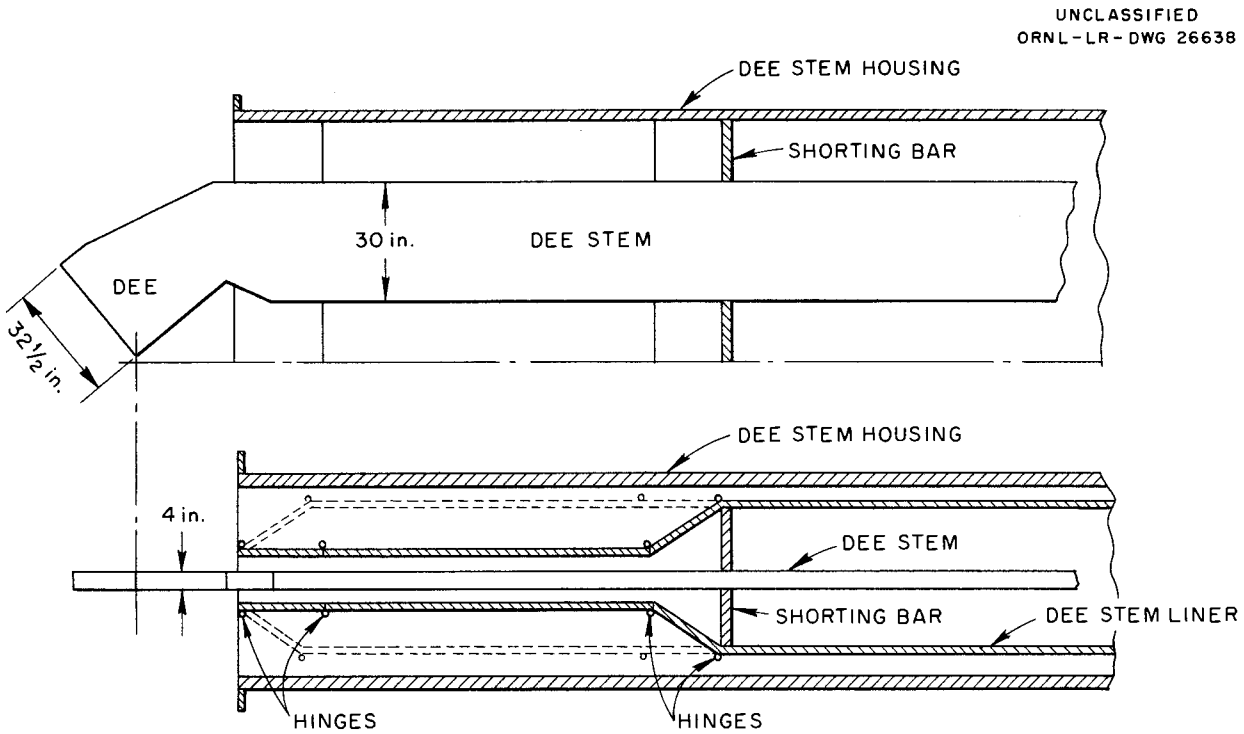


**Fig. 43. Transmission Line with Variable Capacitance.**

## SPECIAL SEPARATIONS

The isotopes of uranium, plutonium and thorium are enriched from special feed materials and distributed on a Commission-wide basis. The isotopes $Th^{230}$, $U^{234}$, $U^{235}$, $U^{236}$, $U^{238}$, $Pu^{239}$, $Pu^{240}$, and $Pu^{241}$ are separated as required, in order to maintain an inventory of these materials. In addition to purified isotopes being made available for research purposes, the experience gained in handling special materials in the electromagnetic separation process permits continuing evaluation of the process for possible larger-scale applications. Present emphasis is on the separation of $Pu^{240}$ and $Pu^{241}$ from highly irradiated plutonium. The instrument development phase of the program has centered about an isotope separator capable of separating quite small quantities of feed materials and of giving higher enrichment factors than can be obtained with the conventional one-mass-unit separators.

### PLUTONIUM SEPARATIONS

Since the last report,[1] seven plutonium separations were completed. Production of separated plutonium products for the period totaled 4.4 g of $Pu^{240}$ and 0.9 g of $Pu^{241}$. Plutonium of two different irradiation levels and containing different amounts of $Pu^{240}$ was used. The data for the several runs are summarized in Table 8.

As is evident from the table, the ion source performance, characterized by process efficiency, was very irregular. This has been traced to leakage of liquid $PuCl_3$ from the graphite feed bottle. Apparently, leakage began when a change was made from C-18 graphite to type APC for feed-container construction. The APC graphite is equally as dense and fine-grained as C-18 and has superior machinability, but apparently it has more connecting voids. The $PuCl_3$ leakage was largely eliminated by changing to Hastelloy C for container material. In Fig. 44 the new metal container is shown beside one of graphite for comparison.

In runs 12 and 14, four-pocket collectors were used to provide for $Pu^{242}$ collection; $Pu^{240}$ was used as the monitoring isotope. In addition to providing for the collection of $Pu^{242}$, it was expected that with this collector design the enrichment and retention of both $Pu^{240}$ and $Pu^{241}$ would be improved. The expected improvement was not realized; in fact, results were substantially poorer than those obtained with standard collectors (see Table 8). The poor results apparently were caused by difficulties in properly monitoring the beam. The presence of the intense $Pu^{239}$ peak (abundance 65%) only 150 v above the $Pu^{240}$ peak (abundance 30%) interfered with the adjusting of the position of the collector in order to optimize the focus.

A survey of the temperature distribution in the plutonium ion source revealed that improvement in temperature control could be made with minor rearrangement of the heat shielding. In particular, the charge container was being heated to a temperature of 680°C by radiation from the manifold and arc chamber heaters. Additional heat shielding between manifold and feed container lowered the temperature of the latter to 580°C and permitted better temperature control with the heaters around the charge container. With this modified heat shielding, temperature control is much smoother, particularly during the startup.

### CHEMICAL RECYCLE AND PRODUCT CHEMISTRY

Chemical operations consisted mainly in the routine recovery and reprocessing (to pure $PuCl_3$) of the plutonium vaporized during previous isotope separations. In addition, the recovery of low-level plutonium used in earlier programs was continued. Recovery of both the 100-Mwd/ton (0.5% $Pu^{240}$) and the 1200-Mwd/ton (5% $Pu^{240}$) material is essentially complete. The final recovery of the material at the 3000-Mwd/ton level (13% $Pu^{240}$) was begun.

Two minor changes in the recycle flowsheet were made in order to speed up the operation and to provide a better product. First, a leaching of the solids from the initial dry recovery of plutonium from the ion source and collector units was introduced. Formerly, the solids were muffled directly. The change has markedly reduced the amount of plutonium held up as $PuO_2$, which is difficult to

[1] *Electronuclear Research Semiann. Prog. Rep. March 20, 1956*, ORNL-2139, p 11.

Table 8. Summary of Plutonium Isotope Separation Runs

| Run No. | | Isotopic Concentration (at. %) | | | | Amount (g of Pu) |
|---|---|---|---|---|---|---|
| | | $Pu^{239}$ | $Pu^{240}$ | $Pu^{241}$ | $Pu^{242}$ | |
| 8 | Pu vaporized | 84.33 | 13.69 | 1.77 | 0.21 | 46.0 |
| | $Pu^{240}$ product[a] | | | | | |
| | $Pu^{241}$ product[a] | | | | | |
| 9 | Pu vaporized | 84.52 | 13.51 | 1.69 | 0.28 | 110.0 |
| | $Pu^{240}$ product | 18.64 | 80.08[b] | 1.14 | 0.14 | 0.350 |
| | $Pu^{241}$ product | 31.62 | 33.39 | 34.50 | 0.49 | 0.097 |
| 10 | Pu vaporized | 87.06 | 11.46 | 1.30 | 0.18 | 61.0 |
| | $Pu^{240}$ product | 19.09 | 79.71 | 1.08 | 0.12 | 0.349 |
| | $Pu^{241}$ product | 37.84 | 16.75 | 43.86 | 1.55 | 0.057 |
| 11 | Pu vaporized | 85.09 | 13.07 | 1.61 | 0.23 | 124.7 |
| | $Pu^{240}$ product | 23.69 | 75.13 | 1.13 | 0.05 | 0.402 |
| | $Pu^{241}$ product | 31.27 | 32.32 | 35.71 | 0.70 | 0.099 |
| 12 | Pu vaporized | 65.08 | 29.72 | 4.33 | 0.87 | 94.1 |
| | $Pu^{240}$ product[a] | | | | | |
| | $Pu^{241}$ product[a] | | | | | |
| 13 | (Terminated early) | | | | | |
| 14 | Pu vaporized | 65.60 | 29.47 | 4.15 | 0.78 | 114.0 |
| | $Pu^{240}$ product (1)[c] | 28.02 | 70.08 | 1.83 | 0.07 | 1.199 |
| | $Pu^{240}$ product (2) | 23.82 | 74.01 | 2.06 | 0.11 | 1.331 |
| | $Pu^{241}$ product (1) | 21.10 | 42.16 | 35.11 | 1.63 | 0.191 |
| | $Pu^{241}$ product (2) | 19.84 | 41.86 | 36.53 | 1.77 | 0.241 |
| | $Pu^{242}$ product (1) | 32.78 | 31.80 | 19.13 | 16.29 | 0.083 |
| | $Pu^{242}$ product (2) | 32.27 | 31.44 | 18.45 | 17.84 | 0.107 |
| 15 | Pu vaporized | 65.37 | 29.67 | 4.16 | 0.80 | 73.0 |
| | $Pu^{240}$ product | 5.86 | 92.19 | 1.84 | 0.11 | 0.768 |
| | $Pu^{241}$ product | 9.02 | 31.01 | 57.96 | 2.01 | 0.204 |

[a]Same collectors used for subsequent completed run.

[b]Isotope desired.

[c]Numbers refer to the two collectors; they were processed separately.

dissolve. The second change was in the preparation of the anhydrous chloride. Formerly the peroxide precipitate was dissolved in HCl and then added dropwise to refluxing hexachloropropene (HCP). In the present method, plutonium(IV) oxalate is reacted with refluxing HCP. The final chlorination step is to react the product of the HCP chlorination with phosgene at 550°C for 12 hr.

Two minor releases of plutonium occurred during the period. First, approximately 500 ml of solution containing 30 mg of plutonium leaked from the glove box containing the liner-wash circulating pump. The release was caused by the failure of the pump seal and subsequent failure of the means provided to retain the leakage. The second spill occurred in the evaporator room of the recycle laboratory, and was caused by the failure by

UNCLASSIFIED
PHOTO 28411

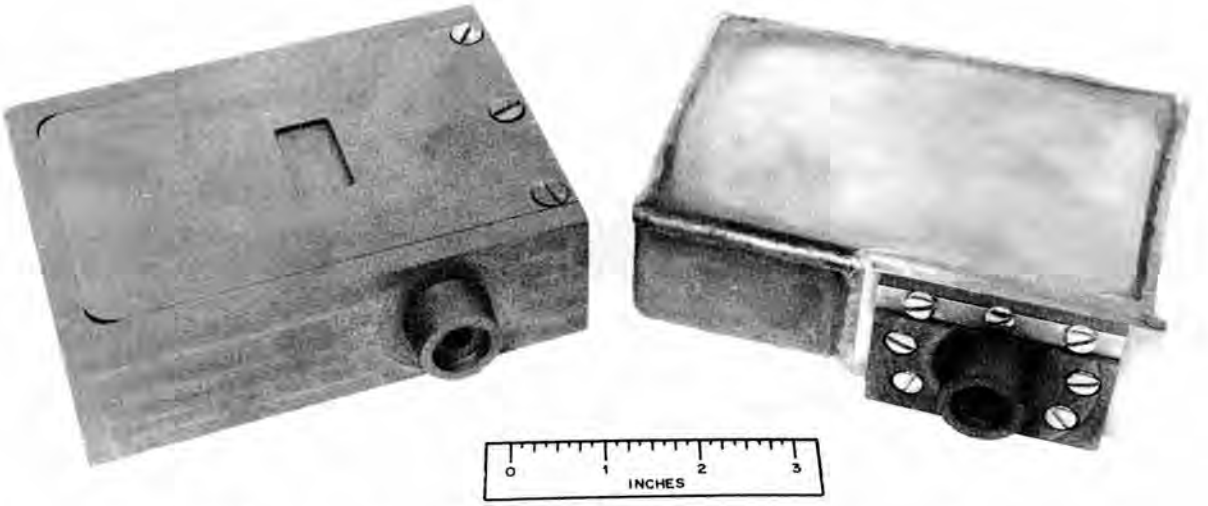


**Fig. 44. Graphite and Hastelloy C Feed Bottles Used in Plutonium Isotope Separation.**

corrosion of the lower flange of a sight glass on a glass-lined storage tank. Approximately 7 gal of solution containing 200 mg of plutonium was lost to the "hot" floor drain system and was subsequently shipped to the X-10 tank farm. No contamination of personnel nor dispersal of plutonium in the building resulted from either incident. The maximum contamination of the air immediately adjacent to the spill was in both incidents approximately 30 $d \cdot min^{-1} \cdot m^{-3}$.

### LOW-INTENSITY ISOTOPE SEPARATOR

Development of the Low-Intensity Isotope Separator (LIIS) was continued with considerable success. This mass spectrograph is designed for special-purpose work, such as the second-stage separation of products from previous separations and the preparation of small amounts of isotopes of especially high purity. Present results indicate that the one-mass-unit enrichment factor will be at least 100, that is, a factor of 3 better than is obtained with the larger calutrons.

At present the LIIS is mounted in the framework of a standard Beta ion source (Fig. 45). The assembly is shown in cross section in Fig. 46. Listed below are the typical performance characteristics of the LIIS:

| | |
|---|---|
| Beam energy | 37.0 kev |
| Accelerating potential | −19.2 kv |
| Arc current | 1.6 amp |
| Arc potential | 135.0 v |
| Average pressure | $2.2 \times 10^{-5}$ mm Hg |
| Collector current, av | 2.23 ma |
| Collector current, peak | 3.0 ma |
| Run length | 5.5 hr |
| Uranium collected | 99.0 mg |
| $UCl_3$ vaporized | 2.50 g |
| Efficiency | 5.7% |
| Feed consumption rate | 351.0 mg of element per hr |

A focal-plane scan (Fig. 47) made with the normal uranium feed illustrates the sharp focus obtained.

Recently a substantial improvement in performance was obtained by placing grounded metal plates adjacent and parallel to the 2-in.-wide beam. The usual gap inside the Beta liner where

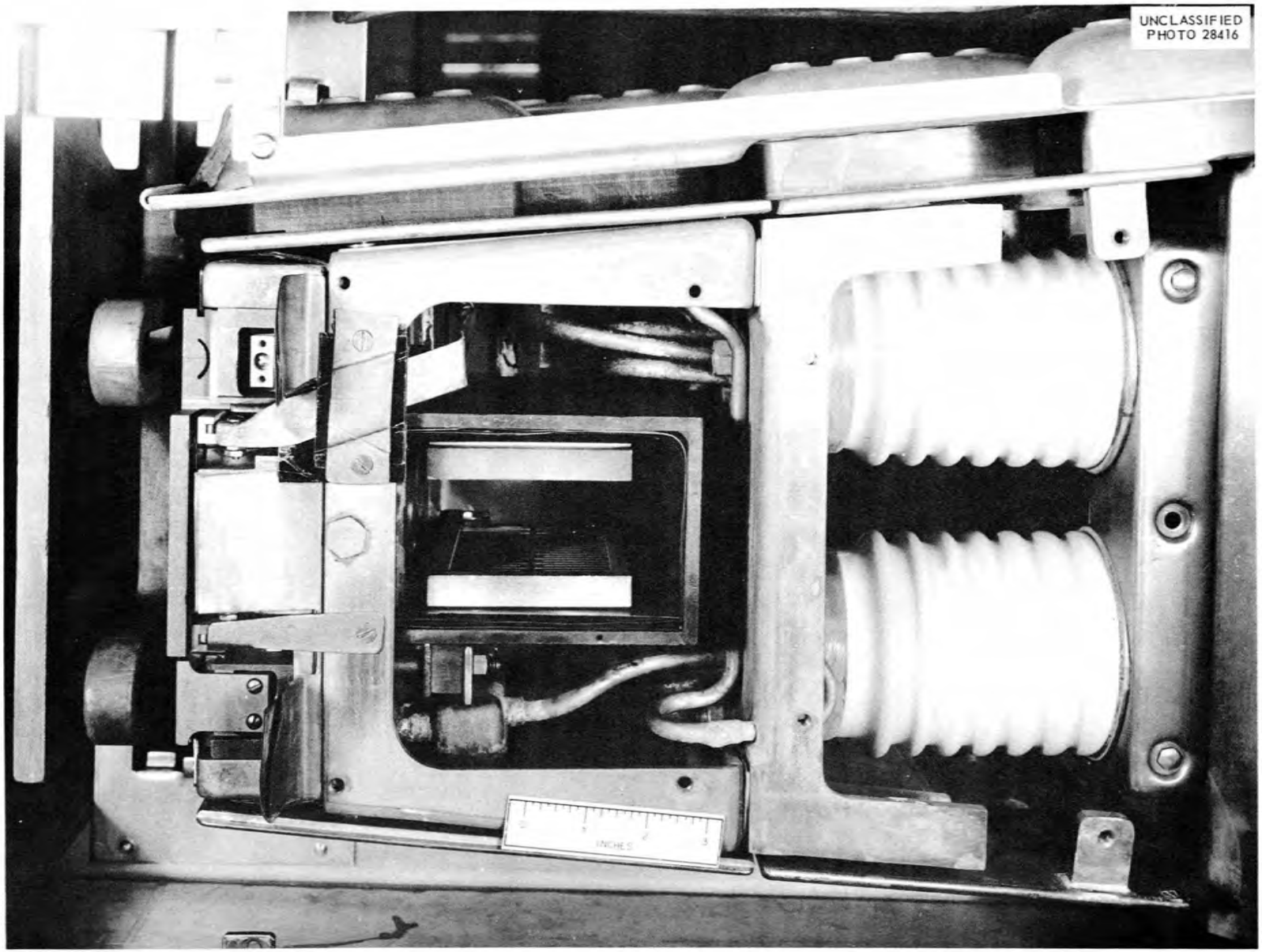


Fig. 45. The Low-Intensity Isotope Separator. The small ion source is mounted in the framework of a Beta ion source.

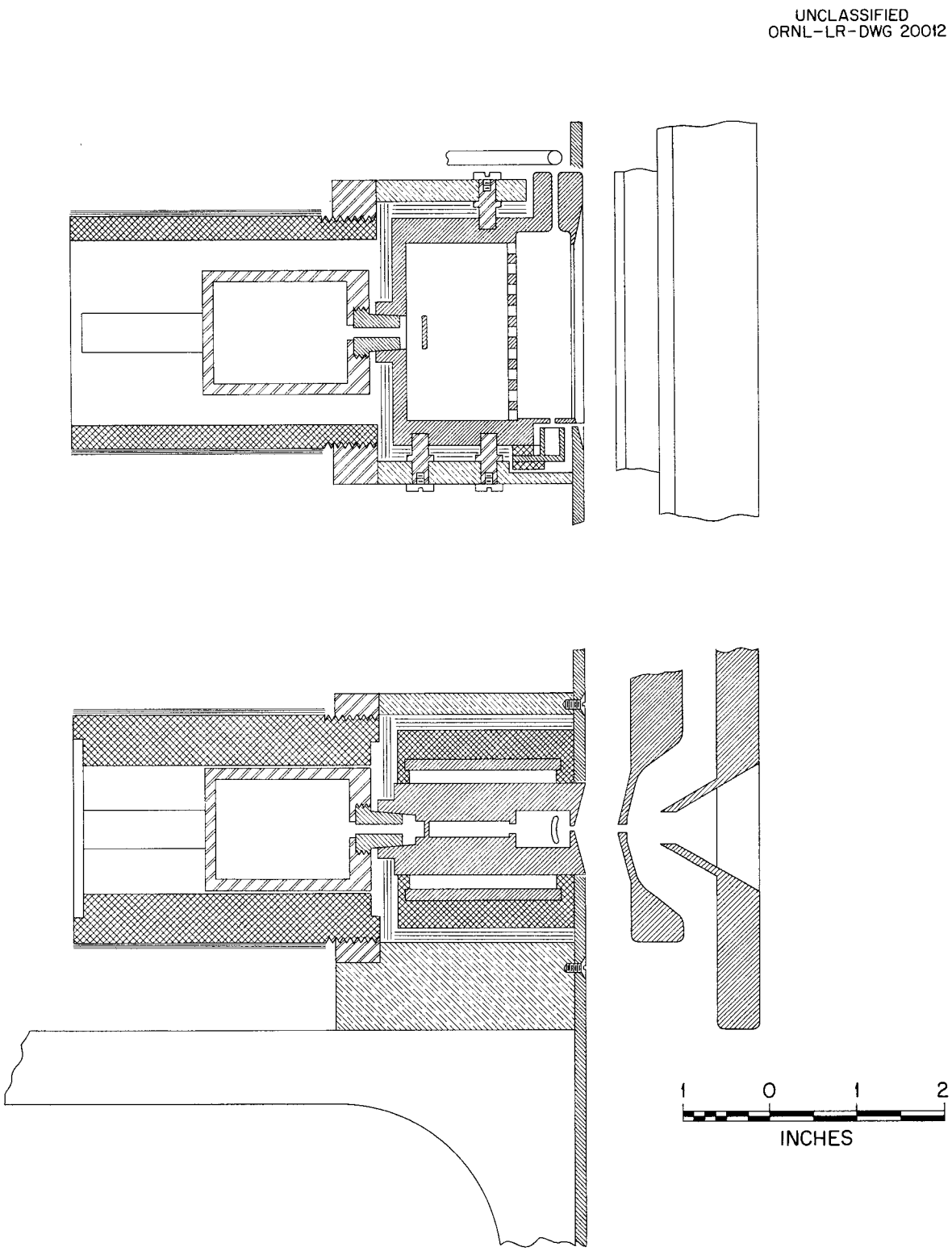


Fig. 46. Low-Intensity Isotope Separator in Cross Section.

the beam passes is approximately 11 in. Before adding the plates, beam response to changes in accelerating voltage, arc current, or arc voltage was extremely sluggish; seconds were required for the beam to recover to its full value. Installation of these side plates completely eliminated the sluggish response. It appears that with the large gap and the small beam, the beam plasma had been slow in collecting enough electrons for neutralizing the large volume. Further, with the large gap, the potential of the center of the plasma with respect to the walls was unnecessarily large.

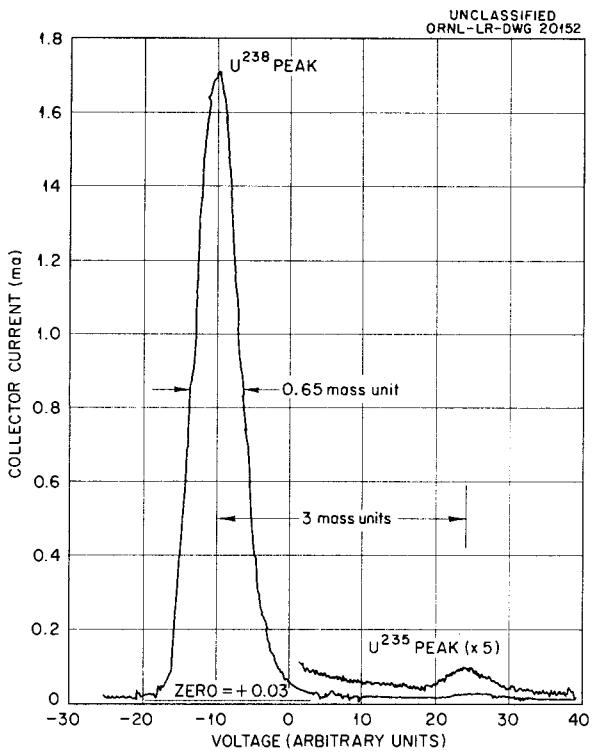


**Fig. 47. Focal Pattern Obtained with LIIS from Normal Uranium Feed.**

With the completion of the work aimed toward stabilizing the performance of the LIIS, actual collections to determine enrichment factors are proceeding. If the results of the scans are borne out by assayed collections, the LIIS will be applied to the separation of the uranium isotopes $U^{234}$ and $U^{236}$ and the plutonium isotopes $Pu^{240}$ and $Pu^{241}$.

## NEW PLUTONIUM FEED MATERIALS

Fabrication of four Pu-Al fuel elements for irradiation in the MTR was completed at ORNL in early 1957. Irradiation of these elements in the MTR is proceeding satisfactorily, with the possible exception that only one beryllium reflector position has been made available for the program. Unless additional reactor space becomes available, the irradiations will not be complete until mid-1958. Consequently, the first isotope separation of the MTR-irradiated plutonium will probably be made during the fall of 1958.

## ISOTOPE SHIPMENTS

The distribution of electromagnetically enriched isotopes of heavy elements to various laboratories is shown in Table 9.

(Note: The Special Separations activities were transferred, as of July 1, 1957, to the Isotopes Division.)

Table 9. Distribution of Isotopes

| Isotope | Shipped To | Amount (g) | Purity (%) |
|---|---|---|---|
| $U^{234}$ | Argonne National Labaratory | 0.005 | 96.88 |
| | General Electric Company (Hanford) | 0.001 | 96.88 |
| | Oak Ridge National Laboratory | 0.1307 | 96.88 |
| | Argonne National Laboratory | 0.048 | 93.44 |
| | AERE, Harwell, U.K. | 0.0991 | 93.44 |
| | K-25 | 0.003 | 93.44 |
| | Oak Ridge National Laboratory | 0.030 | 93.44 |
| | University of California Radiation Laboratory | 0.026 | 93.44 |
| | Oak Ridge National Laboratory | 0.162 | 79.51 |
| | Atomic Energy of Canada, Limited | 0.096 | 51.70 |
| | General Electric Company (Hanford) | 0.015 | 51.70 |
| | Y-12 | 0.104 | 13.50 |
| | Oak Ridge National Laboratory | 1.344 | 10.68 |
| $U^{235}$ | K-25 | 0.003 | 99.994 |
| | Oak Ridge National Laboratory | 2.496 | 99.994 |
| | Argonne National Laboratory | 0.020 | 99.94 |
| | Oak Ridge National Laboratory | 4.998 | 99.93 |
| | Argonne National Laboratary | 2.000 | 99.91 |
| | U.S. Geological Survey | 0.010 | 99.91 |
| | Los Alamos Scientific Laboratory | 1.694 | 99.88 |
| | General Electric Company (Hanford) | 10.000 | 99.70 |
| | Los Alamos Scientific Laboratory | 100.000 | 99.70 |
| $U^{236}$ | AERE, Harwell, U.K. | 0.1007 | 95.48 |
| | K-25 | 0.249 | 95.48 |
| | Naval Research Laboratory | 0.001 | 95.48 |
| | Argonne National Laboratory | 0.028 | 94.77 |
| | Atomic Energy of Canada, Limited | 0.051 | 94.77 |
| | University of California Radiation Laboratory | 0.025 | 94.77 |
| $U^{238}$ | K-25 | 0.001 | 99.9999 |
| | Atomic Energy of Canada, Limited | 4.240 | 99.9997 |
| | Knolls Atomic Power Laboratory | 5.012 | 99.9997 |
| | Knolls Atomic Power Laboratory | 10.000 | 99.9997 |
| | Los Alamos Scientific Laboratory | 14.990 | 99.9997 |
| | University of Califarnia Radiation Laboratory | 5.017 | 99.9997 |
| | Oak Ridge National Laboratory | 0.107 | 99.9994 |
| | Argonne National Laboratory | 0.030 | 99.9988 |
| | K-25 | 0.003 | 99.9956 |
| | Westinghouse Electric Corporation | 25.500 | 99.9956 |
| | Knolls Atomic Power Laboratory | 73.500 | 99.981 |
| | Oak Ridge National Laboratory | 2.000 | 99.981 |
| | Oak Ridge National Laboratory | 2.290 | 99.981 |
| | Oak Ridge National Laboratory | 5.420 | 99.981 |
| | Oak Ridge National Laboratory | 136.900 | 99.981 |
| | Oak Ridge National Laboratory | 150.000 | 99.981 |
| | AEC-SRO | 34.100 | 99.981 |

Table 9 (continued)

| Isotope | Shipped To | Amount (g) | Purity (%) |
|---|---|---|---|
| $U^{238}$ | Westinghouse Electric Corporation | 80.500 | 99.981 |
| | Knolls Atomic Power Laboratory | 140.500 | 99.971 |
| | Knolls Atomic Power Laboratory | 254.5500 | 99.971 |
| | Los Alamos Scientific Laboratory | 10.520 | 99.971 |
| | Los Alamos Scientific Laboratory | 504.000 | 99.971 |
| | Oak Ridge National Laboratory | 1.741 | 99.971 |
| $Pu^{239}$ | Oak Ridge National Laboratory | 0.003 | 99.89 |
| | Oak Ridge National Laboratory | 0.200 | 99.89 |
| | Oak Ridge National Laboratory | 0.002 | 99.81 |
| | Oak Ridge National Laboratory | 0.109 | 99.81 |
| | Phillips Petroleum Company (MTR) | 0.698 | 99.80 |
| $Pu^{240}$ | University of California Radiation Laboratory | 0.202 | 88.10 |
| | Argonne National Laboratory | 0.050 | 87.17 |
| | Argonne National Laboratory | 0.053 | 87.17 |
| | Oak Ridge National Laboratory | 0.052 | 87.17 |
| | Los Alamos Scientific Laboratory | 0.396 | 83.1 |
| | Los Alamos Scientific Laboratory | 0.577 | 80.27 |
| | Phillips Petroleum Company (MTR) | 0.077 | 80.27 |
| | Oak Ridge National Laboratory | 0.151 | 80.08 |
| | Phillips Petroleum Company (MTR) | 0.333 | 79.85 |
| | Argonne National Laboratory | 0.015 | 79.71 |
| | Los Alamos Scientific Laboratory | 1.024 | 74.01 |
| $Pu^{241}$ | Oak Ridge National Laboratory | 0.015 | 62.11 |
| | Brookhaven National Laboratory | 0.042 | 52.37 |
| | Brookhaven National Laboratory | 0.025 | 46.74 |
| | Brookhaven National Laboratory | 0.167 | 40.73 |
| | Oak Ridge National Laboratory | 0.093 | 34.50 |
| | University of California Radiation Laboratory | 0.053 | 22.80 |
| $Th^{230}$ | K-25 | 0.051 | 90.02 |
| | Oak Ridge National Laboratory | 0.002 | 90.02 |
| | Oak Ridge National Laboratory | 0.105 | 87.85 |

# PACKAGE POWER REACTOR

The activities of the Package Power Reactor Group include research and development programs for the Army Reactor Branch, the Maritime Reactor Branch, and the Oak Ridge Operations Office of the Atomic Energy Commission. The work for the Army Reactor Branch consists of research and development in support of the Army Package Power Reactor-1 (APPR-1) and the Army Gas-Cooled Reactor Experiment. Support is being given to the Maritime Reactor Branch on the Maritime Ship Reactor. Technical assistance is being furnished to the Oak Ridge Operations Office on the Puerto Rican Reactor.

## ARMY PACKAGE POWER REACTOR

The contract for the design and construction of the APPR-1 at Fort Belvoir, Virginia, was awarded to Alco Products, Inc., on December 10, 1954. Ground breaking at the Fort Belvoir site occurred in October 1955. One and one-half years later, construction was completed (see Fig. 48), and on April 8, 1957, the reactor went critical. When the reactor was taken up to full power, the load response characteristics of the system were found to be excellent. After a brief testing period, the reactor was dedicated on April 29, 1957. A 700-hr performance test run was started shortly afterwards and was concluded on July 2 with only an 8-hr outage. In general, the entire system exceeded expectation. At present, a six-month training and endurance test is being conducted.

### Fabrication of APPR-1 Fuel Assemblies

The Laboratory was given the responsibility for producing the fuel and control elements for the first core of the APPR-1. The development program was cut short when the contract date for completion of the reactor was advanced six months. The production of the core elements was started as soon as possible and progressed on a satisfactory time schedule. When over half the fuel elements were completed, it was noted that the surface of a finished element was very rough after final pickling. Further examination showed that the roughness was due to pitting of the cladding. This pitting of the type 304L stainless steel was attributed to intergranular attack by the final pickling solution. The attack resulted in grains of the metal actually being corroded free from the surrounding clad metal and falling out.

The reason for this attack on type 304L stainless steel, which should be resistant to intergranular corrosion, was investigated. It was found that the cladding was being carburized and subsequently sensitized during the hot-rolling operation, thereby rendering the cladding susceptible to intergranular attack.

Since the extent of intergranular corrosion of the fuel elements manufactured up to this time was uncertain, these first elements were used only for the APPR-1 zero-power experiment. A second core loading was manufactured by a procedure that eliminated the final pickling of the assemblies. This second fuel loading was completed early in January 1957 and was loaded into the APPR-1. At present, the core has operated without any difficulties for over 10% of the design lifetime.

### Fuel-Melting Experiment

A joint experimental program was undertaken with the Chemistry Division to obtain information on the magnitude of the release of fission products, in gaseous form, during the melting of a stainless-steel-clad fuel element. Information of this type is required for reactor safeguards considerations in predicting fission-product release to the atmosphere in case of a reactor catastrophe.

In the initial phases of the program, small slivers of fuel-plate material, clad on only two sides, were irradiated in the ORNL Graphite Reactor and subsequently were melted by induction heating in a gas stream in a chemical hood. The released gases were collected in filters, chemical absorbents, or in activated charcoal traps. The initial results were very erratic. Subsequently, punched disks containing approximately 10 mg of irradiated $U^{235}$ were substituted for the slivers. Then, to eliminate the effect of exposed edges and to extend the irradiation time, larger, fully clad irradiated samples containing 100 mg of $U^{235}$ were used, and the melting time was increased to approximately 90 sec.

Preliminary results indicated that the gross gamma activity released varied between 1 and

Fig. 48. The APPR-1 Installation at Fort Belvoir, Va.

8%, probably due to differences in total time at temperature, which was difficult to duplicate. The cesium values averaged 9% and were in fair agreement; the iodine values averaged 33%; and the values for vaporized strontium were not clearly different from zero. Larger irradiated samples will be tested when hot-cell facilities become available.

The test programs involving the irradiation of APPR-type fuel elements and control-rod materials will be reported separately.

### Reactor Calculations

Calculations were performed to coordinate the irradiation experiments conducted at the MTR. The calculations were an attempt to predict the neutron-$B^{10}$ reactions to be expected in absorber samples and in a full-scale mockup of the APPR absorber section.

Data from the APPR critical experiment were analyzed and compared with predictions from theory. The prediction of the constructive interference for a five-rod bank, as well as the worth of various other control-rod arrangements, was found to be in agreement with the experimental results. The calculated critical mass was found to be sensitive to assumptions concerning the resonance absorption of neutrons in the stainless steel in the APPR core. Satisfactory agreement with the initial mass measurement was obtained by a two-group method in which the resonance absorption in stainless steel is accounted for by using the measured resonance integral.

To aid in a survey of potential high-temperature moderators, age calculations were made, with the Oracle, for a large variety of materials. Fermi age theory was used for nonhydrogenous materials, and the Flugge-Tittle method was employed for the materials containing hydrogen.

## GAS-COOLED LOOP DESIGN AND CONSTRUCTION

The design and successful operation of high-temperature, gas-cooled reactors require a knowledge of the behavior of materials under complex environmental conditions. Final evaluation of proposed materials must be based on tests conducted under actual or simulated service conditions, because the deleterious effects of radiation, temperature, and gas-metal reactions are intricately interrelated. The AEC has a program under way to provide facilities for such tests by the insertion of gas-cooled test loops into existing reactors.

The Laboratory is designing, constructing, and installing a gas-cooled test loop in the new Oak Ridge Research Reactor (ORR). This facility is intended principally for testing small samples of a variety of materials for gas-cooled reactor application. Test specimens will be exposed in the loop to the neutron and gamma fields of the ORR and to the hot circulating gas at controlled temperatures, pressures, and flow rates.

The in-pile or test section of the $1\frac{15}{16}$-in.-ID loop occupies two lattice positions of the ORR. Equipment associated with the gas system is located in a shielded area approximately 100 ft from the reactor. A reciprocating compressor of the nonlubricated type is used to circulate the gas, which is cooled before it enters the compressor and then is reheated to desired test conditions. Other major pieces of equipment include a high-temperature filter, a gas-to-gas heat exchanger, a gas-to-water cooler, and an electrical-resistance-type gas heater. The structural material for the high-temperature portions of the loop is Inconel. Procurement and fabrication of major components and assembly of the instrument and control panel are under way.

## ASSISTANCE TO OTHER REACTOR PROGRAMS

**Maritime Nuclear Power Program.** – The Maritime Reactor Branch of the AEC has requested technical support on the design and construction of the first nuclear-powered merchant ship. The reactor for this ship, which is being designed by the Babcock & Wilcox Co., will be a pressurized-water type, fueled with low-enriched uranium oxide; the reactor power output will be 68 Mw. The Package Reactor Group, along with other ORNL groups, will review the Nuclear Merchant Ship Reactor design. Technical assistance will also be provided in the testing and construction phases, including backup and supplemental work on the metallurgy and the irradiation testing of the fuel and control materials for the reactor.

**Puerto Rican Reactor Program.** – The Oak Ridge Operations Office requested technical assistance in the preparation of an invitation to bid on a swimming-pool-type research reactor. A 1-Mw reactor, which will be used in a research and

training program, is to be located adjacent to the University of Puerto Rico campus at Mayaguez, Puerto Rico. The invitations were written to give industry the widest possible latitude in providing their own designs for the reactor components. In particular, it is very desirable to provide a reactor design in which the power level can later be increased to 5 Mw, with a minimum amount of physical modification. The AEC will request that the reactor facility be in complete operable condition within 700 days after the contract is let.

Subsequent to the signing of the contract, a technical committee with representatives from ORNL and ORO will be formed to assist in the technical guidance of the program.

**Sponsored ORSORT Summer Studies.** – In the summer of 1956 an ORSORT study was made for a reactor-powered "beachlighter." A beachlighter is a ship used to transport men and materials from ship to shore. For such a vessel to be independent of fuel supply has important military advantages.

The study sponsored and supervised in the summer of 1957 was for a small gas-cooled reactor suitable for transporting by trailer. The reactor system studied was cooled by nitrogen, in a closed-cycle system, and moderated with BeO.

(Note: The activities of the Package Power Reactor Group were transferred, as of October 1, 1957, to the Reactor Projects Division.)

## PREVIOUS PROGRESS REPORTS

Progress reports have been issued by the Electronuclear Research Division for the periods ending on the dates listed below:

| | |
|---|---|
| Y-495 | September 30, 1949 |
| Y-548 | December 31, 1949 |
| Y-584 | March 31, 1950 |
| Y-637 | June 30, 1950 |
| Y-676 | September 30, 1950 |
| Y-722 | December 31, 1950 |
| Y-767 | March 31, 1951 |
| Y-795 | June 30, 1951 |
| ORNL-1173 | September 30, 1951, Part I |
| ORNL-1235 | September 30, 1951, Part II |
| ORNL-1269 | December 31, 1951, Part I |
| ORNL-1270 | December 31, 1951, Part II |
| ORNL-1315 | March 31, 1952, Part II |
| ORNL-1339 | March 31, 1952, Part I |
| ORNL-1345 | June 30, 1952, Part I |
| ORNL-1346 | June 30, 1952, Part II |
| ORNL-1383 | September 30, 1952 |
| ORNL-1531 | March 20, 1953 |
| ORNL-1663 | September 20, 1953 |
| ORNL-1670 | March 20, 1954 |
| ORNL-1795 | September 20, 1954 |
| ORNL-1884 | March 20, 1955 |
| ORNL-2030 | September 20, 1955 |
| ORNL-2139 (Unclassified) | March 20, 1956 |
| ORNL-2140 (Confidential) | March 20, 1956 |

---

## PAPERS PRESENTED DURING THE PERIOD MARCH 21, 1956–OCTOBER 1, 1957

*Southeastern Section of the American Physical Society, Nashville, Tennessee, March 29–31, 1956:*

H. G. Blosser and T. H. Handley, "($n,p$) Cross Section Measurements at Medium Energies."

R. S. Livingston, "A Bev High-Current Accelerator" (an invited paper).

A. Zucker and H. L. Reynolds, "A Semiclassical Model for Elastic Nitrogen-Nitrogen Scattering."

*American Physical Society, Washington, D.C., April 26–28, 1956:*

H. G. Blosser, T. H. Handley, and C. D. Goodman, "($n,\alpha$) Cross Section Measurements at 14 Mev."

M. L. Halbert, T. H. Handley, and A. Zucker, "Excitation Functions for Nitrogen-Induced Nuclear Reactions in Sodium."

J. L. Need and C. D. Goodman, "Energy Distribution of Light Reaction Products from Bombardment of Beryllium by Nitrogen."

A. Zucker, "Nuclear Reactions with 26-Mev Nitrogen Ions" (an invited paper).

*American Nuclear Society, Chicago, Illinois, June 6–8, 1956:*

F. L. Green and J. A. Martin, "Increased Yields of $Mn^{54}$, $I^{125}$, and $I^{125}$ and $I^{130}$ with a 22-Mev Proton Cyclotron."

B. Harmatz, R. S. Livingston, and J. A. Martin, "The Electromagnetic Separation of the Isotopes of the Heavy Elements."

M. L. Winton, F. P. Green, and A. L. Boch, "Response Characteristics of the ORNL Package Reactor Conceptual Design by Analog Simulation."

*International Conference on Nuclear Reactions, Amsterdam, July 2–7, 1956:*

B. L. Cohen, "Energy Distribution of Single Mass Fission Fragments."

B. L. Cohen, "22-Mev Proton-Induced Reactions in Medium Weight Elements."

A. Zucker, "Heavy-Ion Nuclear Physics Research at Oak Ridge National Laboratory."

A. Zucker, "Nitrogen Stripping Reactions on Light Elements."

*American Physical Society, Chicago, Illinois, November 23–24, 1956:*

J. W. Mihelich, B. Harmatz, T. H. Handley, and J. J. Pinajian, "Nuclear Spectroscopy of Neutron-Deficient Isotopes in the Rare Earth Region."

*American Physical Society, New York, January 30–February 2, 1957:*

H. G. Blosser, F. T. Trammell, and H. M. Moseley, "Parameter Calculation Program for Oak Ridge Cyclotron Analogue."

B. L. Cohen, "Anomalous Inelastic Scattering of 23-Mev Protons by Heavy Elements."

C. D. Goodman, "Level Density in $F^{19}$ as Inferred from Nitrogen-Induced Reactions."

E. E. Gross, "Absolute Neutron Spectra from 190-Mev Proton Bombardment of Various Elements."

M. L. Halbert and A. Zucker, "Angular Distribution of $N^{13}$ from $Mg^{25}(N^{14}, N^{13})Mg^{26}$."

R. E. Worsham, H. G. Blosser, and R. S. Livingston, "Design Description of Oak Ridge Cyclotron Analogue."

A. Zucker, M. L. Halbert, T. H. Handley, J. J. Pinajian, and W. H. Webb, "Nitrogen-Induced Neutron Transfer Reactions in Be, C, O, Na, $Mg^{24}$, $Mg^{25}$, $Mg^{26}$."

*Southeastern Section of the American Physical Society, Lexington, Kentucky, April 4–6, 1957:*

H. G. Blosser, "The Oak Ridge Cyclotron Analogue" (an invited paper).

C. B. Fulmer, "Equilibrium Charges of Uranium-235 Fission Fragments in Gases as Functions of Fragment Velocity, Gas Pressure, and Type of Gas."

M. L. Halbert, "Fluorescent Response of CsI(Tl) to Nitrogen Ions."

A. Zucker, "Heavy Ion Induced Reactions" (an invited paper).

*American Physical Society, Washington, April 25–27, 1957:*

B. L. Cohen, "Coincidence Studies of the $Ni^{58}$ $(p,2p)$ Reaction" (post-deadline paper).

B. L. Cohen and C. B. Fulmer, "A Fission-Fragment Mass Separator and the Nuclear Charge Distribution of Single Mass Fission Fragments."

C. B. Fulmer and B. L. Cohen, "Magnetic Analysis of Long Range Particles from Fission of Uranium-235."

C. B. Fulmer and B. L. Cohen, "Scintillation Pulse Height in CsI(Tl) vs Energy and Range in Various Materials vs Energy for Light and Heavy Fission Fragments."

C. D. Goodman and N. F. Ziegler, "A Square-Wave Cyclotron Oscillator."

*International Symposium on Isotope Separation, Amsterdam, April 23–27, 1957:*

R. S. Livingston, "Electromagnetic Separation of the Isotopes of the Heavy Elements."

R. S. Livingston, "Special Isotope Separator for Identification or Purification of Radioactive Species."

*American Physical Society, Notre Dame, Indiana, June 20–22, 1957:*

K. P. Jacob, J. W. Mihelich, and B. Harmatz, "The Decay of $Tm^{168}$ to Levels in $Er^{168}$."

T. J. Ward, K. P. Jacob, J. W. Mihelich, B. Harmatz, and T. H. Handley, "Electron Capture of $Tb^{155}$ to Levels in $Gd^{155}$."

## ARTICLES PUBLISHED DURING THE PERIOD MARCH 21, 1956–OCTOBER 1, 1957

B. L. Cohen, "Anomalous Inelastic Scattering of 23-Mev Protons by Heavy Elements," *Phys. Rev.* **105**, 1549–1555 (1957).

B. L. Cohen, "Proton-Induced Reactions in $Na^{23}$, $Al^{27}$, and $Si^{29}$," *Phys. Rev.* **102**, 453–455 (1956).

B. L. Cohen, A. F. Cohen, and C. D. Foley, "Energy Distribution of Mass-97 Fission Fragments from Thermal-Neutron Fission of U-235," *Phys. Rev.* **104**, 1046–1053 (1956).

B. L. Cohen and S. W. Mosko, "Inelastic Proton Scattering and $(p,d)$ Reactions in Heavy Elements," *Phys. Rev.* **106**, 995–1000 (1957).

M. L. Halbert, "Fluorescent Response of CsI(Tl) to Energetic Nitrogen Ions," *Phys. Rev.* **107**, 647–649 (1957).

M. L. Halbert, T. H. Handley, and A. Zucker, "Excitation Function for Two Nitrogen-Sodium Nuclear Reactions," *Phys. Rev.* **104**, 115–117 (1956).

M. L. Halbert, T. H. Handley, J. J. Pinajian, W. H. Webb, and A. Zucker, "Neutron-Transfer Reactions from the Nitrogen Bombardment of Be, C, O, Na, and $Mg^{24,25,26}$," *Phys. Rev.* **106**, 251–256 (1957).

R. S. Livingston, "Trends in the Design of Cyclotrons After 25 Years," *Ind. Eng. Chem.* **48**, 1231–1237 (1956).

G. H. McCormick, H. G. Blosser, B. L. Cohen, and E. Newman, "($p$,He$^3$) and ($p$,$t$) Cross Section Measurement," *J Nuclear Inorg. Chem.* **2**, 269–270 (1956).

J. W. Mihelich and B. Harmatz, "Some New Isomeric Transitions in Rare Earth Nuclei," *Phys. Rev.* **106**, 1232–1235 (1957).

H. L. Reynolds, D. W. Scott, and A. Zucker, "Nuclear Reactions Produced by Nitrogen on Boron and Oxygen," *Phys. Rev.* **102**, 237–241 (1956).

H. L. Reynolds and A. Zucker, "Elastic Scattering of Nitrogen by Nitrogen," *Phys. Rev.* **102**, 1378–1384 (1956).

W. H. Webb, H. L. Reynolds, and A. Zucker, "Nitrogen-Induced Nuclear Reactions in Aluminum," *Phys. Rev.* **102**, 749–752 (1956).

## ARTICLES SUBMITTED FOR PUBLICATION MARCH 21, 1956–OCTOBER 1, 1957

B. L. Cohen, "Coincidence Studies of the Ni$^{58}$($p$,2$p$) Reaction," to *The Physical Review.*

B. L. Cohen, "Cyclotron and Synchrocyclotrons," to *Handbuch der Physik,* Springer-Verlag, Berlin.

B. L. Cohen and C. B. Fulmer, "A Fission-Fragment Mass Separator and the Nuclear Charge Distribution of Single Mass Fission Fragments," to *The Physical Review.*

C. B. Fulmer, "Scintillation Response of CsI(Tl) Crystals to Fission Fragments and Energy vs Range in Various Materials for Light and Heavy Fission Fragments," to *The Physical Review.*

C. B. Fulmer and B. L. Cohen, "Equilibrium Charges of Fission Fragments in Gases," to *The Physical Review.*

C. B. Fulmer and B. L. Cohen, "Magnetic Analysis of the Long Range Particles from Fission of U$^{235}$," to *The Physical Review.*

M. L. Halbert and A. Zucker, "Angular Distribution of N$^{13}$ from N$^{14}$ on Mg$^{25}$," to *The Physical Review.*

J. W. Mihelich, B. Harmatz, and T. H. Handley, "Nuclear Spectroscopy of Neutron-Deficient Rare Earths (Tb Through Hf)," to *The Physical Review.*

**ORNL-2434**
**Physics and Mathematics**
**TID-4500 (13th ed. Rev.)**

## *INTERNAL DISTRIBUTION*

1. C. E. Center
2. Biology Library
3. Health Physics Library
4-6. Central Research Library
7. Reactor Experimental Engineering Library
8-11. Laboratory Records Department
12. Laboratory Records, ORNL R.C.
13. A. M. Weinberg
14. L. B. Emlet (K-25)
15. J. P. Murray (Y-12)
16. J. A. Swartout
17. E. H. Taylor
18. E. D. Shipley
19. S. C. Lind
20. M. L. Nelson
21. W. H. Jordan
22. R. R. Dickison
23. C. P. Keim
24. R. S. Livingston
25. F. L. Culler
26. H. G. Blosser
27. A. H. Snell
28. A. Hollaender
29. M. T. Kelley
30. G. E. Boyd
31. K. Z. Morgan
32. T. A. Lincoln
33. A. S. Householder
34. C. S. Harrill
35. C. E. Winters
36. D. W. Cardwell
37. D. Phillips
38. P. M. Reyling
39. G. C. Williams
40. R. J. Jones
41. A. L. Boch
42. B. L. Cohen
43. F. T. Howard
44. R. E. Worsham
45. J. A. Martin
46. M. B. Marshall
47. A. Zucker
48. R. W. Johnson
49. J. A. Lane
50. M. J. Skinner
51. R. A. Charpie
52. R. F. Christy (consultant)
53. E. Creutz (consultant)
54. L. P. Smith (consultant)
55. R. L. Thornton (consultant)
56. J. A. Wheeler (consultant)
57. ORNL – Y-12 Technical Library, Document Reference Section

## *EXTERNAL DISTRIBUTION*

58. Division of Research and Development, AEC, ORO
59-662. Given distribution as shown in TID-4500 (13th ed. Rev.) under Physics and Mathematics category (75 copies – OTS)